REFERENCES

1. M. E. Pearce, J. B. Melanko and A. K. Salem, *Phamaceutical Reseach*, **24**, 2007, 2335.
2. J. Yao, G. Zhao, D. Wang and G. Han, *Material Letters*, **59**, 2005, 3652.
3. D. Beydoun, R. Amal, G. Low and S. Mcvoy, *Journal of Nanoparticle Research,* **1**, 1999, 439.
4. X. F. Duan, Y. Huang, R. Agawal and C. M. Leiber, *Nature*, **421**, 2003, 241.
5. H. Zhang, D. R. Yang, X. Y. Ma and D. L. Que, *Material letters*, **59**, 2005, 3037.
6. C. Li, X. Yang, B. Yang, Y. Yan and Y. Qian, *Journal of Crystal Growth*, **291**, 2006, 45.
7. Y. Li, J. Wan, and Z.Gu *Material Science and Engineering* A, **286**, 2000, 106
8. S. I. Nikirenko, Y. Koltypin, Y. Mastai, M. Koltypin and A. Gedanken, *Journal of Material Chemistry*, **12**, 2002, 1450.
9. D. Routkevitch, T. Bigioni, M. Moskovits and J. M. Xu, *Journal of Physical Chemistry*, **100**, 1996, 14037.
10. J. H. Zhan, X. G. Yang, D. W. Wang, S. D. Li, Y. T. Xie, Y. N. Xia and Y. T. Qian, *Advance Materials*, **12**, 2000, 1348.
11. D. Xu, Y. Xu, D. Chen, G. Guo, L. Gui and Y. Tang, *Chemistry and Physic Letters*, **325**, 2000, 340.
12. J. Yang, J. Zeng, S. Yu, L. Yang, G. Zhou and Y. Qian, *Chemistry of Materials*, **12**, 2000, 3259.

13. J. Wu, Y. Jiang, Q. Li, X. Liu and Y, Qian, *Journal of crystal growth*, **235**, 2002, 421.

14. M. Chen, Y. Xie, J. Liu, Y. Xiong, S. Zhang, Y. Qian and X. Liu, *Journal of Material Chemistry*, **12**, 2002, 748.

15. S.Q. sun and T. Li, *Crystal Growth & design*, **7**, 2007, 2367.

16. K. Byrappa and M. Yoshimura; *HAND BOOK OF HYDROTHERMAL TECHNOLOGY; A Technology for Crystal Growth and Materials Processing*, Noyes Publications, New York, 2001.

17. M. Yoshimaru and K. Byrappa, *Journal of Materials Science*, **43**, 2008, 1573.

18. Z. Quan, C. Li, X. Zhang, J. Yang, P. Yang, C. Zhang and J. Lin, *Crystal Growth & Design*, **8**, 2008, 2384.

19. http://en.wikipedia.org/wiki/Cadmium sulfide (September 12, 2011)

20. P. Atkins, T. Overtone, J. Rourke, M. Weller and F. Armstrong; *SHRIVER & ATKINS Inorganic Chemistry*, 4th.Oxford University Press.2006]

21. R. R. Gainov, A. V. Dooglav, I. N. Penkov, I. R. Mukhamedshin, N. M. Mozgova, A. V. Evlampiev and I. A. Bryzgalov, *Physical Review B*, **79**, 2009, 075115.

22. W. Li, *Materials Letters,* **62**, 2008, 243.

23. Z. Liu, D. Xu, J. Liang, W. Lin, W. Yu and Y. Qian, *Journal of Solid State Chemistry*, **178**, 2005, 950.

24. C. Boudias, D. Monceau, *CaRIne Crystallography 3.1*, DIVERGENT S.A. Centre de Transfert, 60200 Compiègne, France, 1989-1998.

25. S. Kumar and T. Nann. *Small*, **2**, 2006, 316.

26. A. Huczko., *Applied Physic A.*, **70**, 2000, 365.

27. G. L. Hornyak, J. Dutta, H. F. Tibbals and A. K. Rao; "*Introduction to nanosciece*", CRC Press, USA, 2008.

28. A. H. Mueller, M. A. Petruska, M. Achermann, D. J. Werder, E. A. Akhadov, D. D. Koleske, M. A. Hoffbauer and V. I. Klimov, *Nano Letters*, **5**, 2005, 1039.

29. J. M. Caruge, J. E. Halpert, V. Bulovic and M. G. Bawendi, *Nano Letters*, **6**, 2006, 2991.

30. S. Coe, W. K. Woo, M. Bawendi, V. Bulovic, *Nature*, **420**, 2002, 800.

31. A. L. Rogach, N. Gaponik, J. M. Lupton, C. Bertoni, D. E. Gallardo, S. Dunn, N. L Pira, M. Paderi, P. Repett, S. G. Romanov, C. O'Dwyer, C. M. S. Torres and A. Eychmuller, *Angewandte Chemie International Edition*, **47**, 2008, 6538.

32. J. Z. Zhang, Z. Wang, J. Liu, S. Chen and G. Liu, *"Self-Assembled Nanostructures"*, Kluwer Academic Publishers, New York, USA, 2003.

33. A. L. Rogach, A. Eychmuller, S. G. Hickey and S. V. Kershaw, *Small*, **3**, 2007, 536.

34. A. Biebersdorf, R. Dietmüller, A. S. Susha, A. L. Rogach, S. K. Poznyak, D. V. Talapin, H. Weller, T. A. Klar and J. Feldmann, *Nano Letters*, 6, 2006, 1559.

35. K. Szendrei, F. Cordella, M. V. Kovalenko, M. Boberl, G. Hesser, M. Yorema, D. Jarzab, O. V. Mikhnenko, A. Gocalinska, M. Saba, F. Quochi, A. Mura, G. Bongiovanni, P. W. M. Blom, W. G. Heiss and M. A. Loi, *Advance Materials*, **21**, 2009, 683.

36. W. T. Sun, Y. Yu, H. Y. Pan, X. F. Gao, Q. Chen and L. M. Peng, *Journal of the American Chemical Society,* **130**, 2008, 1124.

37. G. Hodes, *Journal of Physical Chemistry C*, **112**, 2008, 17778.

38. Y. Zhou, M. Eck and M. Kruger, *Energy & Environmental Science*, **3**, 2010, 1851.

39. W. L. Ma, C. Y. Yang, X. Gong, K. Lee and A. J. Heeger, *Advance Functional Materials*, **15**, 2005, 1617.

40. J. Y. Kim, K. Lee, N. E. Coates, D. Moses, T. Q. Nguyen, M. Dante and A. J. Heeger, *Science*, **317**, 2007, 222.

41. M. Afzaal and P. O'Brien, *Journal of Material Chemistry*, **16**, 2006, 1597.

42. A. K. Rath , M. Bernechea , L. Martinez and G. Konstantatos, *Advance Materials*, **23**, 2011, 3712.

43. S. H. Im, H. Kim, J. H. Rhee, C. S. Lim and S. Seok, *Energy & Environmental Science,* **4**, 2011, 2799.

44. Y. Zhou, M. Eck and M. Kruger, *Energy & Environmental Science,* **3**, 2010, 1851.

45. I. Gur, N. A. Fromer, M. L. Geier and A. P. Alivisatos, *Science*, **310**, 2005, 462.

46. E. R. Hernandez, A. Baeza and M. V. Regi, *ACS Nano*, **5**, 2011, 1259.

47. Y. Weizmann, D. M. Chenoweth and T. M. Swager, *Journal of the American Chemical Society*, **133**, 2011, 3238.

48. N. L. Rosi and C. A. Mirkin, *Chemical Review*, **105**, 2005, 1547.

49. W. Nie, L. An, B. Jiang and X. L. Ji, *Chemistry Letters*, **33**, 2004, 836.

50. F. Shieh, A. E. Saunders, B. A. Korgel, *Journal of Physical Chemistry B*, **109**, 2005, 8538.

51. W. Z. Wang, Y. Geng, P. Yan, F. Y. Liu, Y. Xie and Y. T. Qian, *Inorganic Chemistry Communications*, **2**, 1999, 83.

52. L. Manna, D. J. Millirion, A. Meisel, E. C. Scher and A. P. Alivisatos, Nature Material, 2, 2003, 382.

53. S. G. Thoma, A. Sanchez, P. P. Provencio, B. L. Abrams and J. P. Wilcoxon, *Journal of the American Chemical Society*, **127**, 2005, 7611.

54. S. L. Cumberland, K. M. Hanif, A. Javier, G. A. Khitrov, G. F. Strouse, S. M. Woessner, C. S. Yun, *Chemistry of Materials*, **14**, 2002, 1576.

55. D. J. Crouch, P. O'Brien, M. A. Malik, P. J. Skabra and S. P. Wright, *Chemical Communications*, **12**, 2003, 1454.

56. P. S. Nair, T. Radhakrishnan, N. Revaprasadu, G. Kolawole and P. O'Brien, *Journal of Material Chemistry*, **12**, 2002, 2722

57. F. T. Quinlan, J. Koether, W. Tremel, W. Knoll, S. Rishbud and P. Stroeve, *Langmuir*, **16**, 2000, 4049.

58. D. Ingert and M. P. Pileni, *Advance Functional Materials*, **11**, 2001, 136–139.

59. B. A. Simmons, S. Li, V. T. John, G. L. Mcpherson, A. Bose, W. Zhou and J. He, *Nano Letters*, **2**, 2002, 263.

60. N. Pinna, K. Weiss, H. S. Kongehl, W. Vogel, J. Urban and M. P. Pileni, *Langmuir*, **17**, 2001, 7982.

61. P. V. Radovanovic, C. J. Barrelet, S. Gradecak, F. Qian and C. M. Lieber, *Nano Letters*, **5**, 2005, 1407.

62. M. S. Gudiksen and C. M. Lieber, *Journal of the American Chemical Society*, **122**, 2000, 8801.

63. W.W. Yu, Y. A. Wang, X. Peng, *Chemistry of Materials*, **15**, 2003, 4300.

64. K. Byrappa and T. Adschiri, *Progress in Crystal Growth and Characterization of Materials*, **53**, 2007, 117.

65. M. Yoshimura and K. Byrappa, *Journal of Materials science*, **43**, 2008, 2085.

66. K. Jackowska, A.T. Biegunski and M. Tagowska, *Journal of Solid State Electrochemistry*, 12, 2008, 437.

67. K.S. Shankar and A.K. Raychaudhuri, *Materials Science and Engineering C*, **25**, 2005, 738.

68. B. E. Warren, *X-ray diffraction,* Addison-Wesley Pub. Co., Reading, USA, 1969.

69. D. Keith Bowen and B. K. Tanner, *High Resolution X-Ray Diffraction and Topography,* Taylor & Francis, London, UK, 1998.

70. H. J. Butt, K. Graf and M. Kappl, *Physics and chemistry of interfaces*, Wiley-VCH, Weinheim, Germany, 2003.

71. S. Amelinckx, D. van Dyck, J. V. Landuyt, and G. V. Tandeloo, *Electron microscopy: principles and fundamentals*, Wiley-VCH, Weinheim, Germany, 2003.

72. A. C. C. Yu, M. Mizuno, Y. Sasaki, M. Inoue, H. Kondo, I. Ohta, D. Djayaprawira and M. Takahashi, *Applied Physics Letters,* **82**, 2003, 4352

73. L. Valentini, I. Armentano, J. M. Kenny, C. Cantalini, L. Lozzi and S. Santucci, *Applied Physics Letters,* **82**, 2003, 961.

74. Z. L. Wang, *Journal of Physical Chemistry B*, **104**, 2000, 1153.

75. L. A. Bendersky and F. W. Gayle, *Journal of Research of the National Institute of Standards and Technology,* **106**, 2001, 997.

76. R. Ferraro and K. Nakamoto, *Introductory Raman Spectroscopy,* Academic Press, San Diego, USA, 1994.

77. I. De Wolf, C. Jian and W. M. van Spengen, *Optics and Lasers in Engineering*, **36,** 2001, 213.

78. T. Thongtem, A. Phuruangrat, S. Thongtem, *Journal of Materials Science*, **42**, 2007, 9316.

79. H. H. Perkampus, *UV-VIS spectroscopy and its applications* Springer-Verlag, Berlin, Germany, 1992.

80. X. Michalet, F. Pinaud, T. D. Lacoste, M. Dahan, M. P. Bruchez, A. P. Alivisatos, and S. Weiss, *Single Molecules*, **2**, 2001, 261.

81. A. D. Yoffe, *Advances in Physics*, **50**, 2001, 208.

82. A. P. Alivisatos, *Science*, **271**, 1996, 933.

83. J. H. Park, J. Y. Kim, B. D. Chin, Y. C. Kim, J. K. Kim and O. O. Park, *Nanotechnology*, **15**, 2004, 1217.

84. N. Venkatram, D. N. Rao and M. A. Akundi, *Optics Express*, **13**, 2005, 867.

85. C. H. B. Ng and W. Y. Fan., *Journal of Physical Chemistry B,* **110**, 2006, 20801.

86. D. A. Skoog and J. J. Leary, *Principles of Instrumental Analysis*, 4thed. Saunders College Publishing, Orlando, USA, 1992.

87. L. H. Qu and X. G. Peng, *Journal of the American Chemical Society*, **124**, 2002, 2049.

88. M. Bruchez, M. Moronne, P. Gin, S. Weiss and A. P. Alivisatos, *Science,* **281**, 1998, 2013.

89. W. C. W. Chan and S. M. Nie, *Science*, **281**, 1998, 2016.

90. Q. Li, B. Sun, I. A. Kinloch, D. Zhi, H. Sirringhaus and A. H. Windle, *Chemistry of Materials*, ***18***, 2006, 164.

91. A. P. Alivisatos, *Nature Biotechnology*, **22**, 2004, 47.

92. X. Michalet, F. F. Pinaud, L. A. Bentolila, J. M. Tsay, S. Doose, J. J. Li, G. Sundaresan, A. W. Wu, S. S. Gambhir and S. Weiss, *Science*, **307**, 2005, 538.

93. M. Y. Han, X. Gao, J. Z. Su and S. Nie, *Nature Biotechnology*, **19**, 2001, 631.

94. T. Thongtem, A. Phuruangrat and S. Thongtem, *Material Letters*, **61**, 2007, 3235.

95. Q. Sun and T. Li, *Crystal Growth & Design*, **7**, 2007, 2367.

96. Q. Zhang, F. Huang and Y. Li, *Colloids and Surfaces A: Physicochemical and Engineering Aspects*, **257**, 2005, 497.

97. C. C. Chen, C. Y. Chao and Z. H. Lang, *Chemistry of Materials*, **12**, 2000, 1516

98. H. Ji, J. Cao, J. Feng, X. Chang, X. Ma, J. Liu and M. Zheng, *Material Letters*, **59**, 2005, 3169.

99. M. Nagurathinam, J. Chen, and J. J. Vittal, *Crytal Growth & Design*, **9**, 2009, 2457.

100. H. Zhang, Y. Zhang, J. Yu and D. Yang, *Journal of Physical Chemistry C*, **112**, 2008, 13390.

101. K. J. Wang, G. D. Li, J. X. Li, Q. Wang and J. S. Chen, *Crystal Growth & Design*, **7**, 2007, 2265.

102. B. Zhang, X. Ye, W. Hou, Y. Zhao and Y. Xie, *Journal of Physical Chemistry B*, **110**, 2006, 8978.

103. X.Y. Ma, L. Liu, W.L. Mo, H. Liu, H.Z. Kou and Y. Wang, *Journal of Crystal Growth*, **306**, 2007, 159.

104. Z. Quan, J. Yang, P. Yang, Z. Wang, C. Li and J. Lin, *Crystal Growth & Design*, **8**, 2008, 200.

105. X. Zhu, J. Ma, Y. Wang, J. Tao, B. Lin, Y. Ren, X. Jiang and J. Liu, *Ceramics International*, **34**, 2008, 249.

106. H. Wang, Y.N. Lu, J.J. Zhu, and H.Y. Chen, *Inorganic Chemistry*, **42**, 2003, 6404.

107. H. Bao, X. Cui, C.M. Li, Q. Song, Z. Lu and J. Guo, *Journal of Physical Chemistry C*, **111**, 2007, 17131.

108. L. Chen, W. Zhu, Q. Han, X. Yang, L. Lu and X. Wang, *Materials Letters*, **63**, 2009, 1258.

109. Powder Diffraction File, *JCPDS International Centre for Diffraction Data*, PA 19073-3273, USA, 2001.

110. J. S. Jang, U. A. Joshi and J. S. Lee, *Journal of Physical Chemistry C*, **111**, 2007, 13280.

111. V. Sivasubramanian, A.K. Arora, M. Premila, C.S. Sundar and V.S. Sastry, *Physica E*, **31**, 2006, 93.

112. H. M. Fan, X. F. Fan, Z. H. Ni, Z. X. Shen, Y. P. Feng and B. S. Zou, *Journal of Physical Chemistry C*, **112**, 2008, 1865.

113. A. Pan, R. Liu, Q. Yang, Y. Zhu, G. Yang, B. Zou and K. Chen, *Journal of Physical Chemistry B*, **109**, 2005, 24268.

114. C. Li, X. Yang, B. Yang, Y. Yan and Y. Qian, *Journal of Crystal Growth*, **291**, 2006, 45.

115. H. Wang, P. Fang, Z. Chen and S. Wang, *Journal of Alloys and Compounds*. **461,** 2008, 418.

116. W. Qingqing, X. Gang and H. Gaorong, *Journal of Solid State Chemistry*, **178**, 2005, 2680.

117. X. G. Yue, W. Han, C. C. Wei, Z. H. Qian, C. J. Ming and J. G. Bin, *Transactions Nonferrous Metals Society of China*, **16**, 2006, 105.

118. W. Qingqing, X. Gang and H. Gaorong, *Journal of Solid State Chemistry*, **178**, 2005, 2680.

119. X. Yang, X. Wang and Z. Zhang, *Materials Chemistry and Physics*, **95**, 2006, 154.

120. J. Ota and S. K. Srivastava, *Journal of Physical Chemistry C*, **111**, 2007, 12260.

121. Y. Sun, Q. Han, J. Lu, X. Yang, L. Lu and X. Wang, *Materials Letters*, **62**, 2008, 3730.

122. Q. Han, Y. Sun, X. Wang, L. Chen, X. Yang and L. Lu, *Journal of Alloys Compounds*, **481**, 2009, 520.

123. J. Lu, Q. Han, X. Yang, L. Lu and X. Wang, *Materials Letters*, **61**, 2007, 3425.

124. B. Zhang, X. Ye, W. Hou, Y. Zhao and Y. Xie, *Journal of Physical Chemistry B*, **110**, 2006, 8978.

125. Z. Quan, J. Yang, P. Yang, Z. Wang, C. Li and J. Lin, *Crystal Growth & Design*, **8**, 2008, 200.

126. C. J. Tang, G. Z. Wang, H. Q. Wang, Y. X. Zhang and G. H. Li, *Materials Letters*, **62**, 2008, 3663.

127. Y. Jiang, Y. J. Zhu and Z. L. Xu, *Mateirials Letters*, **60**, 2006, 2294.

128. X. Y. Ma, L. Liu, W. L. Mo, H. Liu, H. Z. Kou and Y. Wang, *Journal of Crystal Growth*, **306,** 2007, 159.

129. J. Lu, Q. Han, X. Yang, L. Lu and X. Wang, *Materials Letters*, **61**, 2007, 2883.

130. X. J. Feng, K. Shankar, O. K. Varghese, M. Paulose, T. J. Latempa,and C. A. Grimes, *Nano Letter*, **8**, 2008,3781.

131. S. Gimenez, A. L. Rogach, A. A. Lutich, D. Gross,A. Poeschl, A. S. Susha, I. Mora-Sero, T. Lana-Villarreal and J. Bisquert, *Journal of applied physics*, **110**, 2011, 014314.

132. Y. Zhang, B. Deng, T. Zhang, D. Gao and A.W. Xu, *Journal of Physical Chemistry C*, **114**, 5073.

133. U. Schubert and N. Hüsing, *Synthesis of Inorganic Materials*, Weinheim, Wiley-VCH; 2000.

134. F. Li, T. Kong, W. Bi, D. Li, Z. Li and X. Huang, *Applied Surface Science*, **255**, 2009, 6285.

135. L. Chu, B. Zhou, H. Mu, Y. Sun and P. Xu, *Journal of Crystal Growth*, **310**, 2008, 5437.

136. J. Zhang and Z. Zhang, *Materials Letters*, **62**, 2008, 2279.

137. X. P. Shen, H. Zhao, H. Q. Shu, H. Zhou and A.H. Yuan, *Journal of Physics and Chemistry of Solids*, **70**, 2009, 422.

138. P. Zhang and L. Gao, *Journal of Material Chemistry*, **13**, 2003, 2007.

139. T. Y. Ding, M. S. Wang, S. P. Guo, G. C. Guo and J. S. Huang, *Materials Letters*, **62**, 2008, 4529.

140. http://en.wikipedia.org/wiki/Polyethylene_glycol (January 6, 2012)

141. http://en.wikipedia.org/wiki/Polyvinyl_alcohol (January 6, 2012)

142. http://en.wikipedia.org/wiki/Polyvinylpyrrolidone (January 6, 2012)

143 http://en.wikipedia.org/wiki/Polyvinylpyrrolidone (January 6, 2012)

APPENDICES

APPENDIX A

The Joint Committee for Powder Diffraction Standards (JCPDS) [109]

1. Cadmium sulfides (CdS)

Name and formula

Reference code:	41-1049
Mineral name:	Greenockite, syn
Common name:	cadmium yellow
PDF index name:	Cadmium Sulfide
Empirical formula:	CdS
Chemical formula:	CdS

Crystallographic parameters

Crystal system:	Hexagonal
Space group:	P63mc
Space group number:	186
a (?):	4.1409
b (?):	4.1409
c (?):	6.7198
Alpha (?):	90.0000
Beta (?):	90.0000
Gamma (?):	120.0000

Measured density:	4.82
Volume of cell:	99.79
Z:	2.00
RIR:	-

Subfiles and Quality

Subfiles:	Inorganic
	Mineral
	Alloy, metal or intermetalic
	Corrosion
	Common Phase
	Educational pattern
	Forensic
	Pigment/Dye
Quality:	Star (S)

Comments

Color:	Yellow
Optical data:	B=2.506, Q=2.529, Sign=+
Additional pattern:	To replace 1-780 and 6-314.
	See ICSD 31074 (PDF 75-1545); See ICSD 60629
	(PDF 77-2306). **References**
Primary reference:	Razik, N., *J. Mater. Sci. Lett.*, **6**, 1443, (1987)
Optical data:	*Dana's System of Mineralogy, 7th Ed.*, **I**, 228, (1944)

Peak list

No.	h	k	l	d [A]	I [%]
1	1	0	0	3.58610	62.0
2	0	0	2	3.35990	91.0
3	1	0	1	3.16380	100.0
4	1	0	2	2.45190	29.0
5	1	1	0	2.07050	48.0
6	1	0	3	1.89980	50.0
7	2	0	0	1.79310	8.0
8	1	1	2	1.76270	31.0
9	2	0	1	1.73250	15.0
10	0	0	4	1.67990	5.0
11	2	0	2	1.58190	3.0
12	1	0	4	1.52130	3.0
13	2	0	3	1.39980	15.0
14	2	1	0	1.35540	5.0
15	2	1	1	1.32870	8.0
16	1	1	4	1.30450	4.0
17	1	0	5	1.25850	9.0
18	2	0	4	1.22590	2.0
19	3	0	0	1.19540	9.0
20	2	1	3	1.15960	14.0
21	3	0	2	1.12620	7.0
22	2	0	5	1.07540	8.0

23	2	2	0	1.03520	3.0
24	2	2	2	0.98930	5.0
25	1	1	6	0.98510	6.0
26	3	0	4	0.97400	2.0
27	2	1	5	0.95430	9.0
28	1	0	7	0.92730	4.0
29	3	1	3	0.90900	7.0
30	4	0	0	0.89650	3.0

Stick Pattern

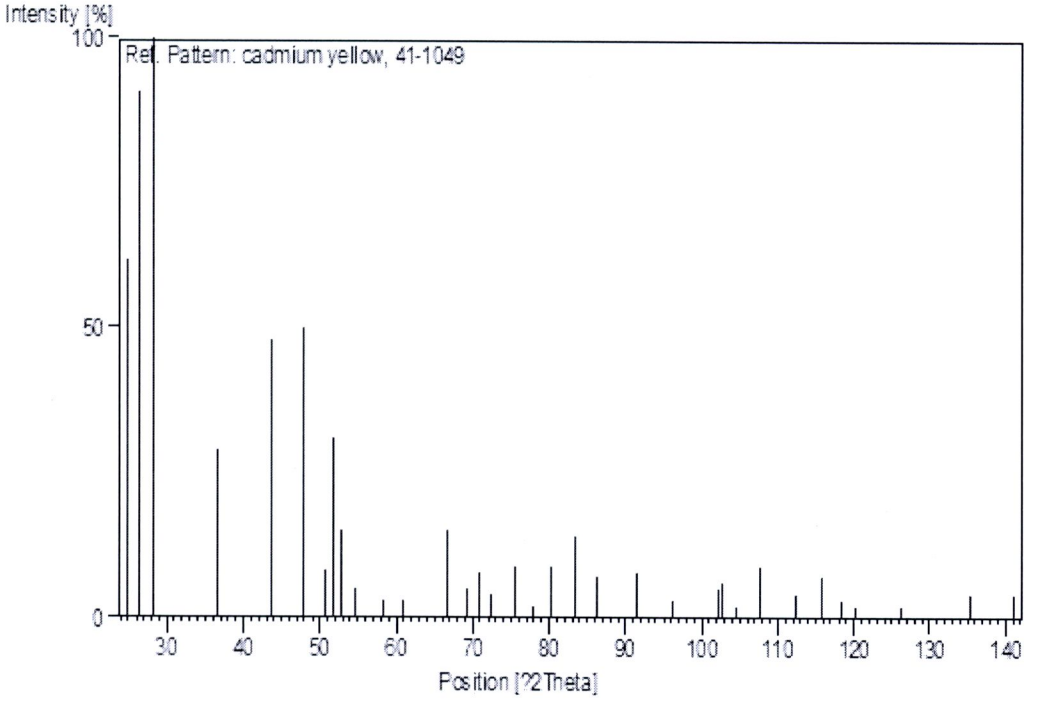

2. Bismuth sulfide (Bi_2S_3)

Name and formula

Reference code:	17-0320
Mineral name:	Bismuthinite, syn
PDF index name:	Bismuth Sulfide
Empirical formula:	Bi_2S_3
Chemical formula:	Bi_2S_3

Crystallographic parameters

Crystal system:	Orthorhombic
Space group:	Pbnm
Space group number:	62
a (?):	11.1490
b (?):	11.3040
c (?):	3.9810
Alpha (?):	90.0000
Beta (?):	90.0000
Gamma (?):	90.0000
Calculated density:	6.81
Measured density:	6.78
Volume of cell:	501.72
Z:	4.00
RIR:	2.10

Subfiles and Quality

Subfiles:	Inorganic
	Mineral
	Alloy, metal or intermetalic
	Common Phase
	Educational pattern
	Forensic
	NBS pattern
Quality:	Indexed (I)

Comments

Color:	Dark gray
General comments:	Measured density from *Dana's System of Mineralogy, 7th Ed.*, **II** 962.
Sample source:	Sample prepared by Glatz, A., Carrier Research and Development Co.
Additional pattern:	Validated by calculated pattern 42-541. See ICSD 201066 (PDF 84-279).
Temperature:	Pattern taken at 25 C.

References

Primary reference:	*Natl. Bur. Stand. (U.S.) Monogr.25*, **5**, 13, (1967)
Structure:	Mumme, W., Watts, J., *Can. Mineral.*,**14**, 322, (1976)

Peak list

No.	h	k	l	d [A]	I [%]
1	1	1	0	7.93600	2.0
2	0	2	0	5.60400	20.0
3	2	0	0	5.56600	6.0
4	1	2	0	5.04000	20.0
5	2	2	0	3.96700	40.0
6	1	0	1	3.74800	18.0
7	1	3	0	3.56900	100.0
8	3	1	0	3.53000	60.0
9	0	2	1	3.25300	16.0
10	2	1	1	3.11800	80.0
11	0	4	0	2.82400	14.0
12	2	2	1	2.81200	50.0
13	3	0	1	2.71700	30.0
14	4	1	0	2.70900	4.0
15	3	1	1	2.64100	18.0
16	2	4	0	2.52100	40.0
17	4	2	0	2.49900	12.0
18	2	3	1	2.45600	10.0
19	0	4	1	2.30500	20.0
20	1	4	1	2.25800	30.0
21	4	3	0	2.24100	12.0
22	5	1	0	2.18800	6.0

23	2	4	1	2.13000	8.0
24	4	2	1	2.11800	10.0
25	2	5	0	2.09600	10.0
26	5	2	0	2.07500	10.0
27	0	0	2	1.99000	18.0
28	4	4	0	1.98500	16.0
29	4	3	1	1.95300	40.0
30	5	0	1	1.94500	30.0
31	1	5	1	1.93700	16.0

Stick Pattern

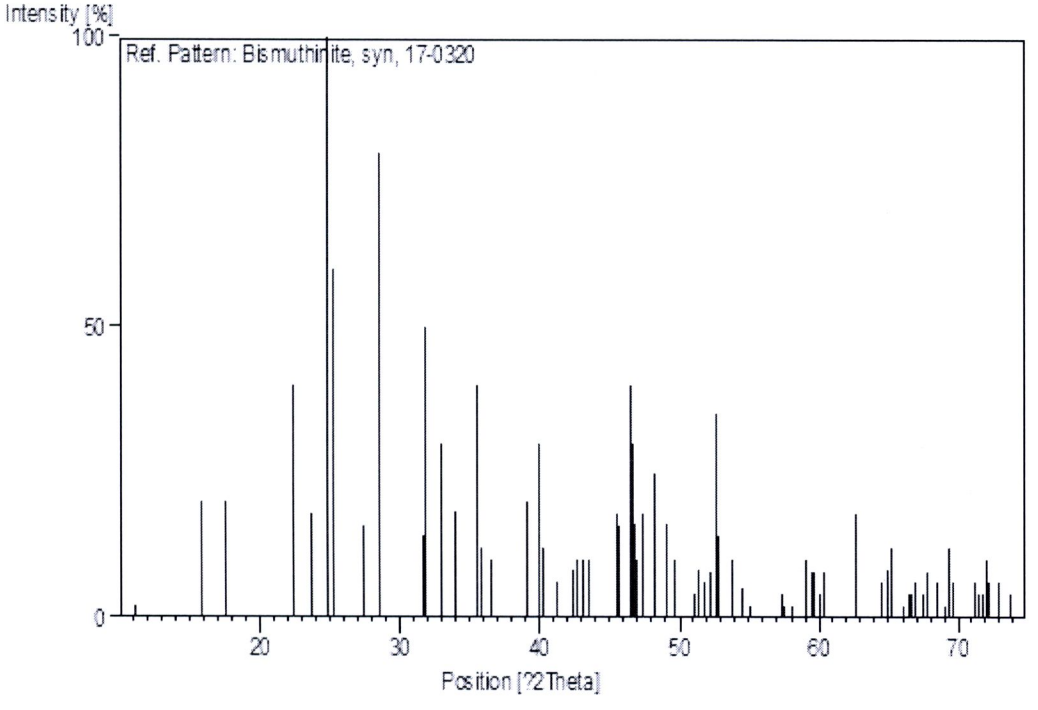

3. Copper sulfide (CuS)

Name and formula

Reference code:	06-0464
Mineral name:	Covellite, syn
PDF index name:	Copper Sulfide
Empirical formula:	CuS
Chemical formula:	CuS

Crystallographic parameters

Crystal system:	Hexagonal
Space group:	P63/mmc
Space group number:	194
a (?):	3.7920
b (?):	3.7920
c (?):	16.3440
Alpha (?):	90.0000
Beta (?):	90.0000
Gamma (?):	120.0000
Calculated density:	4.68
Measured density:	4.67
Volume of cell:	203.53
Z:	6.00
RIR:	-

Subfiles and Quality

Subfiles:	Inorganic
	Mineral
	Alloy, metal or intermetalic
	Corrosion
	Common Phase
	Educational pattern
	Forensic
	NBS pattern
	Superconducting Material
Quality:	Star (S)

Comments

Color:	Dark blue
General comments:	Opaque mineral optical data on specimen from unspecified locality: R_1R_o=7.1, RR_2R_e=23.7, Disp.=16, VHN_{100}=128-138, Color Values=o .224, .226, 6.8, e .283, .287, 23.5, Ref.: IMA Commission Ore Microscopy QDF. Measured density and color from *Dana's System of Mineralogy, 7th Ed.*, **I**.
Sample source:	Sample from Fisher Scientific Company.
Sample preparation:	Annealed at 400 °C for several hours in sulfur atmosphere.

Analysis:	Spectroscopic analysis: <0.1% Si, Zn; <0.01% Ag, Al, Ca, Fe, Mg, Ni; <0.001% B, Mn, Pb.
Optical data:	B = 1.45, Sign = +
Additional pattern:	To replace 1-1281, 3-724 and 3-1090 and validated by calculated pattern 24-60. See ICSD 24586 and 36155 (PDF 76-1725); See ICSD 63327 (PDF 78-2121).
Temperature:	Pattern taken at 26 C.

References

Primary reference: *Natl. Bur. Stand. (U.S.), Circ. 539*, **IV**, 13, (1955)

Peak list

No.	h	k	l	d [A]	I [%]
1	0	0	2	8.18000	8.0
2	1	0	0	3.28500	14.0
3	1	0	1	3.22000	30.0
4	1	0	2	3.04800	65.0
5	1	0	3	2.81300	100.0
6	0	0	6	2.72400	55.0
7	1	0	5	2.31700	10.0
8	1	0	6	2.09700	6.0
9	0	0	8	2.04300	8.0
10	1	0	7	1.90200	25.0
11	1	1	0	1.89600	75.0

12	1	0	8	1.73500	35.0
13	2	0	1	1.63400	4.0
14	2	0	2	1.60900	8.0
15	2	0	3	1.57200	16.0
16	1	1	6	1.55600	35.0
17	1	0	10	1.46300	6.0
18	1	1	8	1.39000	6.0
19	1	0	11	1.35400	8.0
20	2	0	7	1.34300	6.0
21	2	0	8	1.28000	10.0
22	2	1	2	1.22700	6.0
23	2	1	3	1.21000	10.0
24	1	0	14	1.09980	8.0
25	3	0	0	1.09460	10.0
26	2	1	8	1.06070	10.0
27	3	0	6	1.01550	8.0

Stick Pattern

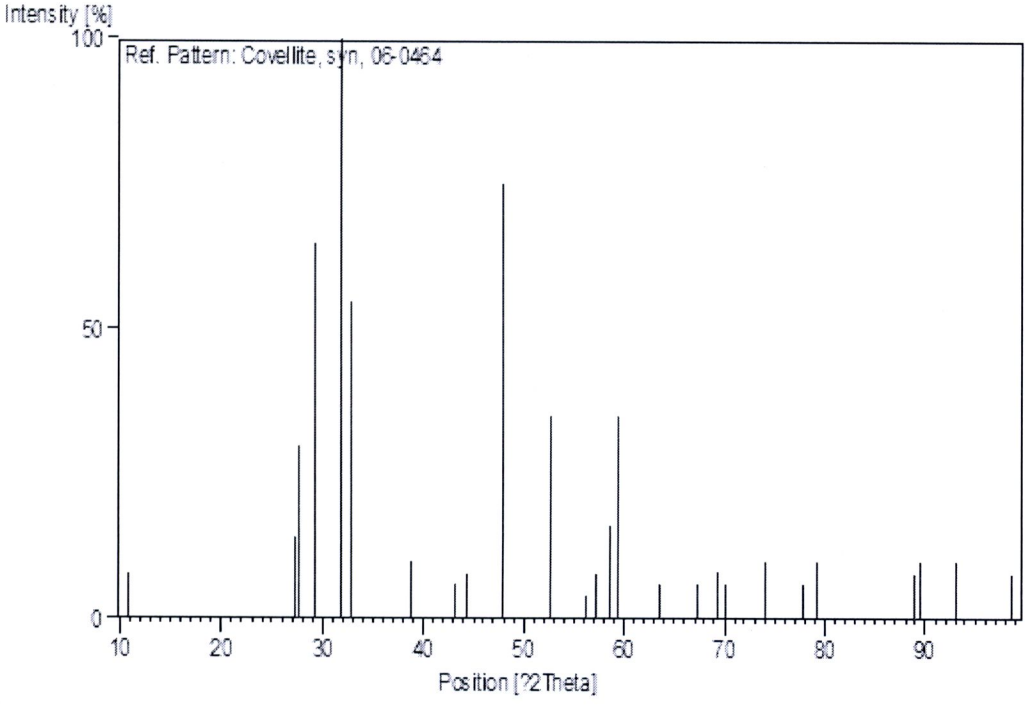

APPENDIX B

Camera constants used for the indexing of SAED pattern

Camera constants (Lλ) at 200 kV

(cm)	D111Au (mm)	R111Au (mm)	D111Auv (A)	Lλ (mm.A)
40	8.70	4.35	2.355	10.2442
60	13.2	6.60	2.355	15.5430
80	17.2	8.60	2.355	20.2530
100	21.2	10.60	2.355	24.9630
120	25.2	12.60	2.355	29.6730
150	31.5	15.75	2.355	37.0912
200	41.5	20.75	2.355	48.8662
250	51.8	25.90	2.355	60.9945

APPENDIX C

Properties and structures of polymers used in present research

1. Polyethylene glycol (PEG) [140]

PEG is a polyether compound with many applications from industrial manufacturing to medicine. It has also been known as polyethylene oxide (PEO) or polyoxyethylene (POE), depending on its molecular weight, and under the tradename Carbowax.

Structure	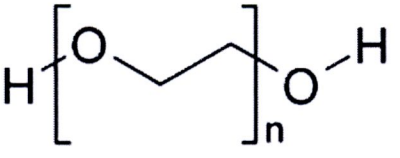
IUPAC name	Poly(oxyethylene) {structure-based} Poly(ethylene oxide) {source-based}
Other names	Carbowax, GoLYTELY, GlycoLax, Fortrans, TriLyte, Colyte, Halflytely, Macrogol, MiraLAX, MoviPrep
Molecular formular	$C_{2n}H_{4n+2}O_{n+1}$
Molar mass	Variable
Flash point	182-287 °C

2. Polyvinyl alcohol (PVA) [141]

PVA is a water-soluble synthetic polymer which has excellent film forming, emulsifying and adhesive properties. It is also resistant to oil, grease and solvent. It is odorless and nontoxic. It has high tensile strength and flexibility, as well as high oxygen and aroma barrier properties. However these properties are dependent on humidity, in other words, with higher humidity more water is absorbed. The water, which acts as a plasticiser, will then reduce its tensile strength, but increase its elongation and tear strength. PVA is fully degradable and dissolves quickly. PVA has a melting point of 230°C and 180–190°C(356-374 degrees Fahrenheit) for the fully hydrolysed and partially hydrolysed grades, respectively. It decomposes rapidly above 200°C as it can undergo pyrolysis at high temperatures.

Structure	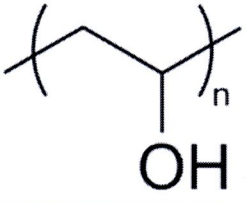
Other names	PVOH; Poly(Ethenol), Ethenol, homopolymer; PVA; Polyviol; Vinol; Alvyl; Alkotex; Covol; Gelvatol; Lemol; Mowiol
Molecular formular	$(C_2H_4O)_x$
Density	1.19-1.31 g/cm^3
Melting point	230 °C
Molar mass	Variable
Flash point	79.44 °C

3. Polyvinylpyrrolidone (PVP) [142]

PVP is soluble in water and other polar solvents. When dry it is a light flaky powder, which readily absorbs up to 40% of its weight in atmospheric water. In solution, it has excellent wetting properties and readily forms films. This makes it good as a coating or an additive to coatings. PVP is a branched polymer, that is its structure is more complicated than linear polymer but it too is in a two-dimensional plane. The structure of a polymer greatly depends on its integrity and strength, formed through cross-links and bonds. A single polymer molecule may consist of hundreds to a million monomers and may have a linear, branched, or network structure. Covalent bonds hold the atoms in the polymer molecules together and secondary bonds then hold groups of polymer chains together to form the polymeric material. Copolymers are polymers composed of two or more different types of monomers.

Structure	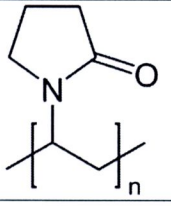
IUPAC name	Polyvinylpyrrolidone
Other names	PVP, Povidone, Polyvidone Poly[1-(2-oxo-1-pyrrolidinyl)ethylen] 1-Ethenyl-2-pyrrolidon homopolymer 1-Vinyl-2-pyrrolidinon-Polymere Copovidone
Molecular formular	$(C_6H_9NO)_n$
Density	1.2 g/cm^3
Melting point	150-180 °C
Molar mass	Variable

4. Hydroxyethyl cellulose (HEC) [143]

HEC is a gelling and thickening agent derived from cellulose. It is widely used in cosmetics, cleaning solutions, and other household products. Hydroxyethyl cellulose and methyl cellulose are frequently used with hydrophobic drugs in capsule formulations, to improve the drugs' dissolution in the gastrointestinal fluids.

Structure	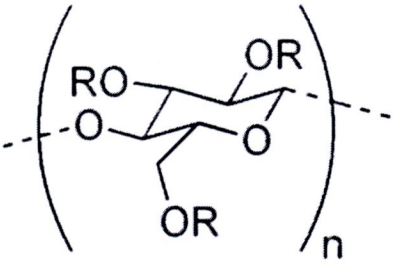 R = H or CH_2CH_2OH
Other names	Cellulose, hydroxyethyl ether; hydroxyethylcellulose; 2-hydroxyethyl cellulose
Molecular formular	Variable
Melting point	140 °C
Molar mass	Variable

CURRICULUM VITAE

Name Mr. Chalermchai Pilapong

Date of birth December 4, 1984

Education

2007 B.Sc (Chemistry, 1st honor) Naresuan University, Thailand

2011 Ph.D. (Chemistry) Chiang Mai University, Thailand

Experiences

1. Teaching Assistance at Department of Chemistry, Faculty of Science, Chiang Mai University
2. Visiting researcher at the School of Chemistry, University of Leeds at the United Kingdom during September, 2010- August, 2011

Publications and patent

1. T. Thongtem, S. Jattukul, C. Pilapong and S. Thongtem, *Current Applied Physics*, Available online 2011 (IF = 1.74)
2. T. Thongtem, C. Pilapong, J. kavinchan, A. Phuruangrat and S. Thongtem, *Journal of Alloys and compounds*, 2010, 500, 195-199 (IF=2.135)
3. C. Pilapong, T. Thongtem and S. Thongtem, *Journal of Alloys and compounds*, 2010, 507, L38-L42 (IF=2.135)
4. T. Thongtem, C. Pilapong and S. Thongtem, *Journal of Alloys and compounds*, 2010, 496, 29-32 (IF=2.135)

5. T. Thongtem, C. Pilapong and S. Thongtem, *Material Letter*, 2010, 64, 111-114 (IF=2.12)
6. T. Thongtem, C. Pilapong and S.Thongtem, *Transactions of Nonferrous Metals Society of China*, 2009, 19, 105-109 (IF=0.676)
7. C. Pilapong, T. Thongtem and S. Thongtem, *Journal of Physics and Chemistry of Solids,* 2009, 71, 712-715 (IF=1.38)
8. T. Thongtem, C. Pilapong and S. Thongtem, *Current Applied Physics*, 2009, 9, 1272-1277 (IF=1.74)

International conferences

1. **Poster presentation** , C. Pilapong, T. Thongtem, D. Zhou, A Simple, Ultrasensitive, Label-free DNA Assay Using Enzyme-Magnetic Nanoparticle Probes , 2011 Northern Region Dalton Division Meeting, 29 June 2011, Sheffield, UK

2. **Poster presentation,** Chaned Wichasilp, Somchai Thongtem, Chalermchai Pilapong, Titipun Thongtem, Effect of polymer- p-type semiconductor nanocomposited electrolyte on the photovoltaic performance of a solid-state dye-sensitized solar cell, ISEPD 2011,8-11 Jan 2011, ChiangMai, Thailand

3. **Poster presentation**, Fabrication of a novel $ZnS/ZnAl_2S_4$ nanocomposite using a facile solvothermal route, The 3rd IEEE International Nanoelectronic Conference, January 3-8, 2010, City University of Hong Kong, China.

4. **Poster presentation**, Large-scale synthesis of Sb_2S_3 spikes by hydrothermal reaction, The 3rd IEEE International Nanoelectronic Conference, January 3-8, 2010, City University of Hong Kong, China.

5. **Poster presentation**, Characterization of MFe_2O_4 (M=Mn, Ni, Cu and Zn) nanoparticles produced using microwave-hydrothermal method, The 3rd International Symposium on Functional Materials.(ISFM2009), June 15-18, 2009, Jinju, Korea

6. **Oral presentation**, Large scale synthesis of CuS nano-hexaplate using the mixed solvent solvothermal method, The 3rd International Symposium on Functional Materials.(ISFM2009), June 15-18, 2009, Jinju, Korea

7. **Poster presentation**, Characterization of flower-like Bi_2S_3 nanostructure synthesized via hydrothermal route, The 15th International Symposium on Intercalation Compounds (ISIC15), May 10-14, 2009, Beijing, China

8. **Oral presentation**, Characterization of CdS Nanorods Synthesized by a Hydroxyethyl Cellulose - Assisted Solvothermal Method, PERCH-CIC Congress VI, May 3-6, 2008, pattaya, Thailand

9. **Poster presentation**, Characterization of MS (M = Cd, Cu, Zn) producted by the 200 °C solvothermal reaction, The 1st International Symposium on Hybrid Materials and Processing. (HyMaP 2008), October 27-29, 2008, Busan, Korea

Scholarships

2010 - 2011	The National Research Council of Thailand
2008 - 2011	Strategic Scholarships for Frontier Research Network for the Join Ph.D. program Thai Doctoral degree from the Commission on Higher Education, Thailand
2007 - 2008	The Center for Innovation in Chemistry (PERCH- CIC)

INTERNATIONAL PUBLICATIONS

Current Applied Physics 9 (2009) 1272–1277

Contents lists available at ScienceDirect

Current Applied Physics

journal homepage: www.elsevier.com/locate/cap

Solvothermal synthesis of CdS nanorods using hydroxyethyl cellulose as a template

Titipun Thongtem [a,*], Chalermchai Pilapong [a], Somchai Thongtem [b]

[a] Department of Chemistry and Center for Innovation in Chemistry, Faculty of Science, Chiang Mai University, 239 Huay Kaew Road, Suthep District, Amphur Muang, Chiang Mai 50200, Thailand
[b] Department of Physics and Materials Science, Faculty of Science, Chiang Mai University, Chiang Mai 50200, Thailand

ARTICLE INFO

Article history:
Received 14 April 2008
Received in revised form 12 February 2009
Accepted 17 February 2009
Available online 26 February 2009

PACS:
81.07.b
81.07.Bc
81.16.Be

Keywords:
CdS nanorods
Solvothermal synthesis
Ethylenediamine
Hydroxyethyl cellulose

ABSTRACT

CdS nanorods were solvothermally produced from $Cd(CH_3COO)_2$ and S powder using ethylenediamine (en) as a solvent and hydroxyethyl cellulose (HEC) as a template. The phase with hexagonal structure was detected using XRD and SAED, which is in perfect accordance with the results obtained by simulation. SEM, TEM and HRTEM revealed the development of nanorods with a number of atoms arranged in crystal lattices. When the appropriate amount of HEC was used, the longest nanorods, with preferential growth in the [001] direction, were produced. Raman spectra showed the fundamental and overtone modes at the same wavenumbers of 301 and 599 cm^{-1}, respectively. Their relative intensities at each temperature were strongly influenced by the anisotropic geometry of the products. Photoluminescence caused by electron–hole recombination was detected at 470 nm and by surface trapping induced emission at 575 nm. The formation mechanism of CdS nanorods was also proposed based on the experimental results.

1. Introduction

CdS is one of the II–VI semiconducting materials having a 2.42-eV band gap at room temperature [1,2]. It has a wide variety of applications, such as laser light-emitting diodes [3], solar cells [4] and optoelectronic devices [4]. There are different methods used to produce this material, such as sonochemistry-assisted microwave synthesis [5], solvothermal reaction [1,4,6,7], and hydrothermal process [3]. The products may have different morphologies, which influence their luminescence properties. Among these morphologies are nanowires [1,4], nanorods [3,6,7], and hexagonal and triangular plates [7,8]. Ethylenediamine functions as a solvent and ligand [3]; but this produces nanorods with irregular morphology and low aspect ratio [3,4,6]. The ratio is better when PVA is added [4]. Some polymers such as PAA, PAN, PVP and PVA can be used to modify the surface chemistry of the crystals and the concentration of soluble species for crystal growing [6]. This improves the uniformity in the length and diameter of CdS nanowires [6,9]. The purpose of the present research was to solvothermally produce CdS nanorods templated by hydroxyethyl cellulose (HEC) in ethylenediamine (en). HEC is water-soluble and easy to wash off. Therefore, it has advantages for use as a templating polymer. HEC is a non-ionic polymer which contributes to the stabilization of ion concentrations [9]. It is inexpensive and easily obtainable.

2. Experiment

Different amounts (0.00, 0.25, 0.50, 0.75 and 1.00 g) of hydroxyethyl cellulose (HEC) were mixed with 0.005 mol $Cd(CH_3COO)_2$ in 50 ml de-ionized water. Each mixture was stirred at 80 °C to form a gel, which was subsequently dissolved in 30 ml ethylenediamine (en), a bidentate ligand. Another 30 ml ethylenediamine dissolved with 0.005 mol sulfur powder was prepared, and mixed with the first en solutions. Reactions proceeded in home-made stainless steel autoclaves at temperatures of 100, 120, 140, 160, 180 and 200 °C for 24 and 72 h. The precipitates were washed with distilled water and ethanol, and dried at 80 °C for 24 h. They were then characterized using: X-ray diffraction (XRD) operated at 20 kV, 15 mA and using the $K\alpha$ line from a Cu target; transmission electron microscopy (TEM), high resolution transmission electron microscopy (HRTEM) and selected area electron diffraction (SAED) operated at 200 kV; scanning electron microscopy (SEM) operated at 15 kV; a Raman spectrometer using a 50 mW Ar laser with a 514.5 nm wavelength; and a luminescence spectrometer using a 210 nm excitation wavelength (λ_{ex}). Diffraction patterns were also simulated using CaRine Crystallography 3.1 software [10], and compared with those obtained from the experimental results.

* Corresponding author. Tel.: +66 (0) 53 943341–45; fax: +66 (0) 53 892277.
E-mail addresses: ttpthongtem@yahoo.com, ttpthongtem@hotmail.com (T. Thongtem).

1567-1739/$ - see front matter © 2009 Elsevier B.V. All rights reserved.
doi:10.1016/j.cap.2009.02.010

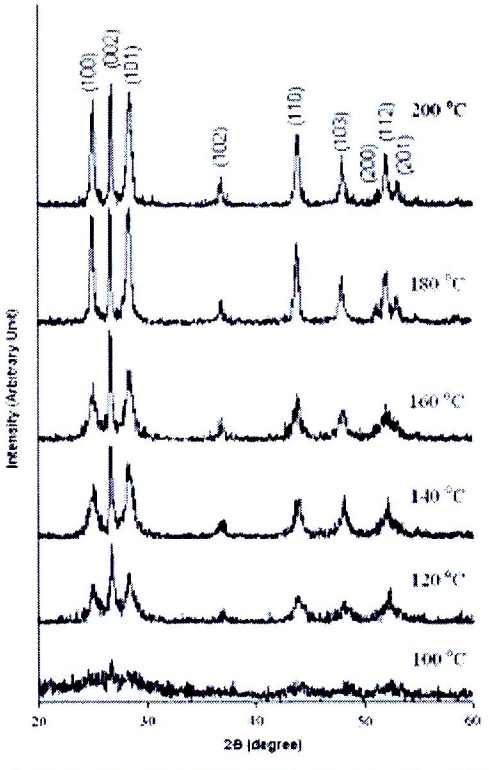

Fig. 1. XRD spectra of the products produced using 0.25 g HEC at different temperatures for 24 h.

3. Results and discussion

3.1. XRD

XRD spectra (Fig. 1) were indexed using Bragg's law of diffraction, and compared with that of the JCPDS software (reference code: 41-1049) [11]. The products produced at different temperatures were identified as CdS (hcp) with $P6_3mc$ space group. At 100 °C and 24 h solvothermal reaction, the spectrum is broad, showing that the product was composed of a number of nanoparticles. At higher solvothermal temperatures, the spectra became sharper and narrower, and the intensities were stronger. The degree of crystallinity continuously increased with an increase in solvothermal temperatures. Crystallite sizes were also enlarged. At 100 °C, the (002) peak was the most dominant, relative to those of the (100) and (101). High crystalline ordering nucleated along the *c*-axis, and the atom ordering in the *x*–*y* planes was at random [12]. It became less dominant at higher temperatures. The (100) and (101) peaks increased at faster rates than the (002) peak. Product crystallinity in the *x*–*y* planes developed along with the preferred orientation in the *c*-axis [12]. The I_{002}/I_{100} and I_{002}/I_{101} intensity ratios are the specification of the preferential growth along the *c*-axis. Two peaks diffracting from the (102) and (103) planes of the nanocrystals at 2θ of 36.52 and 47.84 ° are the characteristics of hcp phase [13]. Calculated lattice parameters for hcp structure [14] are $a = b = 0.413$ nm and $c = 0.669$ nm, which are in accordance with those of the JCPDS software [11]. The present research detected no other characteristic peaks of impurities, showing that the products are pure phase. When the times were prolonged and the amount of HEC was greater (results not shown), CdS (hcp) phase was also detected, as in the above characterization.

3.2. Raman analysis

Raman spectra (Fig. 2a) are very similar to each other although the products were produced at different temperatures. Two main peaks were detected. They corresponded to the first and second

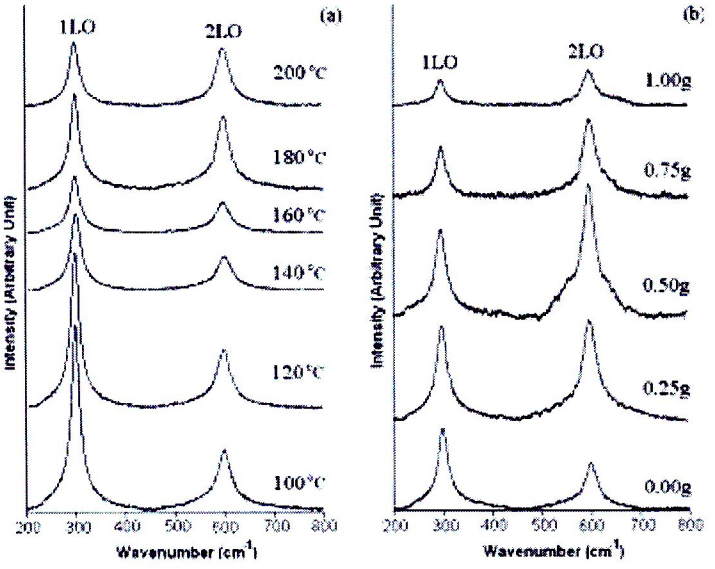

Fig. 2. Raman spectra of CdS produced using (a) 0.25 g HEC at different temperatures for 24 h and (b) different amounts of HEC at 200 °C for 72 h.

longitudinal optical (LO) phonon modes, which are polarized in the x–z face with strong coupling to the excitons along the c-axis [15]. The strong 1LO and weak 2LO modes corresponding to the fundamental and overtone wavenumbers [15,16] were detected at 301 and 599 cm^{-1}, respectively. This is in accordance with previous results obtained by other researchers [17]. Intensity ratios of 2LO/1LO at temperatures of 100, 120, 140, 160, 180 and 200 °C are 0.30, 0.35, 0.42, 0.53, 0.74 and 0.89, respectively. They increased with an increase in the solvothermal temperatures. Their relative intensities were strongly influenced by the anisotropic geometry of the products. As the crystallite sizes increased, the 1LO peaks were weaker and the 2LO peaks became stronger in intensity [12]. Coupling of the 1s–1s state to the LO phonon decreased with the decrease in the quantum crystallite sizes [16]. This was influenced by the lifetime of the 1s–1s state [15]. The 2LO/1LO ratios were the parameters used to specify the strength of the electron–phonon interaction [12]. The two peaks were also detected at the same wavenumbers although HEC was added and its amount was increased (Fig. 2b). The 2LO/1LO ratios became 0.55, 1.01, 1.64, 1.48 and 1.35 for the use of 0.00, 0.25, 0.50, 0.75 and 1.00 g HEC in the process. The ratio is the highest for 0.50 g HEC. Defects of the products can play roles in the spectra as well.

3.3. SEM

SEM images (Fig. 3) show surface morphologies of the products that were produced using a variety of solvothermal temperatures, lengths of time, and amounts of HEC. At 100 °C, 24 h and 0.25 g HEC (Fig. 3a), the product was composed of a number of nanoparticles in clusters. When the temperature was increased to 200 °C (Fig. 3b), a number of nanorods with different orientations were detected. Their axial lengths were rather short. At 200 °C, 72 h and 0.25 g HEC (Fig. 3c), the nanorods were of greater length than the former product. When the amount of HEC was increased, the nanorods became even longer. They were the longest at 0.50 g HEC (Fig. 3d). Close examination of the product showed the elongated nanorods (Fig. 3e) to be perfect, with no defects detected. The nanorods became shorter using 0.75 and 1.00 g HEC (Fig. 3f and g). When less than 0.50 g of HEC was used, it was able to partially adsorb onto the nanorods and cause incomplete capping. But with excess HEC (more than 0.50 g), shorter nanorods were produced due to surplus capping. Hence, their axial growth was limited [5]. Some nanorods were in straight lines and some were bent, depending on the stress developed inside. For each condition, a number of different diameters

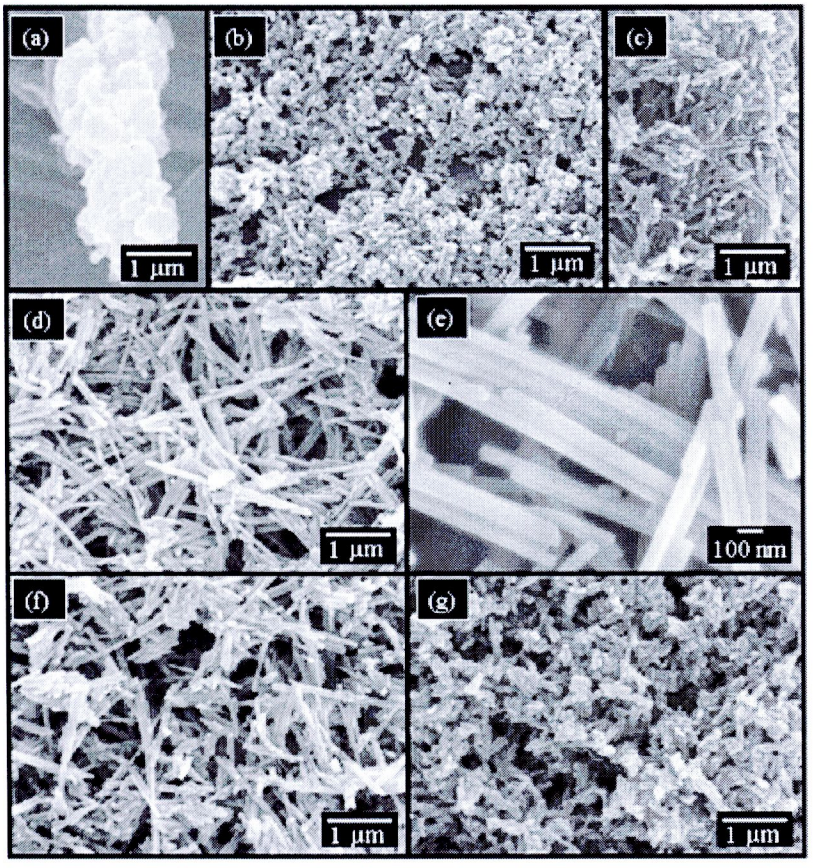

Fig. 3. SEM images of CdS products using (a) 100 °C, 24 h, 0.25 g HEC; (b) 200 °C, 24 h, 0.25 g HEC; (c) 200 °C, 72 h, 0.25 g HEC; (d and e) 200 °C, 72 h, 0.50 g HEC; (f) 200 °C, 72 h, 0.75 g HEC and (g) 200 °C, 72 h, 1.00 g HEC.

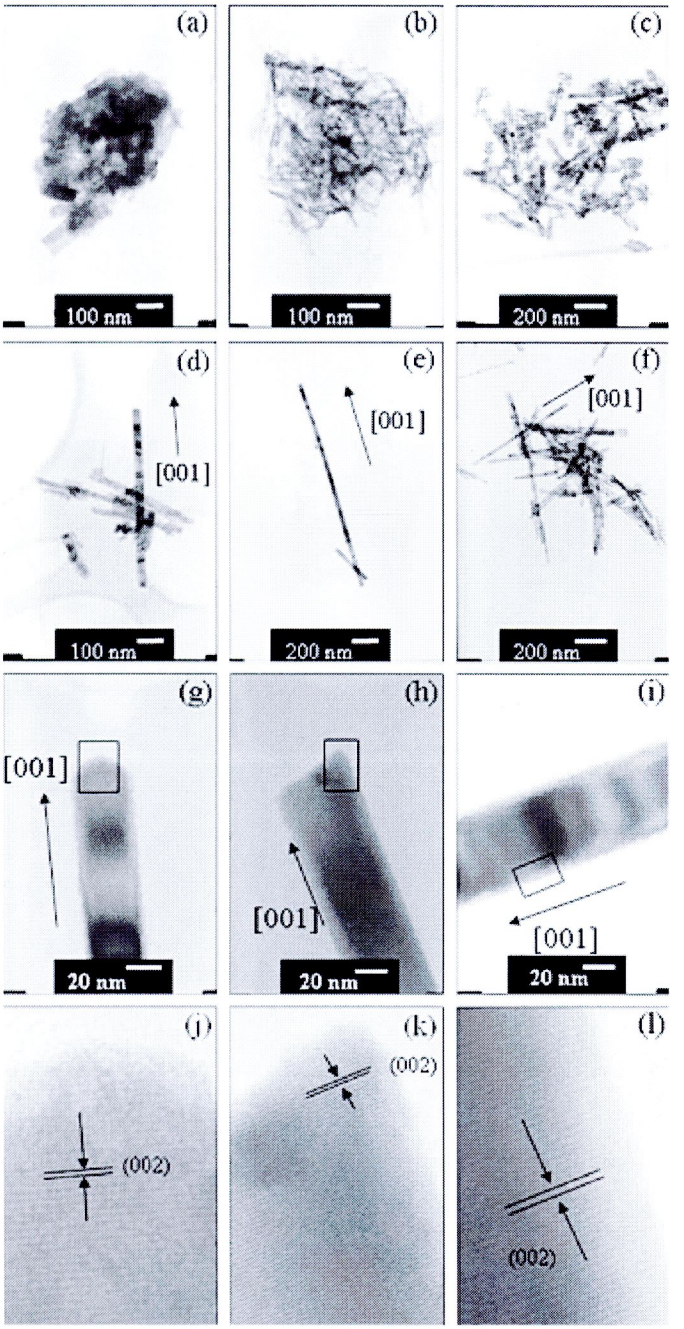

Fig. 4. TEM and HRTEM images of CdS produced using (a) 200 °C 72 h, 0.00 g HEC; (b) 100 °C 24 h, 0.05 g HEC; (c) 200 °C 24 h, 0.25 g HEC; (d, g and j) 200 °C 72 h, 0.25 g HEC; (e, h and k) 200 °C 72 h, 0.50 g HEC and (f, i and l) 200 °C 72 h, 0.75 g HEC.

and axial lengths of the nanorods were detected. This indicated that they nucleated at various times. Their growth rates were probably different as well.

3.4. TEM and HRTEM

TEM and HRTEM images (Fig. 4) show the morphologies of the products produced using a variety of solvothermal temperatures, lengths of time, and amounts of HEC. For HEC-free system (Fig. 4a), the product was very fine nanoparticles in clusters although the temperature was as high as 200 °C and the time was as long as 72 h. At 100 °C, 24 h and 0.25 g HEC (Fig. 4b), the product was composed of a number of nanorods aligned in different directions; but the SEM image in Fig. 3a shows the characteristics of nanoparticles in clusters. This disparity was caused by differences in magnification. The results show that HEC can play a role in templating the nanorods. When the temperature was increased to 200 °C (Fig. 4c) and the time prolonged to 72 h (Fig. 4d), the nanorods became longer. To produce still longer nanorods, more HEC was required. Their lengths were increased to the longest value of 1.570 nm for 200 °C, 72 h and 0.50 g HEC (Fig. 4e), and decreased with the use of excess HEC (Fig. 4f). High magnification TEM images (Fig. 4g–i) show that the nanorods grew in the [001] direction although they were produced at different conditions. Close examination of the products revealed some defects contained in the nanorods as well. HRTEM images (Fig. 4j–l) at the squares of the corresponding images of Fig. 4g–i show a number of the (002) planes aligning in systematic arrays. These show lattice atoms aligning in their crystal lattices. Their growth in the [001] direction is normal to the (002) planes. Each of them grew in the [001] direction (Fig. 4c–f). Growth direction of the nanorods is in accordance with the previous description of the XRD results.

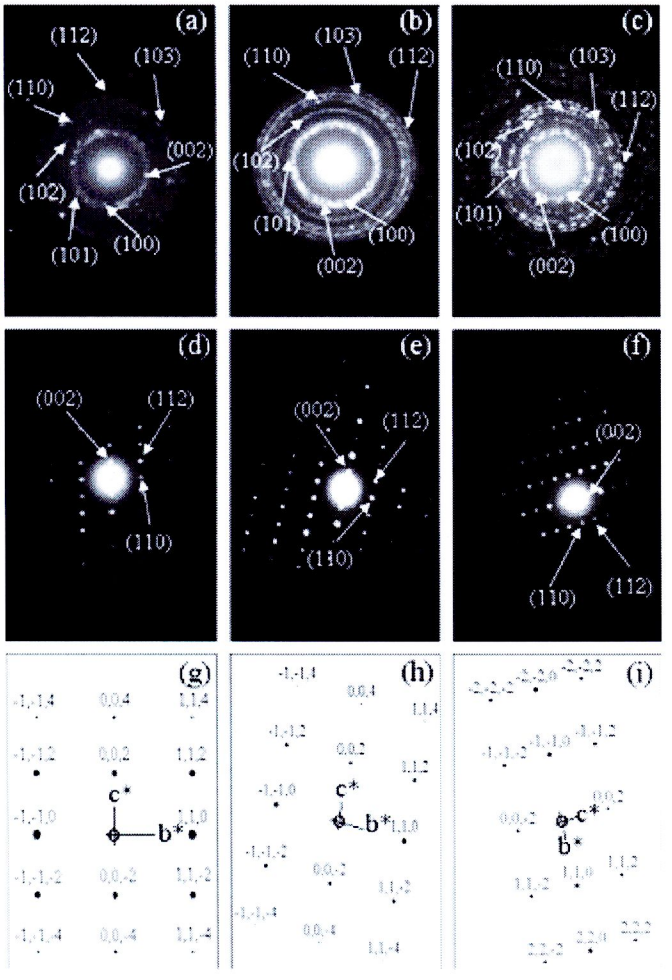

Fig. 5. PXRD and simulated patterns of ZnS produced using (a) 200 °C, 72 h, 0.00 g HEC; (b) 100 °C, 24 h, 0.25 g HEC; (c) 200 °C, 24 h, 0.25 g HEC; (d and g) 200 °C, 72 h, 0.25 g HEC; (e and h) 200 °C, 72 h, 0.50 g HEC and (f and i) 200 °C, 72 h, 0.75 g HEC.

3.5. SAED and simulation

SAED patterns (Fig. 5a–c) of the nanorods in Fig. 4a–c show bright concentric rings corresponding to their diffraction planes. The rings are diffuse and hollow showing that the products were composed of a number of nanosized particles. Diameters of the rings were measured from the diffraction patterns on the films. The interplanar spaces of the diffraction planes were calculated [16] and compared with those of the JCPDS software [11]. The patterns correspond to CdS (hcp). Other SAED patterns (Fig. 5d–f) at the squares of the corresponding images of Fig. 4g–i appear as symmetric and systematic arrays of bright spots, showing that a number of atoms were arranged in crystal lattices. The patterns were interpreted [7,19] and specified as CdS (hcp) [11]. Calculated electron beams [7,19] are in the same direction of $[\bar{1}10]$, the direction that the electron beams were sent to the crystal facets. Diffraction patterns with a $[\bar{1}10]$ zone axis were simulated (Fig. 5g–i) [10]. The simulated spots in the specified crystallographic planes are in systematic and symmetric arrays. The interpreted and simulated patterns are thus in good accordance. The a^*, b^* and c^* lattice vectors are in the [100], [010] and [001] directions, respectively. For the crystal structure, the corresponding lattice vectors are the same although the products were produced under different conditions.

3.6. Proposed mechanism

To produce CdS nanorods, $Cd(CH_3COO)_2$ + HEC gel reacted with ethylenediamine (en), a strongly bidentate ligand, to form $[Cd(en)_n]^{2+}$ complex ions. At the same time, S powder was reduced by ethylenediamine to form S^{2-} ions. $[Cd(en)_n]^{2+}$ and S^{2-} ions were mixed and further reacted in home-made stainless steel autoclaves at different temperatures, lengths of time, and amounts of HEC. Finally, CdS (hcp) was produced. The CdS nuclei that formed were not fully developed (nascent). Initially, HEC adsorbed onto the side walls of the nuclei, which caused termination of lateral growth. Their tips were uncovered, axial growth proceeded very rapidly. As seen using TEM and HRTEM, growth in the x and y directions was limited. The nuclei grew in the z or [001] direction via the diffusion process. Hence, CdS nanorods were produced. These CdS nanorods grew in the same direction as those prepared by other researchers [8]. To form the longest nanorods, the appropriate amount of HEC was used. The details are explained in the above section. The present research shows that HEC played an important role in one dimensional growth of CdS nanorods in the stainless steel autoclaves. HEC concentrations have a strong influence in templating and limiting the axial lengths of the nanorods.

3.7. Photoluminescence

Photoluminescent (PL) spectra (Fig. 6) were analyzed using 210 nm excitation wavelength (λ_{ex}). Two distinct emissions were detected at approximately 470 and 575 nm, which are very close to results previously reported [8]. Some energy was lost during the characterization, and the emission of longer wavelengths than λ_{ex} was detected. The first peaks were caused by the electron-hole recombination, and the second by surface trapping induced emission [8]. The use of 0.50 g HEC resulted in the strongest intensity of the recombination band. The intensity of the surface trapping induced emission band was between those of the 1.00 g HEC and the HEC-free system. The lesser intensity of the HEC-free product was caused by non-capping. But for excess HEC, the stronger surface emission was caused by surplus capping [8]. The present results thus show that HEC dosages have an influence on the PL emissions of the products. The use of 0.50 g HEC was the appropriate amount to produce the longest nanorods with the strongest recombination intensity. Compared to the 515 nm wavelength of bulk CdS (hcp) [9], the 470 nm wavelength of the current nanorods is blue-shifted due to the quantum size effect [1,8]. The extent of blue-shift increased with a decrease in particle sizes or an increase in the surface-to-volume ratios.

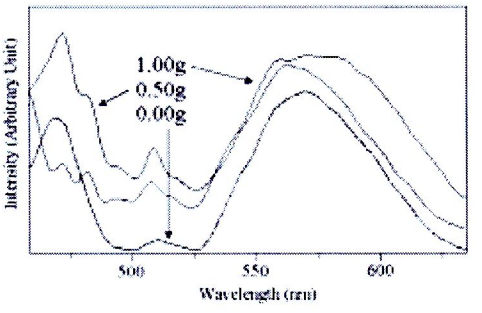

Fig. 6. PL spectra of CdS produced using different HEC dosages at 200 °C for 24 h.

4. Conclusions

CdS nanorods were successfully produced by 100–200 °C solvothermal reactions in ethylenediamine containing different amount of HEC. The hcp phase was detected using XRD and SAED. Diffraction models were also simulated and are in accordance with the interpreted patterns. SEM, TEM and HRTEM revealed the presence of nanorods composed of atoms in a lattice array. A mechanism was also proposed according to the analytical results. Two main peaks of Raman spectra were detected at 301 and 599 cm^{-1}, which were, respectively, specified as the fundamental and overtone modes. There were two distinct emission peaks at approximately 470 and 575 nm, although the products were produced under different conditions.

Acknowledgements

We are extremely grateful to the Thailand Research Fund (TRF), NANOTEC, a member of NSTDA, Ministry of Science and Technology, Thailand, and Center for Innovation in Chemistry (PERCH-CIC), Commission on Higher Education (CHE), Ministry of Education, for financial support.

References

[1] X. Cuo-yue, W. Han, C. Chuan-wei, Z. Hai-qian, C. Je-ming, J. Guang-bin, Trans. Nonferrous Met. Soc. China 16 (2006) 105–109.
[2] X.F. Shen, A.H. Yuan, F. Wang, JM. Hong, Z. Xu, Solid State Commun. 133 (2005) 19–22.
[3] Q. Zhao, L. Hou, R. Huang, S. Li, Inorg. Chem. Commun. 6 (2003) 1459–1462.
[4] J. Yao, C. Zhao, D. Wang, G. Han, Mater. Lett. 59 (2005) 3652–3655.
[5] C. Tai, W. Cao, Ultrason. Sonochem. 13 (2006) 350–356.
[6] H. Wang, P. Fang, Z. Chen, S. Wang, J. Alloys Compd. 461 (2008) 418–422.
[7] T. Thongtem, A. Phuruangrat, S. Thongtem, Mater. Lett. 61 (2007) 3235–3238.
[8] M. Chen, L. Pan, J. Cao, H. Li, C. Ji, X. Ma, Y. Zheng, Mater. Lett. 60 (2006) 3842–3845.
[9] W. Qingqing, X. Gang, H. Caorong, J. Solid State Chem. 178 (2005) 2880–2885.
[10] E. Boudias, D. Monceau, CaRIne Crystallography 3.1, 17 rue du Moulin du Roy, F-60300 Senlis, France, 1989–1998.
[11] Powder Diffraction File, JCPDS International Centre for Diffraction Data, PA 19073-3273, USA, 2001.
[12] S. Jang, D.A. Jeon, J.S. Lee, J. Phys. Chem. C 111 (2007) 13280–13287.
[13] V. Sivasubramanian, A.K. Arora, M. Premila, C.S. Sundar, V.S. Sastry, Physica E 31 (2006) 93–98.
[14] C. Suryanarayana, M.G. Norton, X-ray Diffraction, A Practical Approach, Plenum Press, NY, 1998.
[15] A. Pan, R. Liu, Q. Yang, Y. Zhu, C. Yang, B. Zou, K. Chen, J. Phys. Chem. B 109 (2005) 24268–24272.
[16] C. Li, X. Yang, B. Yang, Y. Yan, Y. Qian, J. Cryst. Growth 291 (2006) 45–51.
[17] J. Lee, Thin Solid Films 451–452 (2004) 170–174.
[18] T. Thongtem, S. Kaowkhong, S. Thongtem, Ceram. Int. 33 (2007) 1449–1453.
[19] T. Thongtem, A. Phuruangrat, S. Thongtem, Mater. Lett. 62 (2008) 454–457.

Journal of Physics and Chemistry of Solids 71 (2010) 712–715

Contents lists available at ScienceDirect

Journal of Physics and Chemistry of Solids

journal homepage: www.elsevier.com/locate/jpcs

Polymer-assisted hydrothermal synthesis of Bi_2S_3 nanostructured flowers

Chalermchai Pilapong [a], Titipun Thongtem [a,*], Somchai Thongtem [b]

[a] Department of Chemistry, Faculty of Science, Chiang Mai University, Chiang Mai 50200, Thailand
[b] Department of Physics and Materials Science, Faculty of Science, Chiang Mai University, Chiang Mai 50200, Thailand

ARTICLE INFO

Article history:
Received 8 May 2009
Received in revised form
28 October 2009
Accepted 3 November 2009

Keywords:
A. Chalcogenides
B. Chemical synthesis
C. Electron microscopy
C. Raman spectroscopy
C. X-ray diffraction

ABSTRACT

Nanostructured Bi_2S_3 was hydrothermally produced from Bi_2O_3 and thiocarbohydrazide in acidic solutions containing PVA, PEG and PVP. By using XRD, SAED and Raman spectrometry, the products were orthorhombic Bi_2S_3 with four vibration modes at 139.6, 253.7, 310 and 968.9 cm^{-1}. The phase was also in accordance with the diffraction patterns obtained by simulation. SEM, TEM and HRTEM show that the products are clusters of nanorods produced in polymer-free solution, and nanostructured flowers of nanospears, nanorods and nanoplates in the respective PVA-, PEG- and PVP-added solutions, with their growths in the same direction of [0 0 1]. A formation mechanism was also proposed according to their phase and morphologies.

1. Introduction

Semiconducting chalcogenides are materials which have attracted a great deal of interest, due to their potential applications in IR spectroscopic, thermoelectric and optoelectronic devices [1–4]. Bi_2S_3 is one of these materials, which has been used as a lamellar structure with a 1.3 eV (2.08×10^{-19} J) direct band gap [1,4–6], and is a promising candidate for photovoltaic converters and photodiode arrays [4,5]. There have been several recent reports on hydrothermal and solvothermal productions of Bi_2S_3 semiconducting materials: Bi_2S_3 nanorods in water containing HCl [1] and tartaric acid [2]; single-crystalline Bi_2S_3 nanorods [4]; irregular and agglomerated particles and rod-shaped Bi_2S_3 crystallites in KOH-free and KOH-added solutions [5]; Bi_2S_3 nanorods using Span80 and SDS as surfactants [6]; Bi_2S_3 nanorods and nanostructured flowers in solutions containing 1–2 cm^3 HNO_3 [7]; and Bi_2S_3 flower-like patterns with well-aligned nanorods in distilled water containing L-cysteine [8]. In the present study, Bi_2S_3 clusters of nanorods and nanostructured flowers were hydrothermally produced in acidic solutions. Their shapes and sizes were influenced by different polymers with different molecular weights (MWs) dissolved in these solutions. It is effective, inexpensive, environmentally benign and appropriate for large-scale production.

2. Experiment

To produce nanostructured Bi_2S_3, 0.005 mol Bi_2O_3 and 0.010 mol thiocarbohydrazide (CH_6N_4S) were mixed in 20 cm^3 H_2O containing 1 cm^3 37% HCl. Subsequently, solutions were formed by the addition of 1 g each of 125,000 MW PVA, 20,000 MW PEG and 30,000 MW PVP. These solutions were thoroughly mixed by stirring for 0.5 h (1800 s). At this stage, the solutions became a yellow-tea color. They were further processed in homemade stainless autoclaves at varying temperatures and times. Finally, black precipitates were produced, which were separated, washed and dried, for further analysis.

3. Results and discussion

Fig. 1a shows XRD spectra of Bi_2S_3 produced by a hydrothermal method under different conditions. All XRD spectra were indexed and interpreted as orthorhombic Bi_2S_3 with the Pbnm space group, as given in JCPDS no. 17-0320 [9]. The products are pure phase, without detection of any impurities such as Bi_2O_3 and Bi. In polymer-free solutions at 100 °C (373 K) for 2 h (7200 s), XRD peaks are rather broad, specifying that lattice atoms were in a state of disorder to some degree. When only the temperature was increased to 200 °C (473 K), or when both the temperature was increased to 200 °C (473 K) and the time to 20 h (72,000 s), the spectra became narrower and sharper. This was also true for the products produced in polymer-added solutions. Lattice atoms became more completely ordered, and the products had a higher degree of crystallinity.

* Corresponding author. Tel.: +66 53 943341; fax: +66 53 892277.
E-mail addresses: tpchongtem@yahoo.com, tpchongtem@hotmail.com (T. Thongtem).

0022-3697/$ - see front matter © 2009 Elsevier Ltd. All rights reserved.
doi:10.1016/j.jpcs.2009.12.073

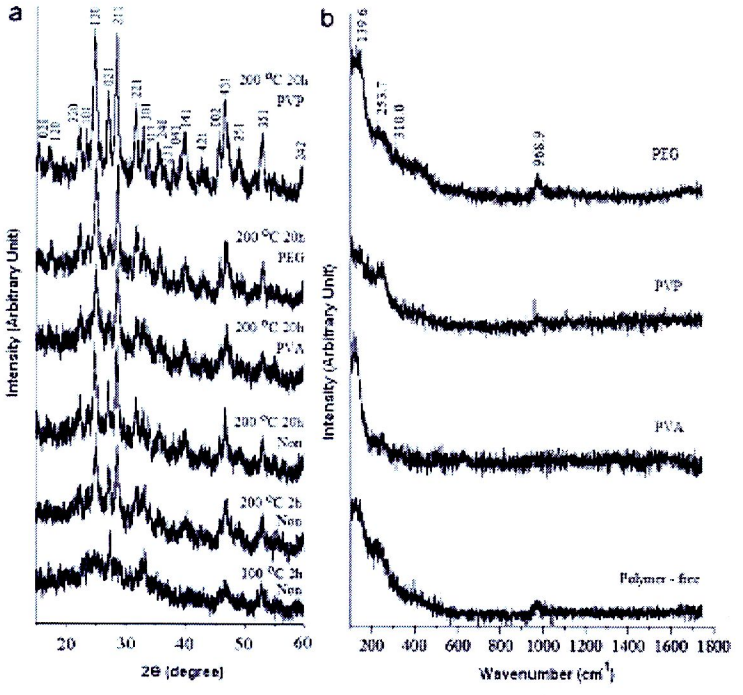

Fig. 1. (a) XRD spectra of Bi_2S_3 hydrothermally produced in polymer-free (non) and polymer-added solutions at different temperatures and times. (b) Raman spectra of Bi_2S_3 hydrothermally produced in a polymer-free solution and solutions containing one of PVA, PVP and PEG at 200 °C(473 K) for 20 h (72,000 s).

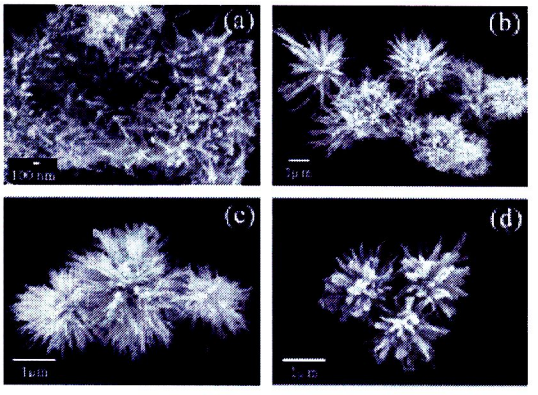

Fig. 2. SEM images of Bi_2S_3 hydrothermally produced at 200 °C(473 K) for 20 h (72,000 s): (a) polymer-free and (b–d) PVA-, PEG- and PVP-added solutions, respectively.

The definite existence of Bi_2S_3 was analyzed using a Raman spectrometer. The spectra (Fig. 1b) show four vibration modes, at 139.6, 253.7, 310 and 968.9 cm^{-1}. The first is in accordance with the 139.4 cm^{-1} mode of Bi_2S_3 nanorods, specified as the surface phonon vibration [4]. The second corresponds with the vibration mode of Bi_2S_3 nanorods at 252 cm^{-1} [4] and 259 cm^{-1} [2], and Bi_2S_3 nanoribbons and hierarchical nanostructures at 250 cm^{-1} [3,10], specified as the vibration mode of Bi–S bonds [10]. The detections of the third and fourth were in accordance with those of Bi_2S_3 nanorods at 312 and 975 cm^{-1} [2]. These detections strongly support the above XRD analysis.

SEM images show that nanostructured Bi_2S_3 was produced in different solutions. In polymer-free solution, the product (Fig. 2a) was composed of a number of nanorods in clusters. They (Fig. 2b–d) became flower-like clusters of nanospears, nanorods and nanoplates in PVA-, PEG- and PVP-added solutions, respectively. It is noteworthy that these polymers functioned as templates which controlled both the shapes and sizes of the nanocrystals. They became lengthened, as well. These microsized flowers nucleated and grew from cores, controlled by the polymers (templates). Compared to a previous report [7], Bi_2S_3 nanorods and nanostructured flowers were hydrothermally produced from $Bi(NO_3)_3 \cdot 5H_2O$ and thiourea (NH_2CSNH_2) in a solution containing a different amount of HNO_3. In order to control the product morphologies. In 1 cm^3 HNO_3 added solution, the product was Bi_2S_3 nanorods with different orientations. Nanostructured flowers, which are different from the present results, were produced when 2 cm^3 HNO_3 was used. Their morphologies were controlled by the acidity of the solutions.

Figs. 3–5 show TEM and HRTEM images, and SAED and simulated patterns of the products produced in different solutions. In polymer-free solution, the product (Fig. 3a and b) was nanorods with very smooth surfaces, and different diameters—controlled by nucleation and growth, and growing in the [001] direction. In polymer-added solutions, the products were flower-like clusters of nanospears (Fig. 4a) and nanoplates (Fig. 5a). Some stress developed inside these nanocrystals as well, such as bent nanospears (Fig. 4a–c). The analysis shows that the nanorods, nanospears and nanoplates grew in the same direction of [001] (Figs. 3a–d, 4e and 5b). Their growth direction is in

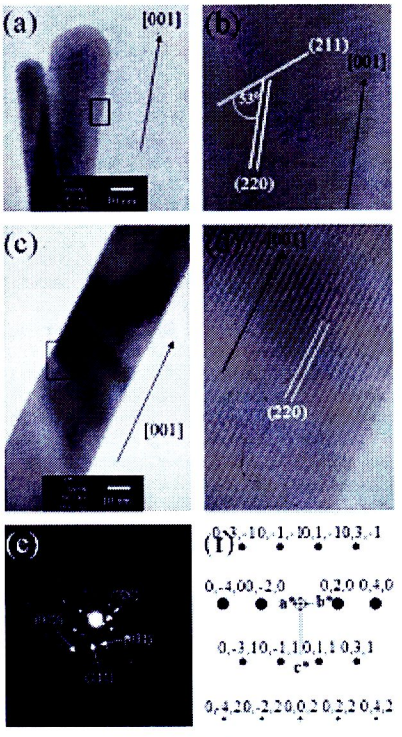

Fig. 3. TEM and HRTEM images and SAED and simulation patterns of Bi_2S_3 hydrothermally produced using 200 °C (473 K) and 20 h (72,000 s): (a and b) for polymer-free solution—(b) was enlarged from the square in (a), and (c–f) for PEG-added solution—(d) and (e) were characterized at the square in (c).

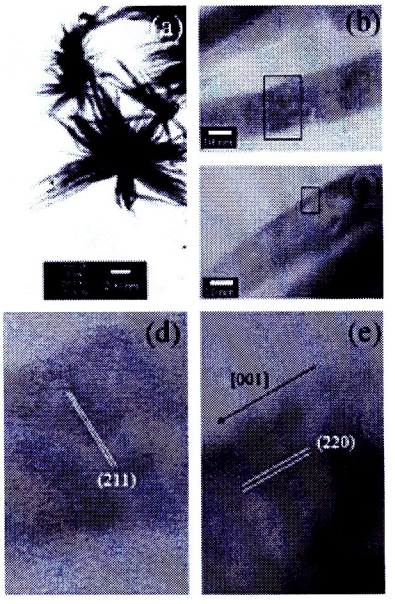

Fig. 4. TEM and HRTEM images of Bi_2S_3 hydrothermally produced in PVA-added solution at 200 °C (473 K) for 20 h (72,000 s)—(d) and (e) were enlarged from the squares in (b) and (c), respectively.

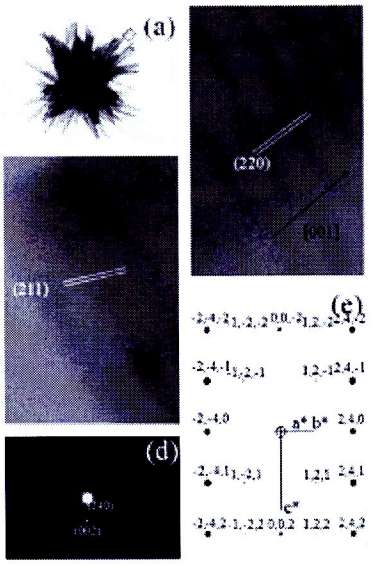

Fig. 5. TEM and HRTEM images and SAED and simulation patterns of Bi_2S_3 hydrothermally produced in PVP-added solution at 200 °C (473 K) for 20 h (72,000 s)—(b) and (d) were characterized at the square in (a), but (c) was characterized on other flower (not shown).

accordance with results characterized by other researchers [1,8,11,12]. A number of crystallographic planes composing these nanocrystals were detected. They include the (2 2 0) planes (Figs. 3b, 3d, 4e and 5b), which are parallel to the [0 0 1] direction. But the (2 1 1) planes (Figs. 3b, 4d and 5c) were at different angles to the growth direction, depending on the orientation of the corresponding nanocrystals. SAED patterns (Figs. 3e and 5d) of a nanorod and nanoplate of the microsized flowers show a single crystal of Bi_2S_3 [9] with the [1 0 0] and [2–1 0] as zone axes, respectively. Simulated diffraction patterns [13] (Figs. 3f and 5e) appear as systematic arrays of spots, corresponding to different crystallographic planes of a Bi_2S_3 [9] single crystal.

For the present research, the formation of Bi_2S_3 is proposed as follows: at room temperature, Bi_2O_3 reacted with HCl to form $BiCl_3$ [14].

$$Bi_2O_3 + 6HCl \rightarrow 2BiCl_3 + 3H_2O$$

Bi^{3+} formed complex with CH_5N_4S [14–16]; the color of the resulting solutions was that of yellow tea.

$$Bi^{3+} + 3CH_5N_4S \rightarrow [Bi(CH_5N_4S)_3]^{3+} \text{ (yellow tea)}$$

$[Bi(CH_5N_4S)_3]^{3+}$ complex hydrothermally decomposed, and Bi_2S_3 black precipitates were produced.

$$[Bi(CH_5N_4S)_3]^{3+} \rightarrow Bi_2S_3 \text{ (black)}.$$

In a polymer-free solution, Bi_2S_3 nuclei formed and grew into nanorods along the [0 0 1] direction, due to their Bi–S inherent chain type structure [1,15], which simultaneously clustered into groups. In polymer-added solutions, nuclei clustered into very tiny spheres, with a number of active sites on these spherical

surfaces at which nanocrystals (nanospears, nanorods and nanoplates) grew. Simultaneously, polymer molecules adsorbed on the side walls of these nanocrystals, of which the lateral growths were inhibited to some extent. The tips were the most active, and these nanocrystals became lengthened [5]. Their Bi–S inherent chain type structure [1,5,15] influenced the promotion of formation of the nanocrystals, growing from cores as well. Thus Bi_2S_3 nanocrystals grew out of the active sites on the spheres, and flower-like clusters were finally produced.

4. Conclusions

Nanostructured Bi_2S_3 was successfully produced by a 200 °C (473 K) 20 h (72,000 s) hydrothermal reaction. The products were orthorhombic Bi_2S_3 with four vibration modes at 139.8, 253.7, 310 and 958.9 cm^{-1}. Different products were produced: clusters of nanorods in polymer-free solution and nanostructured flowers of nanospears, nanorods and nanoplates in solutions containing PVA, PEG and PVP, respectively. Growths of these nanocrystals, produced in both polymer-free and polymer-added solutions, were in the same direction of [0 0 1].

Acknowledgements

I would like to give thank the Office of Commission on Higher Education, Thailand, for supporting this research under the Strategic Scholarships for Frontier Research Network of the Joint Ph.D. Research Program, and the National Research University Project for Chiang Mai University.

References

[1] J. Liu, Q. Han, X. Yang, L. Lu, X. Wang, Mater. Lett. 61 (2007) 3425–3428.
[2] J. Dai, S.K. Srivastava, J. Phys. Chem. C 111 (2007) 12260–12264.
[3] Y. Sun, Q. Han, J. Liu, X. Yang, L. Lu, X. Wang, Mater. Lett. 62 (2008) 3730–3732.
[4] X. Yang, X. Wang, Z. Zhang, Mater. Chem. Phys. 85 (2004) 154–157.
[5] X. Zhu, J. Ma, Y. Wang, J. Tao, S. Lin, Y. Ren, X. Jiang, J. Liu, Ceram. Int. 34 (2008) 249–251.
[6] X.Y. Ma, J. Liu, W.L. Mo, H. Liu, H.Z. Kou, Y. Wang, J. Cryst. Growth 306 (2007) 159–165.
[7] A. Phuruangrat, T. Thongtem, S. Thongtem, Mater. Lett. 63 (2009) 1485–1488.
[8] S. Zhang, X. Ye, N. Hou, Y. Zhao, Y. Xie, J. Phys. Chem. B 110 (2006) 8575–8585.
[9] Powder Diffract. File, JCPDS-ICDD, 12 Campus Boulevard, Newtown Square, PA 19073-3273, USA, (2001).
[10] Q. Han, Y. Sun, X. Wang, L. Chen, X. Yang, L. Lu, J. Alloys Comp. 481 (2009) 525–528.
[11] Z. Qian, J. Yang, P. Yang, Z. Wang, C. Li, J. Lin, Cryst. Growth Design 8 (2008) 200–207.
[12] C.J. Tang, C.Z. Wang, H.Q. Wang, Y.X. Zhang, C.H. Li, Mater. Lett. 62 (2008) 3563–3565.
[13] C. Boudias, D. Monceau, CaRIne Crystallography 3.1, DIVERGENT S.A., Centre de Transfert, 60200 Compiegne, France, (1989–1998).
[14] Y. Jiang, Y.J. Zhu, Z.L. Xu, Mater. Lett. 60 (2006) 2294–2298.
[15] J. Liu, Q. Han, X. Yang, L. Lu, X. Wang, Mater. Lett. 61 (2007) 2883–2885.
[16] R. He, X. Qian, J. Yin, Z. Zhu, J. Cryst. Growth 252 (2003) 505–510.

Journal of Alloys and Compounds 500 (2010) 195–199

Contents lists available at ScienceDirect

Journal of Alloys and Compounds

journal homepage: www.elsevier.com/locate/jallcom

Microwave-assisted hydrothermal synthesis of Bi_2S_3 nanorods in flower-shaped bundles

Titipun Thongtem[a,*], Chalermchai Pilapong[a], Jutarat Kavinchan[a], Anukorn Phuruangrat[b,*], Somchai Thongtem[b]

[a] Department of Chemistry, Faculty of Science, Chiang Mai University, Chiang Mai 50200, Thailand
[b] Department of Physics and Materials Science, Faculty of Science, Chiang Mai University, Chiang Mai 50200, Thailand

ARTICLE INFO

Article history:
Received 18 January 2010
Received in revised form 22 March 2010
Accepted 31 March 2010
Available online 8 April 2010

Keywords:
Semiconductors
Chemical synthesis
Luminescence
Scanning electron microscopy
Transmission electron microscopy
X-ray diffraction

ABSTRACT

Bi_2S_3 nanorods in flower-shaped bundles were successfully synthesized from the decomposition of Bi–thiourea complexes under the microwave-assisted hydrothermal process. X-ray powder diffraction (XRD) patterns and field emission scanning electron microscopy (FE-SEM) show that Bi_2S_3 has the orthorhombic phase and appears as nanorods in flower-shaped bundles. A transmission electron microscopic (TEM) study reveals the independent single Bi_2S_3 nanorods with their growth along the [0 0 1] direction. A possible formation mechanism of Bi_2S_3 nanorods in flower-shaped bundles is also proposed and discussed. Their UV–vis spectrum shows the absorbance at 596 nm with its direct energy band gap of 1.82 eV.

1. Introduction

In recent years, the fabrication of nanomaterials and nanodevices has been widely and deeply researched due to the novel properties comparing to their normal counterparts, and strong dependence on their characteristics such as shape, size and crystallinity [1,2]. Among them, one-dimensional (1D) nanostructures possess unique physical, chemical and electron-transport properties, different from those of bulky and isotropic materials [2–4].

Binary metal chalcogenides of $A_2^{V}X_3^{V}$ (A = As, Sb, Bi; X = S, Se, Te) semiconductors have a number of applications including photoconducting targets of television cameras, electronic and optoelectronic devices, thermoelectric devices, and infrared (IR) spectroscopy [2,4–8]. Bismuth sulfide (Bi_2S_3) has a 1.3 eV direct band gap, and is suitable for application in photovoltaic materials, photodiode arrays, sensors and IR spectroscopy photovoltaic converters, thermoelectric cooling technologies based on the Peltier effect [2,3,5,7–10]. The convention hydrothermal (CH) method has been widely used to synthesize the Bi_2S_3 nanomaterials [1–7]. It was able to control the morphologies: nanorods, nanowires, agglomerated particles and urchinlike [1–8].

Herein, an economical method to synthesize Bi_2S_3 nanorods in flower-shaped bundles by microwave-assisted hydrothermal (MH) method is reported. This method is simple, fast and inexpensive, as compared to the convention hydrothermal (CH) one.

2. Experimental procedure

The analytical grade chemicals: bismuth nitrate pentahydrate ($Bi(NO_3)_3\cdot 5H_2O$), thiourea (NH_2CSNH_2) and polyvinylpyrrolidone (PVP) were used without further purification. To synthesize Bi_2S_3 flower-like structure, 0.005 mole $Bi(NO_3)_3\cdot 5H_2O$ and 0.001 mole NH_2CSNH_2 were dissolved in 60 ml distilled water and followed by 0.5 ml 37% HNO_3 and 0.5 g PVP adding, respectively. The mixture was stirred for 30 min at room temperature and put into a 100 ml Teflon-lined autoclave, which was tightly closed, heated up to 200 °C by a 300 W microwave radiation, held at this temperature for 1 h, and then naturally cooled to room temperature. After the microwave-assisted hydrothermal process, the product was filtered, washed with distilled water and absolute ethanol for several times, and dried at 80 °C for 24 h. This process was also repeated by using the convention hydrothermal method, heated by an electric oven, at 200 °C for 24 h.

The products were analyzed using an X-ray diffractometer (D8 Advance, Bruker Ltd., Germany) with Cu Kα radiation in the 2θ range from 3° to 80°. The Raman spectra was recorded on HORIBA JOBIN YVON T64000 Raman spectrometer using 50 mW Ar laser with λ = 514.5 nm. The morphology of the product was characterized by a JEM-6335F scanning electron microscope (SEM, JEOL Ltd., Japan) and JEM-2010 transmission electron microscope (TEM, JEOL Ltd., Japan). The room temperature UV–vis spectrum was collected on a UV/VIS spectrometer PerkinElmer LAMBDA 40 at wavelength range of 200–1300 nm with the scanning rate of 0.5 nm s^{-1}.

* Corresponding author. Tel.: +66 53 943344; fax: +66 53 892277.
E-mail addresses: sthongtem@yahoo.com (T. Thongtem), phuruangrat@hotmail.com (A. Phuruangrat).

0925-8388/$ – see front matter © 2010 Elsevier B.V. All rights reserved.
doi:10.1016/j.jallcom.2010.03.240

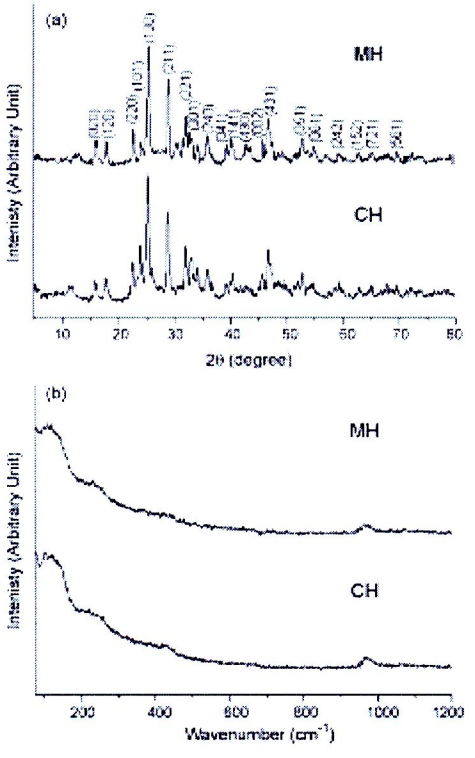

Fig. 1. (a) XRD patterns and (b) Raman spectra of Bi_2S_3 synthesized by the conventional hydrothermal and microwave-assisted hydrothermal methods.

3. Results and discussion

Fig. 1a shows the XRD patterns of the products synthesized by the MH and CH methods. All diffraction peaks match very well with the Bi_2S_3 JCPDS no. 17-0320 [11] with no detection of any impurities. The XRD intensity synthesized by the MH is higher than that synthesized by the CH. It implies that Bi_2S_3 synthesized by the first is better crystalline than Bi_2S_3 synthesized by the second. All the diffraction peaks of the Bi_2S_3 nanorods in flower-shaped bundles were shifted towards the lower angles, as compared to the JCPDS database, caused by an increase in their interplanar spaces. This may be attributed to the existence of the stress in the lattice of Bi_2S_3 nanorods in flower-shaped bundles. EDX spectrum of Bi_2S_3 produced by the MH method (un-shown result) detected only Bi and S peaks, in accordance with its constituents. Quantitative EDX analysis showed that the atomic ratio of Bi:S is 38:62, very close to the composition of Bi_2S_3. A definite existence of Bi_2S_3 was analyzed using a Raman spectrometer as shown in Fig. 1b. The spectra show four vibration modes, at 139.5, 253.7, 310.0 and 958.9 cm^{-1}. The first is in accordance with the 139.4 cm^{-1} mode of Bi_2S_3 nanorods, specified as the surface phonon vibration [12]. The second corresponds with the vibration mode of Bi_2S_3 nanorods at 252.0 and 259 cm^{-1} [12,13] and Bi_2S_3 nanoribbons and hierarchical nanostructures at 250 cm^{-1}, specified as the vibration mode of Bi–S bonds [14,15]. The detections of the third and fourth were in accordance with those of Bi_2S_3 nanorods at 312 and 975 cm^{-1} [13]. In the FTIR spectrum of PVP, it shows the wave numbers at 3450, 2930, 1675, 1420 and 1290 cm^{-1} – assigned to be the OH stretching vibration, CH_2 unsymmetrical stretching vibration, CO stretching vibration, CH_2 bending vibration and CN stretching vibration, respectively [16,17]. There was no detection of these impurity peaks in the FTIR spectrum of Bi_2S_3 (un-shown result), which implied that the product was pure phase.

SEM images of Bi_2S_3, prepared by the MH and CH methods, are given in Fig. 2. Only Bi_2S_3 irregular crystalline (Fig. 2a) with the average size of 1.5 μm was synthesized by the CH process. These nanorods agglomerate together to form clusters, and are not separate as independent nanorod bundles. Comparing to the synthesis of large-scale single-crystalline Bi_2S_3 nanowires by a simple one-step hydrothermal reaction of $Bi(NO_3)_3{\cdot}5H_2O$ and $Na_2S_2O_3$ at 180 °C for 2 days, the product contained a large quantity of nanowires with their lengths of hundreds of nanometers to a few microns range [18]. When microwave radiation was used as the heating source, the clearly independent Bi_2S_3 nanorods in flower-shaped bundles were detected. The use of microwave radiation as heating source shows the formation of uniform and perfect Bi_2S_3 flower-like bundles with the approximate diameter of 3–4 μm including the approximate length of the nanorods of 1–2 μm. The anisotropic growth of the Bi_2S_3 crystallites was further confirmed by the TEM analysis.

Fig. 3 shows TEM images of Bi_2S_3 nanorods in flower-shaped bundles synthesized by the MH method. The Bi_2S_3 flowers of Fig. 3a and b are composed of more than a hundred of individual Bi_2S_3 nanorods grow from the Bi_2S_3 cores. It is obvious that the morphology of Bi_2S_3 nanorods in flower-shaped bundles with 3–5.5 μm in size is in accordance with the SEM image (Fig. 2b) shown above. Fig. 3c shows the broken Bi_2S_3 nanorods form the Bi_2S_3 flower-like cores. The length of the individual nanorod of Bi_2S_3 is approximately 500–1500 nm. The growth direction of Bi_2S_3 nanorods in flower-shaped bundles was studied using high resolution trans-

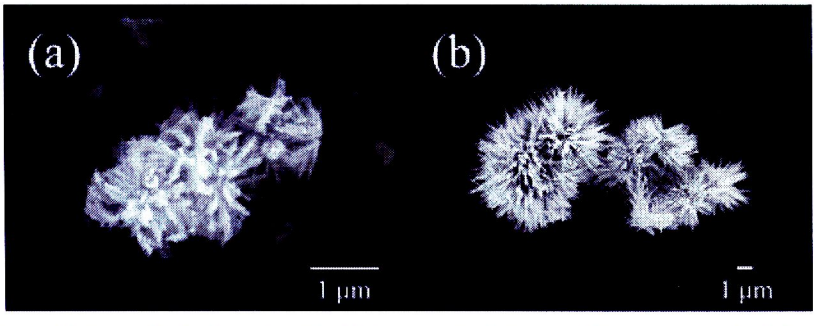

Fig. 2. SEM images of Bi_2S_3 nanorods in bundles synthesized by the (a) conventional hydrothermal and (b) microwave-assisted hydrothermal methods.

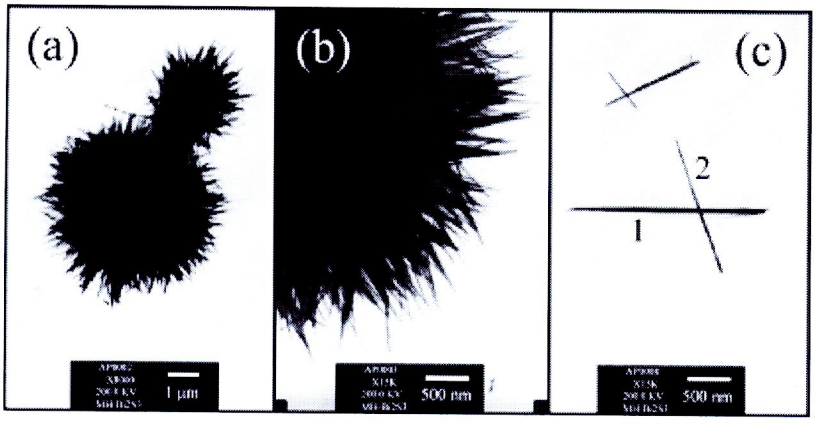

Fig. 3. TEM images of Bi_2S_3 nanorods in flower-shaped bundles synthesized by the MH method at (a) low and (b) high magnifications. (c) The broken nanorods from the flower-like cores.

mission electron microscopy (HRTEM) and selected area electron diffraction (SAED). They were characterized on areas 1 and 2 of TEM image (Fig. 3c). HRTEM images of Fig. 4a and c show lattice fringes of crystallographic planes with 3.98 Å space in parallel with the nanorods, corresponding to the (2 2 0) planes of orthorhombic Bi_2S_3 phase. The HRTEM images demonstrate that the Bi_2S_3 nanorods synthesized by the MH and CH methods grow along the [0 0 1] direction – in accordance with the growth direction of Bi_2S_3 nanorods and nanowires characterized by other researchers [1,3,19]. Both SAED patterns in areas 1 and 2 appear as bright spots composing electron diffraction patterns (Fig. 4b and d), revealing that individual Bi_2S_3 nanorods broken from flower-like cores are single crystal Bi_2S_3 with high degree of crystallinity. The SAED patterns can be indexed as the orthorhombic phase of Bi_2S_3 (JCPDS

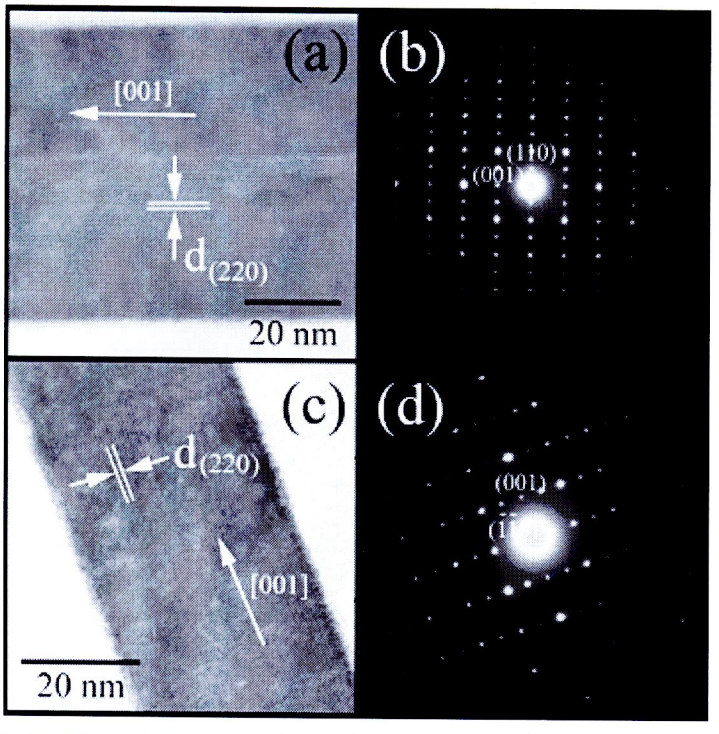

Fig. 4. HRTEM images and SAED patterns of Bi_2S_3 nanorods in bundles synthesized by the (a and b) conventional hydrothermal and (c and d) microwave-assisted hydrothermal methods.

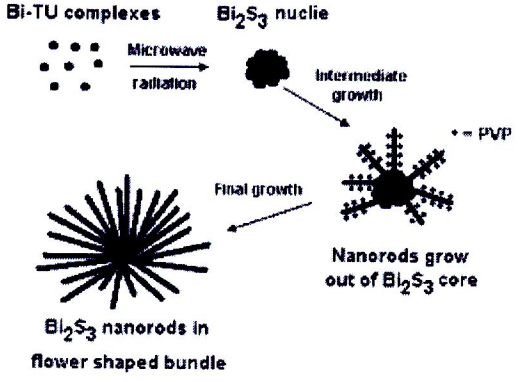

Fig. 5. Schematic illustration for the formation mechanism of Bi_2S_3 nanorods in flower-shaped bundles.

no. 17-0320) with the same [1 1 0] zone axes, which further confirm that the structure of the nanorods is orthorhombic phase, in accordance with the XRD analysis.

The formation mechanism of Bi_2S_3 nanorods in flower-shaped bundles is schematically shown in Fig. 5. First, the strong complex action between Bi^{3+} and thiourea (TU) leads to the formation of Bi–TU complexes [9]. For NH_2CSNH_2 compound, it has pair electrons on nitrogen and sulfur atoms, which have the great coordinating ability with inorganic metal cations, such as Cd^{2+}, Cu^{2+} and Pb^{2+} to form the metal–thiourea complexes [20]. Under microwave-assisted hydrothermal process, the Bi–TU complexes decomposed and formed the Bi_2S_3 nuclei. Then the Bi_2S_3 nanorods grew on the surface of Bi_2S_3 nuclei to form Bi_2S_3 nanorods in flower-shaped bundles. The formation reactions may be described as follows.

$$Bi^{3+} + TU \rightarrow Bi\text{–}TU \text{ complexes} \quad (1)$$

$$Bi\text{–}TU \text{ complexes} \rightarrow Bi_2S_3 \quad (2)$$

The growth process of Bi_2S_3 nanorods in flower-shaped bundles contains mainly two stages – the nucleation and crystal growth. For the present research, $Bi(NO_3)_3$ reacts with TU to form Bi–TU complexes at the initial stage. At the intermediate stage, the Bi–TU complexes decomposed to produce Bi_2S_3 nuclei by the microwave-assisted hydrothermal process. At this stage, PVP adsorbed on Bi_2S_3 nuclei – leading to the Bi_2S_3 nucleation as seeds which act as initial nuclei for particle growth. When the particles reach the critical dimension, PVP absorbed on the small particles by the side linked Bi_2S_3 units forming infinite chains parallel to the *c*-axis acting as a template for the formation of Bi_2S_3 nanorods in flower-shaped bundles. The final stage is the Bi_2S_3 nanorods in flower-shaped bundles, obtained by a novel microwave hydrothermal method, - homogeneous in size and form much similar to a flower with thorns found in nature [9,10,21]. In general, the growth of 1D Bi_2S_3 nanomaterials is a preferential growth direction along the *c*-axis due to the difference bonding in Bi_2S_3 structure. Bi_2S_3 is a lamellar structure with linked Bi_2S_3 units forming infinite chains parallel to the *c*-axis. The stronger covalent bond between the planes perpendicular to the *c*-axis supports higher growth rate along the *c*-axis. The much weaker van der Waals bonding between the planes perpendicular to the *a*-axis limits the growth of the fibers in the horizontal direction and supports their cleavage to form one-dimensional nanostructure [22].

The optical property of the product was investigated by UV–vis spectroscopy. Fig. 5 presents the UV–vis absorbance spectrum, and $(\alpha h\upsilon)^2$ vs. $h\upsilon$ curve of Bi_2S_3 nanorods in flower-shaped bundles synthesized by the MH method. The UV–vis spectrum showed the blue shifted absorption at 595 nm as compared to the 953 nm absorption for bulk Bi_2S_3 [23]. It can be attributed to the excitonic absorbance due to the quantum confinement at low dimension compared to its bulk counterparts [23]. The direct band gap of the product was calculated from its optical absorption spectrum by plotting $(\alpha h\upsilon)^2$ vs. $h\upsilon$ curve where α is the absorbance, h the Planck constant and υ the frequency [24] is shown in Fig. 5b. The direct band gap (E_g) of the Bi_2S_3 semiconducting nanorods in flower-shaped bundles was determined to be at 1.82 eV. This value is in good agreement with the 1.85 eV band gap of Bi_2S_3 nanowires [22], and 1.8 eV band gap of Bi_2S_3 thin films [24].

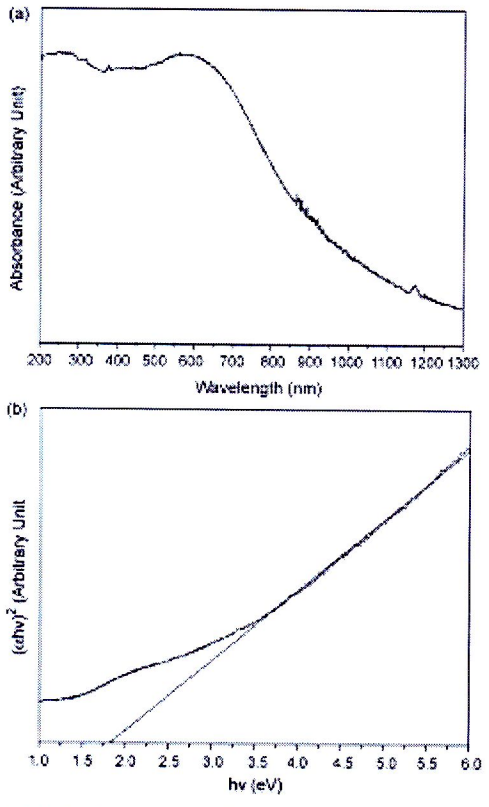

Fig. 6. (a) UV–vis absorbance, and (b) $(\alpha h\upsilon)^2$ vs. $h\upsilon$ curve of Bi_2S_3 nanorods in flower-shaped bundles synthesized by the microwave-assisted hydrothermal method.

4. Conclusions

Microwave-assisted hydrothermal reaction has emerged as an alternative route of fine powder synthesis. It was demonstrated that this simple method can be used to synthesize Bi_2S_3 nanostructure. XRD, SEM and TEM analyses proved that the product is orthorhombic Bi_2S_3 nanorods in flower-shaped bundles with the size of 3–5.5 μm. The microwave-assisted hydrothermal process for the synthesis of nanomaterials is shown to be very effective, inexpensive, short reaction time and environmentally benign. The direct energy band gap of the product was determined to be 1.82 eV – in agreement with those of other researchers.

Acknowledgements

This research was supported by the National Nanotechnology Center (NANOTEC), a member of National Science and Technology Development Agency (NSTDA), Ministry of Science and Technology, and the Thailand Research Fund, Bangkok, Thailand.

References

[1] Z.J. Zhang, X.Y. Chen, J. Phys. Chem. Solids 70 (2009) 1121–1131.
[2] L. Tian, H.Y. Tan, J. Vittal, Cryst. Growth Des. 8 (2008) 734–736.
[3] C.J. Yang, C.Z. Wang, H.Q. Wang, Y.X. Zhang, C.H. Li, Mater. Lett. 62 (2008) 3953–3955.
[4] Q. Han, J. Chen, X. Yang, L. Lu, X. Wang, J. Phys. Chem. C 111 (2007) 14072–14077.
[5] L. Lu, Q. Han, X. Yang, L. Lu, X. Wang, Mater. Lett. 61 (2007) 3425–3428.
[6] C. Xie, Z.P. Qiao, M.H. Zeng, X.M. Chen, S.L. Cao, Cryst. Growth Des. 4 (2004) 313–316.
[7] X. Zhu, J. Ma, Y. Wang, J. Tao, B. Lin, Y. Ren, X. Jiang, J. Liu, Ceram. Int. 34 (2008) 249–251.
[8] Y. Jiang, Y. Zhu, Z. Liu, Mater. Lett. 60 (2006) 2294–2298.
[9] A. Phuruangrat, T. Thongtem, S. Thongtem, Mater. Lett. 63 (2009) 1466–1468.
[10] T. Thongtem, A. Phuruangrat, S. Wannapop, S. Thongtem, Mater. Lett. 64 (2010) 122–124.
[11] Powder Diffract. File, JCPDS-ICDD, Newtown Square, PA, USA, 2001.
[12] X. Yang, X. Wang, Z. Zhang, Mater. Chem. Phys. 93 (2006) 154–157.
[13] J. Ota, S.K. Srivastava, J. Phys. Chem. C 111 (2007) 12260–12264.
[14] Y. Sun, Q. Han, J. Liu, X. Yang, L. Lu, X. Wang, Mater. Lett. 62 (2008) 3730–3732.
[15] Q. Han, Y. Sun, X. Wang, L. Chen, X. Yang, L. Lu, J. Alloys Compd. 481 (2009) 520–525.
[16] X. Su, Y. Liu, C. Shao, Y. Liu, C. Xu, Chem. Phys. Lett. 424 (2006) 340–344.
[17] T.-T. Tseng, W.J. Tseng, Ceram. Int. 35 (2009) 2837–2844.
[18] Y. Yu, W.T. Sun, Mater. Lett. 63 (2009) 1917–1920.
[19] Y. Yu, C.H. Jin, R.H. Wang, Q. Chen, L.M. Peng, J. Phys. Chem. B 109 (2005) 18772–18776.
[20] S.H. Yu, J. Yang, Z.H. Han, Y. Zhou, R.Y. Yang, Y.T. Qian, Y.H. Zhang, J. Mater. Chem. 9 (1999) 1283–1287.
[21] D.P. Volanti, D. Keyson, L.S. Cavalcante, A.Z. Simões, M.R. Joya, E. Longo, J.A. Varela, P.S. Pizani, A.G. Souza, J. Alloys Compd. 459 (2008) 537–542.
[22] W. Li, Mater. Lett. 62 (2008) 243–245.
[23] M. Salavati-Niasari, D. Ghanbari, F. Davar, J. Alloys Compd. 488 (2009) 442–447.
[24] V.V. Kriedenko, S.N. Kartore, C.H. Shokate, Mater. Chem. Phys. 64 (2000) 166–169.

Materials Letters 64 (2010) 111–114

Contents lists available at ScienceDirect

Materials Letters

journal homepage: www.elsevier.com/locate/matlet

Large-scale synthesis of CuS hexaplates in mixed solvents using a solvothermal method

Titipun Thongtem [a,*], Chalermchai Pilapong [a], Somchai Thongtem [b]

[a] Department of Chemistry, Faculty of Science, Chiang Mai University, Chiang Mai 50200, Thailand
[b] Department of Physics and Materials Science, Faculty of Science, Chiang Mai University, Chiang Mai 50200, Thailand

ARTICLE INFO

Article history:
Received 29 May 2009
Accepted 6 October 2009
Available online 9 October 2009

Keywords:
Nanomaterials
X-ray techniques
Electron microscopy
Luminescence
Optical materials and properties

ABSTRACT

Large-scale covellite CuS hexaplates were successfully synthesized by the 200 °C solvothermal reactions of $CuCl_2{\cdot}2H_2O$ and $(NH_4)_2S$ in C_2H_5OH–H_2O mixed solvents containing HCOOH as a pH stabilizer, including different amounts and molecular weights (MWs) of polyethylene glycol (PEG). By using XRD and SAED, CuS (hcp) was detected. XRD peaks of the product, synthesized in a solution containing 5 g PEG6000 and 1.5 ml HCOOH for 5 h, are in accordance with those of the simulation and database. The (110) peak shows the preferential growth, corresponding to the hexaplates, characterized using SEM, TEM and HRTEM. CuS hexaplates with the (100) and (010) lattice planes at an angle of 120° were detected on the flat surface, and the (002) lattice plane on the edge. UV–vis absorption edge was detected at 610 nm (2.03 eV), and the PL emission at 361 nm (3.43 eV). Phase and morphology formations were also explained according to the experimental results.

1. Introduction

Transition metal chalcogenides are semiconducting materials which exhibit novel properties, due to their differences in shapes, sizes, crystallinities and compositions. CuS is one of these materials having a wide range of potential applications in nonlinear optical devices, solar radiation absorbers, high capacity cathode materials and photocatalysts [1,2]. Recently, some researchers have succeeded in synthesizing CuS with different morphologies by different methods [1–10], but only a few for CuS hexaplates. The purpose of the present research was to synthesize CuS hexaplates by solvothermal reactions in solutions containing HCOOH with different amounts and MWs of PEG. The method is extremely effective, inexpensive, environmentally benign and appropriate for large-scale synthesis.

2. Experiment

The procedure was to dissolve 0.005 mol 98% $CuCl_2{\cdot}2H_2O$ and 1, 5 and 10 g PEG with different molecular weights (PEG6000, PEG8000, PEG10000, PEG12000, and PEG20000) in mixed solvents containing 9:1 volume ratio of C_2H_5OH:H_2O and 1.5 ml 98% HCOOH (a pH stabilizer) each. The solutions (green) were continuously stirred, and each 0.005 mol $(NH_4)_2S$ (20% in water) was added. Solvothermal reactions proceeded at 200 °C for 1, 3 and 5 h. Finally, black precipitates were synthesized, separated by filtration, washed with distilled water and 95% ethanol, dried at 70 °C for 8 h, and intensively characterized to determine their phase, morphologies, crystallographic planes, and energies of absorption and emission.

3. Results and discussion

XRD patterns obtained from the experiment, simulation [11] and JCPDS database no. 06-0464 [12] are shown in Fig. 1. The as-synthesized product was a hexagonal structure covellite CuS, with no detection of any impurities. Its diffraction peaks are narrow and sharp, specifying that the X-ray radiation reflected and diffracted from atoms in lattice order. Calculated lattice constants [13], $a=b=3.78$ Å and $c=16.32$ Å, are also in accordance with those of the JCPDS database [12]. This simulated pattern is used to specify that the experimental pattern could exist in reality. The 2θ Bragg's angles and relative intensities (I_R) of the diffraction peaks obtained from the experiment, simulation and database are in good accordance. Experimental I_R of the (110) peak is significantly stronger than those of the simulation and database, which indicates the preferential growth process.

TEM images (Fig. 2a and b) show a plate with two orientations: flat-lying and edge-standing images. The plate was in the shape of a hexagon with 75–100 nm edged length and 22 nm thick. The (100) and (010) lattice planes (Fig. 2c) with the same planar spaces of 3.3 Å were detected on the flat-lying image. These planes make an angle of 120° relative to each other, which is in accordance with the 120° basal plane of an hcp structure. A number of parallel planes with 8.2 Å apart were also detected on the edge-standing image (Fig. 2d). They correspond with the (002) crystallographic planes, to which the c axis

* Corresponding author. Tel.: +66 53 943344; fax: +66 53 892277.
E-mail addresses: ttpnongtem@yahoo.com, ttpnongtem@hotmail.com (T. Thongtem).

0167-577X/$ – see front matter © 2009 Elsevier B.V. All rights reserved.
doi:10.1016/j.matlet.2009.10.004

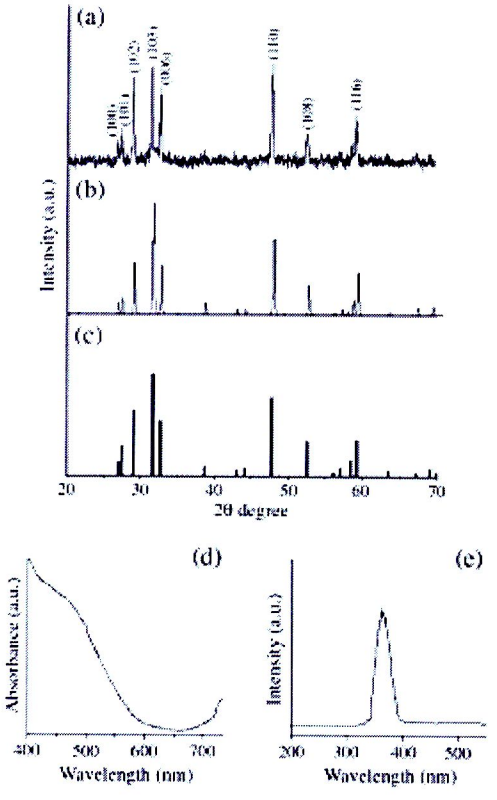

Fig. 1. XRD pattern of the (a) synthesized product produced in 5 g PEG6000-added solution containing 1.5 ml HCOOH at 200 °C for 5 h with its patterns obtained from the (b) simulation, (c) JCPDS database and its (d) UV–vis absorption and (e) PL emission spectra.

of the hcp structure was normal. This detection is also in accordance with that characterized by Cao et al. [3]. Thus hcp structure influenced the formation of hexaplates for the present process. SAED pattern (Fig. 2e) through a flat-lying hexaplate shows regular hexagonal array of diffraction spots, corresponding to the basal plane of its structure, with the electron beam in the [001] direction. This pattern corresponds to a single crystal of hcp covellite CuS [12]. A simulated ED pattern (Fig. 2f) appears as systematic arrays of spots, corresponding to the experimental SAED pattern.

Different products were synthesized under different conditions. HCOOH is a rather weak electrolyte with low degree of dissociation, which is a good pH stabilizer [7]. For 5 g PEG6000 and 1 h, the product (Fig. 3a) was composed of nanoplatelets and nanoparticles. $CuCl_2{\cdot}2H_2O$ reacted with $(NH_4)_2S$ to form CuS nuclei. Subsequently, these nuclei grew to form nanoplatelets and nanoparticles. As the reaction time passed, the product became larger by the Ostwald ripening process: larger particles grow at the expense of smaller ones [14]. More nanoplates and less nanoparticles were detected in the product synthesized for 3 h (Fig. 3b). There were a number of hexagonal plates with no nanoparticles existing in the product of 5 h synthesis (Fig. 3c). Each CuS nuclei grew to form platelets, composing of hcp unit cells in lattice order. Growth proceeded according to the crystal structure, which were associated with energies of different faces on the nuclei, specifying the final shape [6]. Intrinsic anisotropic characteristics of CuS hexagonal crystal structure have the strong influence on the product shapes [8]. PEG is a dominant surfactant, which play a role in changing surface energies of growing crystal faces [9], by selective adsorbing on different faces of nuclei or seeds [1]. Growth in the [110] direction became faster and that in the [001] direction was slower [9]. Hexaplates, surrounded by the (100), (010), (−110), (−100), (0−10) and (1−10) planes, were synthesized. Their sizes were also influenced by the concentration and diffusion of nuclei in the solutions. Solubilities, reactivities and other properties of the reagents and the precursors (intermediates) play the role in the product morphologies, by influencing the growth and self-assemblies of nuclei [6].

When different amounts of PEG6000 with the same prolonged time of 5 h were used, different morphologies were synthesized. For 1 g PEG6000, the product (Fig. 3d) was composed of non-uniform plates and nanoparticles, caused by the incomplete capping on the CuS crystallographic faces. When 10 g PEG6000 was used, nanoparticles were no longer detected. The plates shaped like a hexagon still exist in the product (Fig. 3e), but they were in clusters. Thus excess PEG6000 was no longer required for the present condition.

Morphologies of the products synthesized at 200 °C for 5 h in the solutions containing different MWs of 5 g PEG were also studied. By using PEG6000, the degree of HCOOH in stabilizing a pH became lessened. Thus formation mechanism changed. Individual nanoparticles and plate-shaped particles (Fig. 3f) with different geometries from above (Fig. 3c) were synthesized. When PEGs with heavier MWs or longer chain molecules were used, the degree in prohibiting the growth of individual nanoparticles and plate-shaped particles became more intense. For PEG10000, their chain molecules were long enough to entangle these nuclei in the solution to form clusters with active sites on their surfaces, at which the nuclei grew to form clusters of plate-shaped particles (Fig. 3g). These clusters gradually transformed into incomplete flower-like shapes for PEG12000 (Fig. 3h), and complete flower-like shapes for PEG20000 (Fig. 3i) afterwards. These plates self-assembled into clusters and flower-like clusters, in order to reduce their surface areas and to minimize the interfacial free energies [6].

UV–vis absorption spectrum (Fig. 1d) of CuS hexaplates dispersed in absolute ethanol, shows the absorption edge at 610 nm (2.03 eV). A broad absorption peak of near-IR region indicates the presence of covellite CuS, which is in accordance with those obtained by Gao et al. [4] and Guo et al. [2]. A PL spectrum of solid CuS hexaplates (Fig. 1e) was determined using a 300 nm (4.13 eV) excitation wavelength. Its emission peak is 361 nm (3.43 eV), and is in accordance with the emission of CuS nanoplates at 339 nm (3.665 eV) determined by Zhang et al. [1].

4. Conclusions

CuS (hcp) with different morphologies were solvothermally synthesized in C_2H_5OH–H_2O mixed solvents containing a pH stabilizer (HCOOH) with different amounts and MWs of PEG. Covellite CuS was detected. Its hexagonal plates, synthesized in a solution containing 1.5 ml HCOOH and 5 g PEG6000 for 5 h, were composed of the (100) and (010) parallel lattice planes on the flat surface and (002) plane on the edge. Absorption edge of CuS hexagonal plates was detected at 610 nm (2.03 eV), with its emission at 361 nm (3.43 eV). Formation of CuS with different morphologies was also explained according to the experimental results.

Acknowledgement

The research was supported under the National Research University Project for Chiang Mai University, by the Commission on Higher Education, Ministry of Education, Thailand.

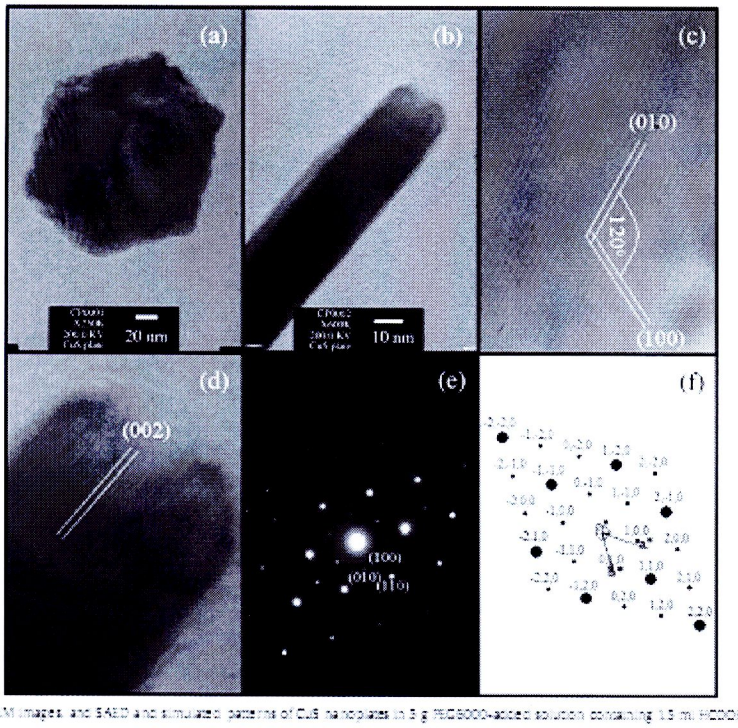

Fig. 2. TEM and HRTEM images and SAED and simulated patterns of CuS nanoplates in 5 g PEG6000-added solution containing 1.5 mL HCOOH at 200 °C for 5 h.

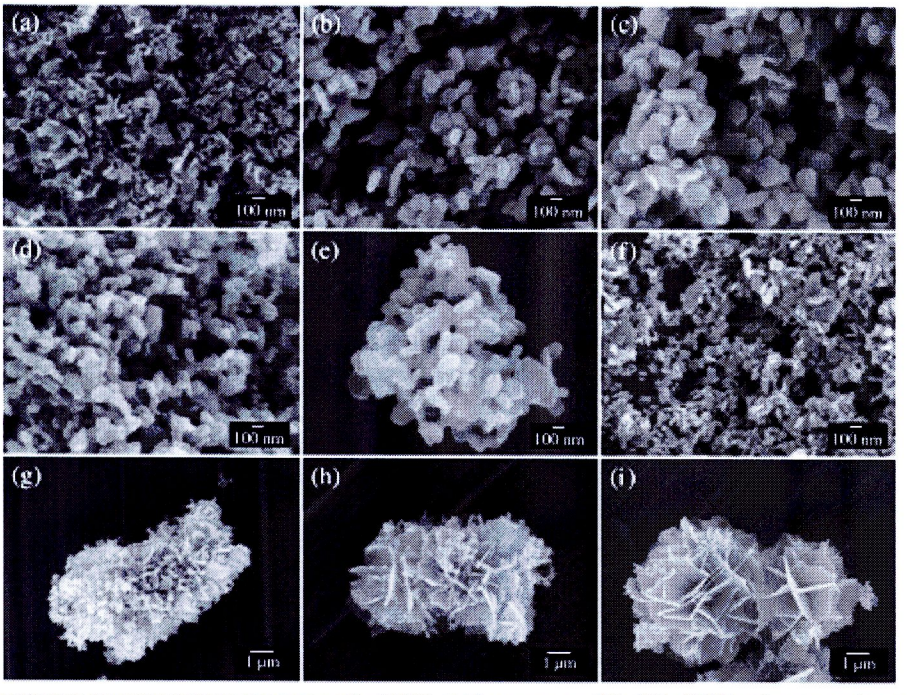

Fig. 3. SEM images of the products synthesized in the solution containing 1.5 mL HCOOH with different amounts and MWs of PEG at 200 °C for different reaction times: (a) 5 g PEG6000, 1 h; (b) 5 g PEG6000, 3 h; (c) 5 g PEG6000, 5 h; (d) 1 g PEG6000, 5 h; (e) 10 g PEG6000, 5 h; (f) 5 g PEG8000, 5 h; (g) 5 g PEG10000, 5 h; (h) 5 g PEG12000, 5 h; and (i) 5 g PEG20000, 5 h.

References

[1] Zhang J, Zhang Z. Mater Lett 2008;62:2278–81.
[2] Ding TY, Wang MB, Guo SY, Guo DC, Huang R. Mater Lett 2008;62:4529–31.
[3] Liu Y, Qin D, Wang J, Cao Y. Mater Chem Phys 2007;102:201–6.
[4] Zhang P, Gao L. J Mater Chem 2003;13:2007–10.
[5] Thongtem T, Phuruangrat A, Thongtem S. J Mater Sci 2007;42:9316–23.
[6] Shen XF, Zhao H, Shui HQ, Zhou H, Yuan AH. J Phys Chem Solids 2009;70:422–7.
[7] Gong W, Yu SH, Qian HS, Luo LB, Liu XM. Chem Mater 2005;15:2013–5.
[8] Li R, Kong T, Bi W, Li D, Li X, Huang X. Appl Surf Sci 2009;255:6283–8.
[9] Chu L, Zhou B, Mu H, Sun Y, Xu F. J Cryst Growth 2008;310:5437–40.
[10] An C, Wang S, He J, Wang Z. J Cryst Growth 2008;310:2565–9.
[11] Boudias C, Monceau D. CaRIne Crystallography 3.1. DIVERGENT S.A., Centre de Transfert, 60200 Compiègne, France; 1989–1998.
[12] Powder Diffract. File: JCPDS-ICDD. 12 Campus Boulevard, Newtown Square, PA 19073-3273, U.S.A.; 2001.
[13] Suryanarayana C, Norton MG. X-ray Diffraction A Practical Approach. New York: Plenum Press; 1998.
[14] Schubert U, Hüsing N. Synthesis of Inorganic Materials, Weinheim, Wiley-VCH; 2000. p. 150–8 379.

Journal of Alloys and Compounds 507 (2010) 139–142

Contents lists available at ScienceDirect

Journal of Alloys and Compounds

journal homepage: www.elsevier.com/locate/jallcom

Letter

Hydrothermal synthesis of double sheaf-like Sb_2S_3 using copolymer as a crystal splitting agent

Chalermchai Pilapong [a], Titipun Thongtem [a,*], Somchai Thongtem [b]

[a] Department of Chemistry, Faculty of Science, Chiang Mai University, Chiang Mai 50200, Thailand
[b] Department of Physics and Materials Science, Faculty of Science, Chiang Mai University, Chiang Mai 50200, Thailand

ARTICLE INFO

Article history:
Received 6 March 2010
Received in revised form 2 August 2010
Accepted 4 August 2010
Available online 11 August 2010

Keywords:
Electron microscopy
Nanomaterials
Sensors
X-ray techniques

ABSTRACT

Double-sheaves of antimony sulfide were synthesized by the 200 °C and 24 h hydrothermal reaction in the acidic solution, containing copolymer – a crystal splitting agent. Using X-ray technique, electron microscopy, and Raman as well as UV–visible NIR absorption spectroscopy, the products were specified as orthorhombic Sb_2S_3 composing of Sb and S with five vibration modes, in the shape of spears in bundles with the [0 0 1] growth direction and 2.38 eV direct energy gap. A diffraction pattern was also simulated, and is in good accordance with that obtained by the interpretation.

1. Introduction

Antimony sulfide (Sb_2S_3, stibnite), a chain-structured V–VI chalcogenide semiconductor with orthorhombic crystal structure [1,2], has good photosensitivity and high thermoelectric power [1,3], and has 1.78–2.50 eV direct band gap – in the visible and near IR range [3]. Its property is generally controlled by the morphologies with different defects and concentrations. A number of methods have been used to synthesize antimony sulfide with different morphologies: nanocrystals by a microwave synthesis [3], dendrites by the crystallization of amorphous colloidal microspheres [4], and straw-tied-like architectures, nanoribbons and sub-microwires by a hydrothermal process [1,5,6].

In the present research, double-sheaves of Sb_2S_3 crystals were hydrothermally synthesized using copolymer as a crystal splitting agent – another function of the copolymer. This method is extremely effective, inexpensive, environmentally benign and appropriate for large-scale synthesis.

2. Experiment

To synthesize Sb_2S_3, 0.005 mol antimony acetate and 0.01 mol thiourea were dissolved in 50 ml H_2O containing 0.5 ml HNO_3. Different amounts of copolymer, poly (vinyl-n-butyral-co-vinyl alcohol-co-vinyl acetate), were added to the mixtures with continuous stirring. The products were hydrothermally synthesized in home-made stainless steel autoclaves at 200 °C for 6–24 h, and further characterized to determine their phase both by interpretation and simulation [7], morphologies, vibrations and energy gap.

3. Results and discussion

XRD pattern (Fig. 1a) was indexed and specified as orthorhombic Sb_2S_3 phase (Pbnm space group) with no detection of any impurities such as Sb_2O_3. Calculated lattice parameters [a = 11.25 Å, b = 11.34 Å and c = 3.82 Å] are in good accordance with those of the JCPDS no. 42-1393 [2].

For the present research, thiourea was hydrolyzed in acidic solution at elevated temperature to produce S^{2-} [8].

$$NH_2CSNH_2 + H_2O \rightarrow NH_2CONH_2 + S^{2-} + 2H^+$$

Simultaneously, Sb^{3+} reacted with S^{2-} in aqueous (aq) solution containing acid to form Sb_2S_3 (s).

$$2Sb^{3+}(aq) + 3S^{2-}(aq) \rightarrow Sb_2S_3(s)$$

EDX spectrum (Fig. 1b) proved that there are antimony and sulfur existing in this product. Cu and C stem from copper stub and carbon tape, were also detected. Quantitative analysis shows that the atomic ratio of Sb:S is 21.67:31.16 – in accordance with antimony sulfide chemical formula.

Its Raman shift (Fig. 1c) was specified as five vibration modes. Sharp peaks at 188.8 and 253.4 cm^{-1} proved that the product

* Corresponding author. Tel.: +66 53 943344; fax: +66 53 892277.
E-mail addresses: tpinongtem@yahoo.com, tpinongtem@hotmail.com (T. Thongtem).

0925-8388/$ – see front matter © 2010 Elsevier B.V. All rights reserved.
doi:10.1016/j.jallcom.2010.08.008

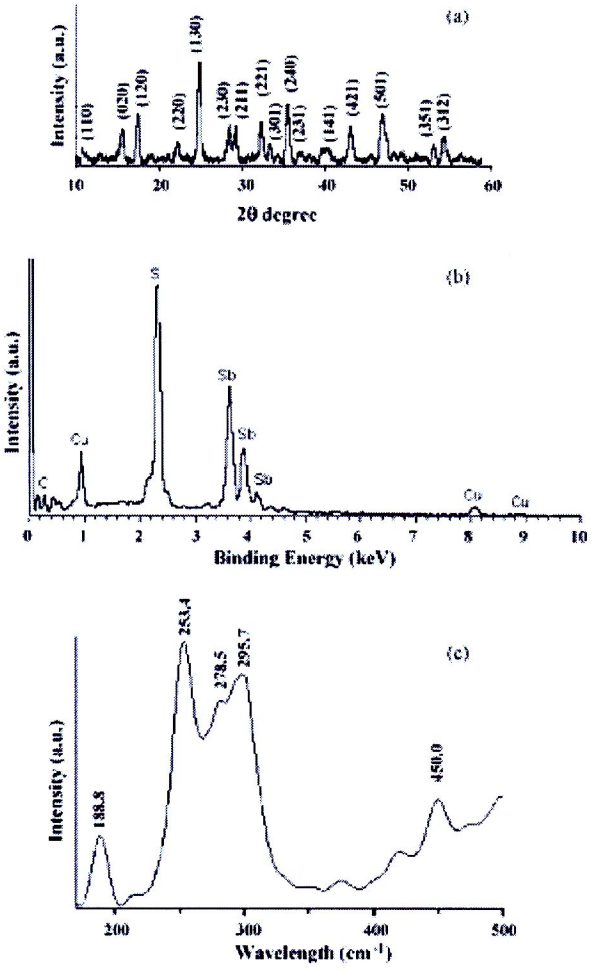

Fig. 1. (a) XRD pattern, (b) EDX spectrum, and (c) Raman shift of Sb_2S_3 synthesized by the 200 °C and 24 h hydrothermal reaction in a solution containing 1 g copolymer.

is good crystalline. Two peaks at 278.5 and 295.7 cm^{-1} are in accordance with the symmetric vibrations of SbS_3 pyramidal units having C_3, symmetry [9,10], and the 450.0 cm^{-1} peak the S–S vibrations [9] or the symmetric stretching of Sb–S–S–Sb structural units [10].

SEM images (Fig. 2) show external morphologies of the products synthesized under different conditions. For 6 h and 1 g copolymer synthesis, the product is composed of bunches of oval plates tied together at the middle. When the time was lengthened to be 12 h, these plates slowly developed into branches, remaining fastened at the middle with both sides spreading out – similar to a wheat sheaf or a bundle of filamentary crystals. For 24 h and 1 g copolymer, more filamentary crystals were produced on each bundle and the extent of spreading became wider. The bundles have the shape of double sheaf-like structures. Each of the filamentary or ribbon-like crystals has sharp point, having the shape of a spear. Incomplete sheaf-like bundles were synthesized for 24 h and 0.5 g copolymer, and a number of nanorods with different sizes and orientations for 24 h in copolymer-free solution. These sheaf-like structures could form by crystal splitting during their growth and grew along the preferential direction into ribbon-like branches. The degree of spreading depends on their splitting ability which increases with the prolonged time increase. The splitting ability was also controlled by copolymer in the solution. By reducing its amount, the degree of splitting became lowered and the sheaf-like bundle was incomplete. In copolymer-free solution, there were a number of nanorods with different sizes and orientations appearing as the product [11].

Fig. 3 shows TEM and HRTEM images, SAED and simulated patterns of Sb_2S_3 synthesized using 1 g copolymer at 200 °C for 24 h. Its TEM image shows an individual ribbon in the shape of a spear, growing along the [0 0 1] direction. HRTEM analysis on a ribbon-like crystal proved that the ribbon is single crystal, composing of the (2 2 0) parallel crystallographic planes with 0.39 nm apart in parallel with the [0 0 1] growth direction. The SAED pattern shows the systematic array of diffraction spots of orthorhombic

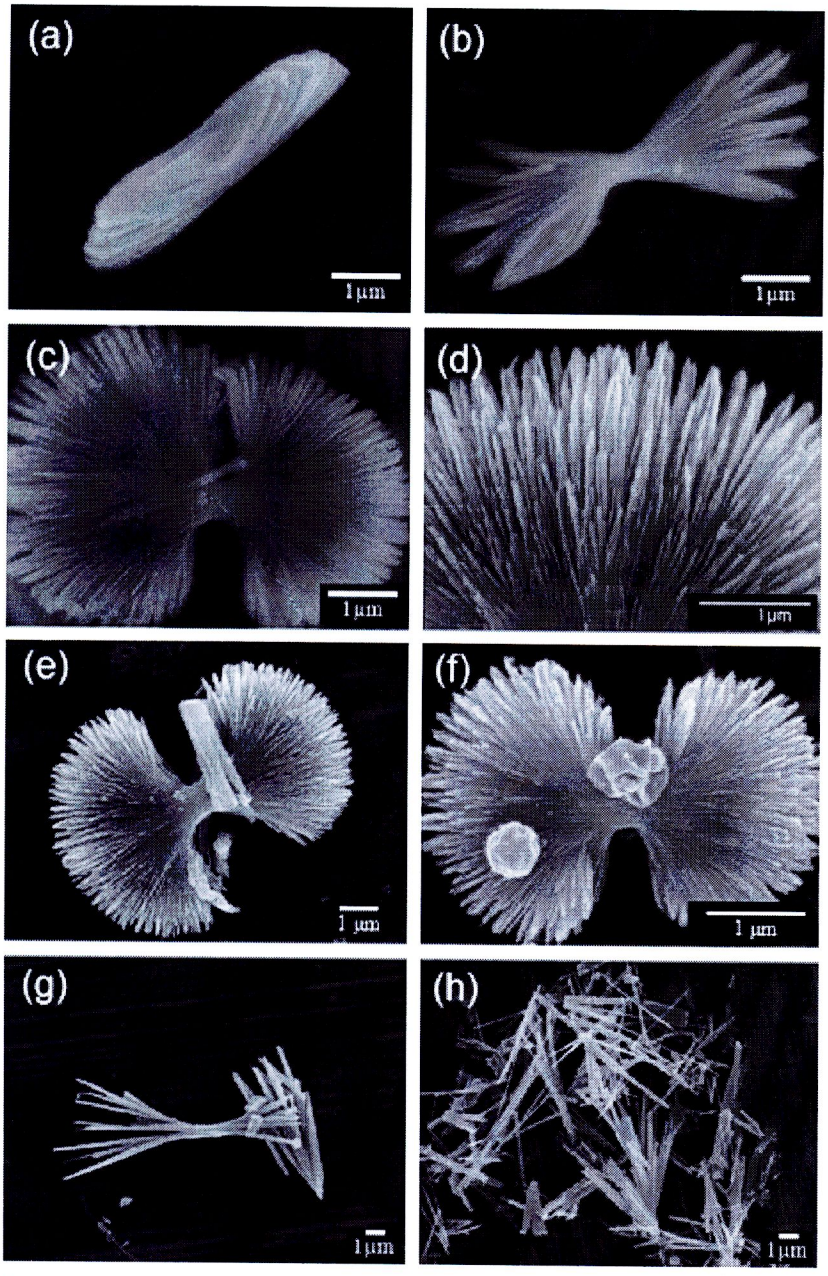

Fig. 2. SEM images of Sb_2S_3 synthesized at 200 °C for different lengths of time and amounts of ascorbyme: (a) 6 h, 1 g; (b) 12 h, 1 g; (c) 24 h, 1 g; (g) 24 h, 0.5 g; and (h) 24 h, ascorbyme-free.

Sb_2S_3 single crystal [2] with electron beam in the [1 0 3] direction, corresponding to the diffraction pattern obtained by simulation [7].

To get an insight into the growth mechanism of sheaf-like structure, its crystal structure (Fig. 4) was simulated [7]. It is made up of infinite chains of stoichiometric composition of atoms running normal to the b axis. The binding of these Sb_2S_3 structure chains in the b direction is considerably weaker than the one along the chains – leading to easily cleavage along its (0 1 0) planes. Thus, the growing crystal was split. Crystal splitting is also associated with

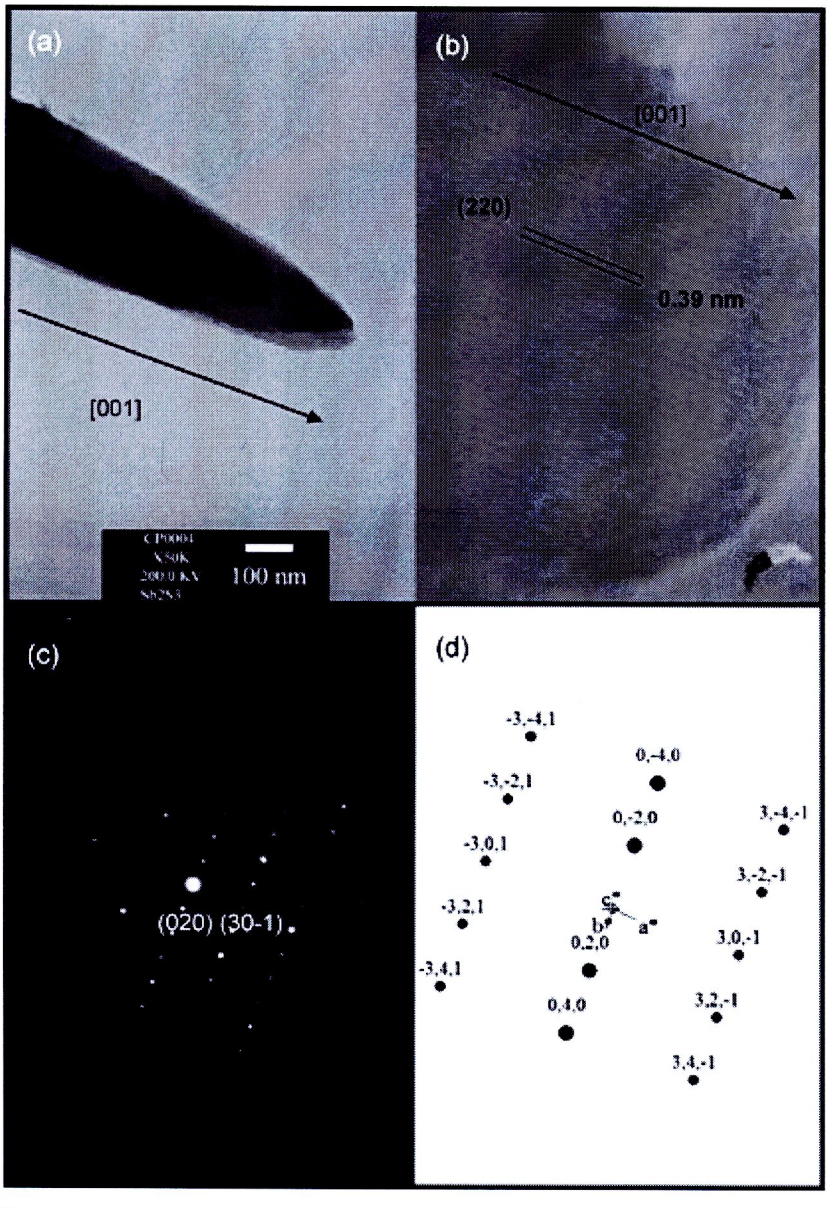

Fig. 3. TEM and HRTEM images and SAED and simulated patterns of Sb_2S_3 nanoribbons synthesized by the 200 °C and 24 h hydrothermal reaction in a solution containing 1g copolymer.

rapid crystal growth, due to the supper saturation that exceeds a certain critical value, especially for some specified condition [11].

Fig. 5 shows the relationship of $(\alpha h\nu)^2$ and photon energy $(h\nu)$ for the direct allowed transition, where α (=−(log T)/t) is the total absorption coefficient, T the transmittance of photon through the suspension in ethanol (C = 0.001 g cm^3) containing in the Spectroscopy cell with the path length (t) of 10.00 mm, t (=$bC\rho$) the effective thickness, and ρ the density of Sb_2S_3 [12]. The absorption edge energy, determined by extrapolation the curve to α = 0, corresponds to the 2.38 eV energy gap. This value is in the 1.78–2.50 eV energy gap range of nano-Sb_2S_3 determined by other researchers [13].

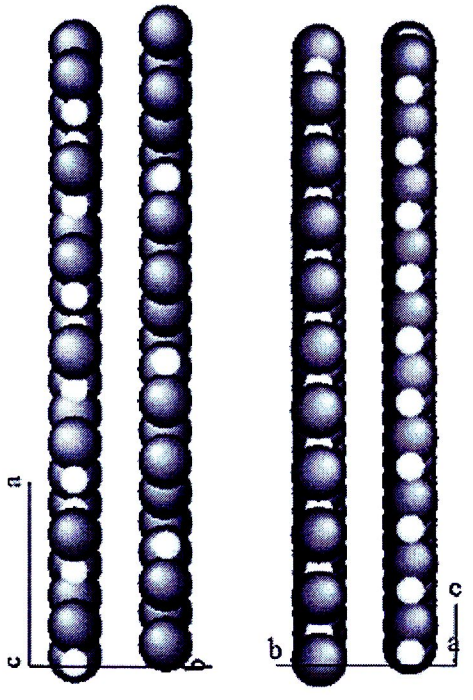

Fig. 4. Crystal structure of Sb_2S_3 composing of Sb (white balls) and S (black balls).

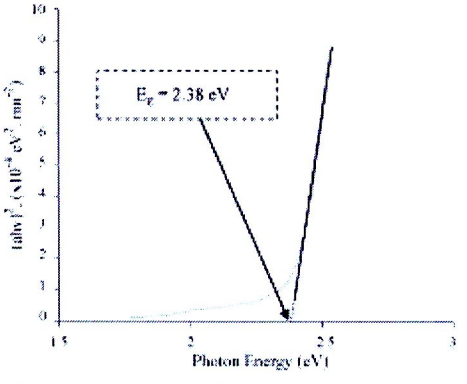

Fig. 5. The relationship between $(\alpha h\nu)^2$ and photon energy ($h\nu$) of Sb_2S_3 synthesized by the 200 °C and 24 h hydrothermal reaction in the solution containing 1 g copolymer.

4. Conclusions

Pure double sheaf-like structured Sb_2S_3 was successfully synthesized in acidic solution containing 1 g copolymer by the 200 °C and 24 h hydrothermal reaction – the environmentally benign process. Its phase, constituents, morphology and Raman vibrations – including its 2.38 eV direct energy gap were clearly detected.

Acknowledgement

This research was supported by the National Nanotechnology Center (NANOTEC), a member of National Science and Technology Development Agency (NSTDA), Ministry of Science and Technology, Thailand.

References

[1] D. Wang, C. Song, X. Fu, K. Lu, J. Cryst. Growth 281 (2005) 611–615.
[2] Powder Diffraction File, ICPDS-ICDD, 12 Campus Boulevard, Newtown Square, PA 19073-3273, USA, 2001.
[3] H. Yang, X. Su, A. Tang, Mater. Res. Bull. 42 (2007) 1357–1363.
[4] X. Cao, Y. Xie, L. Li, J. Solid State Chem. 177 (2004) 2021–2026.
[5] Q. Xie, Z. Liu, M. Shao, L. Kong, W. Yu, Y. Qian, J. Cryst. Growth 252 (2003) 570–574.
[6] C.Q. Zhu, P. Liu, H.Y. Miao, J.P. Zhu, X.B. Bian, Y. Liu, B. Chen, X.B. Wang, Mater. Res. Bull. 43 (2008) 2535–2542.
[7] C. Boudias, D. Monceau, CaRIne Crystallography 3.1, DIVERGENT S.A. Centre de Transfert, 60200 Compiègne, France, 1989–1998.
[8] A. Phuruangrat, C. Thongtem, S. Thongtem, Mater. Lett. 63 (2009) 1538–1541.
[9] C. An, K. Tang, Q. Yang, Y. Qian, Inorg. Chem. 42 (2003) 8061–8065.
[10] M.A. El Idrissi Raghni, B. Bonnet, M.L. Hafid, J. Olivier-Fourcade, J.C. Jumas, J. Alloys Compd. 260 (1997) 7–11.
[11] J. Yang, A.P. Alivisatos, Nano Lett. 6 (2006) 2701–2706.
[12] S. Tsunekawa, T. Fukuda, A. Kasuya, J. Appl. Phys. 87 (2000) 1318–1321.
[13] Q.A. Zhu, M. Dong, C. Zhang, C. Yong, S. Xiang, J. Cryst. Growth 311 (2009) 3651–3655.

Current Applied Physics 12 (2012) 23–30

Contents lists available at SciencesDirect

Current Applied Physics

journal homepage: www.elsevier.com/locate/cap

Hydroxyethyl cellulose-assisted hydrothermal synthesis of Bi_2S_3 urchin-like colonies

Titipun Thongtem [a,b,*], Siriprapha Jattukul [a], Chalermchai Pilapong [a], Somchai Thongtem [b,c]

[a] Department of Chemistry, Faculty of Science, Chiang Mai University, Chiang Mai 50200, Thailand
[b] Department of Physics and Materials Science, Faculty of Science, Chiang Mai University, Chiang Mai 50200, Thailand
[c] Materials Science Research Center, Faculty of Science, Chiang Mai University, Chiang Mai 50200, Thailand

ARTICLE INFO

Article history:
Received 25 January 2011
Received in revised form
18 April 2011
Accepted 18 April 2011
Available online 28 April 2011

Keywords:
Bi_2S_3
Urchin-like colonies
Hydrothermal reaction
Hydroxyethyl cellulose (HEC)
Ultraviolet–visible spectroscopy

ABSTRACT

Orthorhombic Bi_2S_3 with different morphologies was successfully synthesized by the acid-catalyst hydrothermal reactions of bismuth nitrate ($Bi(NO_3)_3$) and thiourea (NH_2CSNH_2) solutions containing different amounts of hydroxyethyl cellulose (HEC). Phase, morphologies, and optical properties were characterized by X-ray diffraction, selected area electron diffraction, scanning and transmission electron microscopy, and ultraviolet–visible spectroscopy. The products, hydrothermally synthesized in the HEC-free, 0.25 g HEC-added, 0.5 g HEC-added and 1.00 g HEC-added solutions, were respectively proved to be orthorhombic Bi_2S_3 irregular nanorods, complete urchin-like colonies of regular nanorods, incomplete urchin-like colonies of regular nanorods, and highly crystalline regular nanorods growing along the [001] direction. Tauc band gaps of the orthorhombic Bi_2S_3 nanorods, synthesized in the HEC-free, 0.25 g HEC-added, and 1.00 g HEC-added solutions were determined to be 3.0, 1.75 and 1.8 eV, respectively. Formation mechanism of orthorhombic Bi_2S_3 nanorods, synthesized in the HEC-free and HEC-added solutions, was also discussed at great detail.

1. Introduction

One-dimensional (1D) Bi_2S_3 nanostructures such as nanorods and nanowires are very interesting chalcogenide semiconductors, for both fundamental and technological applications. The 1D Bi_2S_3 nanostructures exhibit not only novel electronic and optical properties - intrinsically associated with their low dimensionality and quantum confinement effect, but also the representative of critical components in the potential nanoscale device applications [1–4]. In the past decades, 1D Bi_2S_3 nanostructures have been synthesized and characterized by both top-down and bottom-up approaches [5–7]. Major challenges, however, remain as full benefits of the 1D nanostructures – the development of suitable chemical strategies for the rational synthesis, and organization and integration of these nanoscale building blocks. The architectural control of Bi_2S_3 nanostructures with well defined shape and texture is the main goal to obtain the materials with widely varying properties [8].

Not long ago, Bi_2S_3 with different morphologies were successfully synthesized by a hydrothermal process: nanoparticles, nanorods, nanobelts, and nanoflowers [8], networks of cross-linked single crystalline nanowires [10], urchin-like structure [11], chrysanthemum-like microcrystals [12], nanorods [4,13,14], mat-like architecture [15], nanoflowers and nanocabbages [16], and flower-like patterns with well-aligned nanorods [17].

In the present research, Bi_2S_3 nanostructure with the shapes of irregular nanorods, complete urchin-like colonies of regular nanorods, and highly crystalline regular nanorods was synthesized in the solutions containing bismuth nitrate, thiourea, and different amounts of hydroxyethyl cellulose (HEC) via an acid-catalyst hydrothermal reaction. Formation mechanism of orthorhombic Bi_2S_3 nanorods, complete and incomplete urchin-like colonies, and highly crystalline nanorods was also studied. HEC is an inexpensive and easily obtainable nonionic polymer, which contributes to the stabilization of ion concentration [18]. It has been widely used in cosmetics, cleaning solutions, and capsule formulations. To the best of our knowledge, there are no Bi_2S_3 products have ever been synthesized using HEC as a template and capping agent via the hydrothermal synthesis. The success in synthesizing of these products may lead to commercial scale production in the near future.

2. Experimental procedure

All chemicals used in this experiment were analytical grade and used without further purification. The procedure was to mix 5 mmol of bismuth nitrate ($Bi(NO_3)_3$) and 10 mmol of thiourea (NH_2CSNH_2)

* Corresponding author. Department of Chemistry, Faculty of Science, Chiang Mai University, Chiang Mai 50200, Thailand. Tel.: +66 53 943344; fax: +66 53 892277.
E-mail addresses: ttpthongtem@yahoo.com, ttpthongtem@hotmail.com (T. Thongtem).

1567-1739/$ – see front matter © 2011 Elsevier B.V. All rights reserved.
doi:10.1016/j.cap.2011.04.017

in water containing nitric acid (HNO_3). Subsequently, different amounts (0.00, 0.25, 0.50 and 1.00 g) of hydroxyethyl cellulose (HEC) were added to form mixtures, which were followed by 15 min stirring at room temperature. The reactions proceeded in home-made stainless steel autoclaves at varying temperatures and lengths of time. Finally, the precipitates were synthesized, separated by filtering, washed with deionized water and 95% ethanol several times, and dried at 80 °C for 24 h. The final products were characterized using X-ray diffraction (XRD) operating at 20 kV and 15 mA with Kα line of a Cu target; scanning electron microscopy (SEM) operating at 15 kV; and transmission electron microscopy (TEM) and high resolution TEM (HRTEM) as well as selected area electron diffraction (SAED), operating at 200 kV. For TEM and HRTEM experiments, the as-synthesized powders were dispersed in ethanol by ultrasonic vibration. Then, small drops of the dispersions were transferred to holey carbon films supported on copper grids. The energy band gap (E_g) was also determined from their absorbance recorded by UV–visible spectrophotometer in combination with the equation proposed by Wood and Tauc [19–21].

3. Results and discussion

3.1. XRD

Fig. 1 shows XRD spectra of the products synthesized using different conditions. Their diffraction peaks were indexed and specified as orthorhombic Bi_2S_3 with no detection of any impurities such as Bi_2O_3 and metallic bismuth. Calculated lattice parameters were a = 11.15 Å, b = 11.27 Å and c = 3.96 Å, which were in good accordance with those of the JCPDS file no.17-0320 [22]. In HEC-free solutions, and at 160 °C and 180 °C for 2 h, the diffraction peaks were rather broad, indicating that the products were not good crystalline with lattice atoms in disorder arrangement. By increasing only the temperature to 200 °C, or both the temperature to 200 °C and the time to 20 h, the spectra became narrower and sharper, and the lattice atoms became more ordered. When different amounts of HEC were also added to the solutions, and the hydrothermal process was done at 200 °C for 20 h, the crystalline degree continuously increased with an increase in the amounts of HEC adding, and the lattice atoms were in better order. The spectrum was the sharpest and highest, for 1.00 g HEC-added solution. At this stage, the product was the best crystal and the lattice atoms were at the most order.

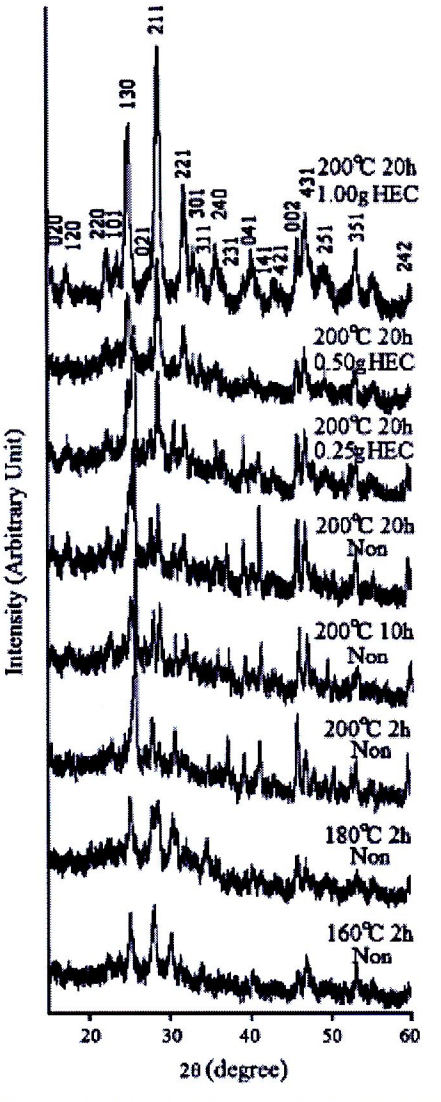

Fig. 1. XRD spectra of Bi_2S_3 hydrothermally synthesized in the solutions containing different amounts of HEC at different temperatures and lengths of time.

3.2. SEM, TEM and HRTEM

Figs. 2 and 3 show SEM, TEM and HRTEM images of Bi_2S_3 hydrothermally synthesized in the acid-catalyst solutions containing different amounts of HEC at 200 °C for 20 h. In HEC-free solution (Figs. 2a and 3a–c), a number of irregular nanorods with different sizes and orientations clustered together in group. Their surfaces were very smooth. The (211) crystallographic planes tilted at an angle of 88° to the corresponding axial nanorod. In 0.25 g HEC-added solution (Figs. 2b and 3d–f), the clusters became urchin-like shape, and were composed of a number of well-aligned regular nanorods with 50 nm diameter radiated from the central cores and self-organized into perfect spherical-like colonies. A number of the (220) crystallographic planes were detected to be parallel with their [001] preferential growth direction, in good accordance with the previous reports [5–7,21,23,24]. These urchin-like colonies will not be separated into discrete nanorods even by the ultrasonic vibration, indicating that these architectures were closely connected and combined together in groups. When HEC was increased to be 0.50 g, the urchin-like colonies (Figs. 2c and 3g–i) were not complete, and the regular nanorods were partially oriented to their centers. The (220) planes were still in parallel with the [001] growth direction. In 1.00 g HEC-added solution (Figs. 2d, 3j–l), the urchin structure was no longer detected. The product was composed of regular nanorods clustered in groups, of which their growth directions remained in the [001] direction – in parallel with the (220) planes.

3.3. SAED and simulation

The SAED patterns of Bi_2S_3 hydrothermally synthesized at 200 °C for 20 h in the solutions containing different amounts of HEC are shown in Fig. 4a–c. They clearly demonstrated that the

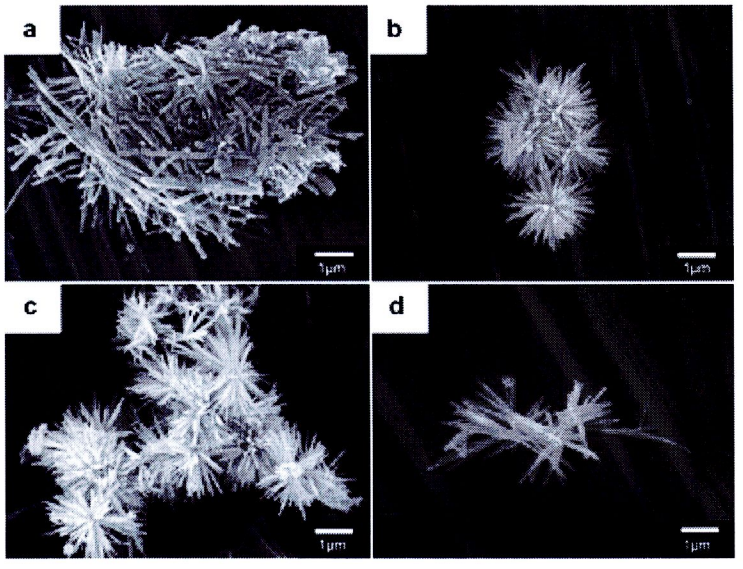

Fig. 2. SEM images of Bi_2S_3 hydrothermally synthesized in the solutions containing (a) 0.00 g, (b) 0.25 g, (c) 0.50 g, and (d) 1.00 g HEC at 200 °C for 20 h.

products were single crystalline in nature with the electron beam in the [100] direction, although they were synthesized using different masses of HEC. These patterns were also indexed [25,26] and interpreted as orthorhombic Bi_2S_3 [22]. A simulated electron diffraction pattern [27] (Fig. 4d) appeared as systematic array of spots, corresponding to these three SAED patterns.

3.4. Formation mechanism

In the present research, the formation of Bi_2S_3 was proposed as follows. At elevated temperature, thiourea was hydrolyzed to produce H_2S via the acid-catalyst hydrolysis process, which was followed by the generation of HS^-. Subsequently, HS^- reacted with

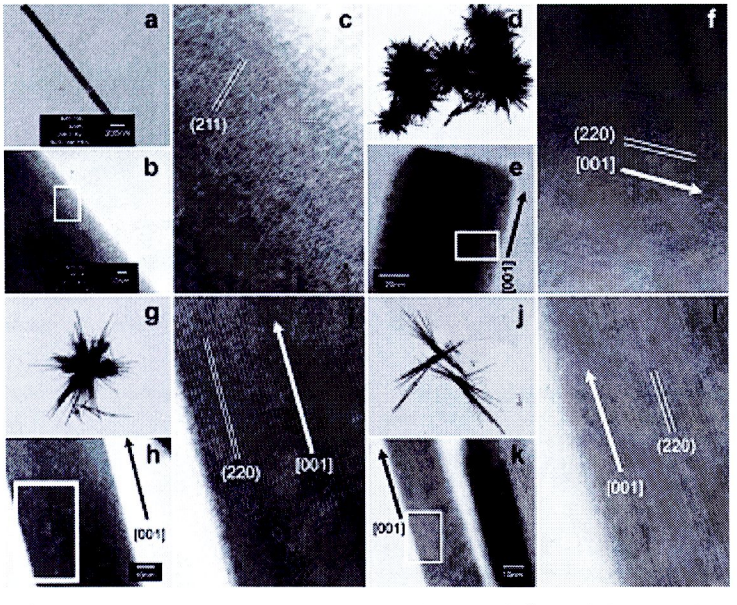

Fig. 3. TEM and HRTEM images of Bi_2S_3 hydrothermally synthesized in the solutions containing (a–c) 0.00 g, (d–f) 0.25 g, (g–i) 0.50 g, and (j–l) 1.00 g HEC at 200 °C for 20 h.

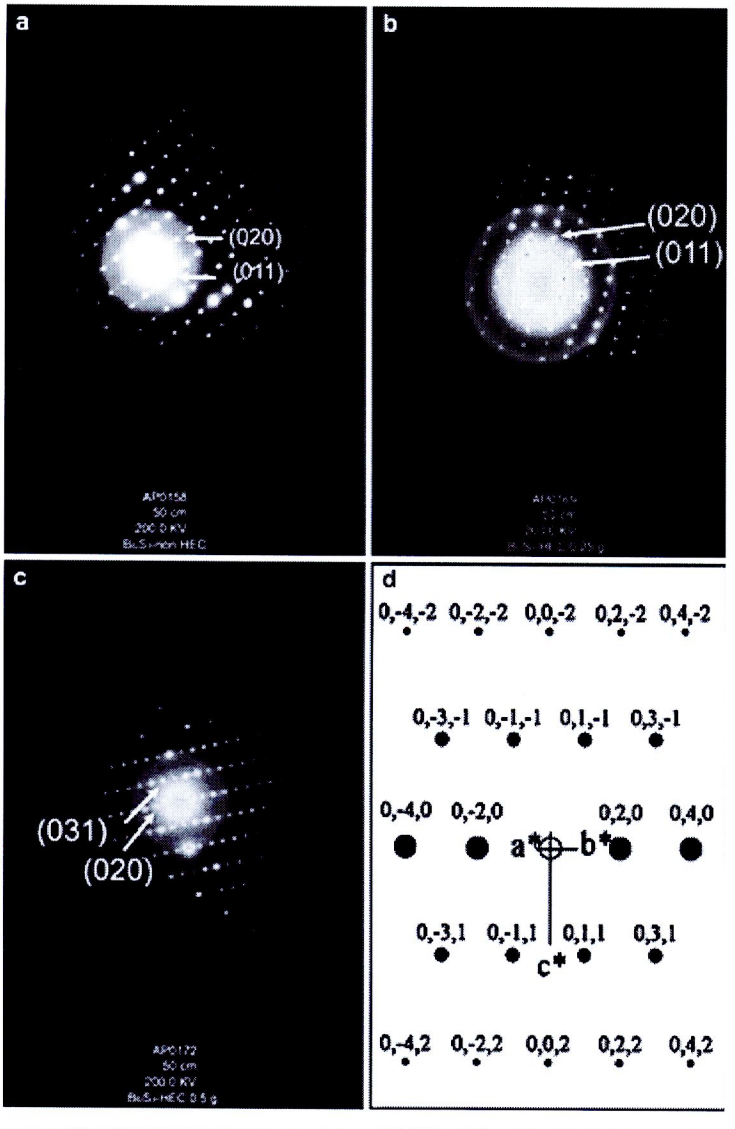

Fig. 4. SAED patterns of Bi_2S_3 hydrothermally synthesized in the solutions containing (a–c) 0.00, 0.25 and 1.00 g HEC at 200 °C for 20 h, respectively, and (d) the simulated pattern.

Bi^{3+} in aqueous (aq) solution by the hydrothermal reaction to form Bi_2S_3 precipitate.

$$NH_2CSNH_2 + H_2O \rightarrow NH_2CONH_2 + H_2S \quad (1)$$

$$H_2S \rightarrow HS^- + H^+ \quad (2)$$

$$2Bi^{3+}(aq) + 3HS^-(aq) + 3H_2O \rightarrow Bi_2S_3(s) + 3H_3O^+ \quad (3)$$

Bi_2S_3 is a laminated structure with infinite chains along the [001] direction (Fig. 5). There are two layers per unit cell. The Bi–S interactions along the infinite chains are mainly covalent, but the layers are held together by a weaker van der Waals interatomic attraction [24,28]. These support the higher growth rate along the [001] direction, and the lower rate along the horizontal direction. During the 200 °C and 20 h hydrothermal synthesis in HEC-free solution, Bi_2S_3 nuclei formed and grew along the [001] direction [5–7,21,23,28] of irregular nanorods with different orientations, grouping together as a cluster. HEC is a long macromolecule with a number of hydroxyl groups. It functions as a soft template and capping agent. At high temperature, some long-chain molecules could be broken into shorter ones. When 0.25 g HEC was added to

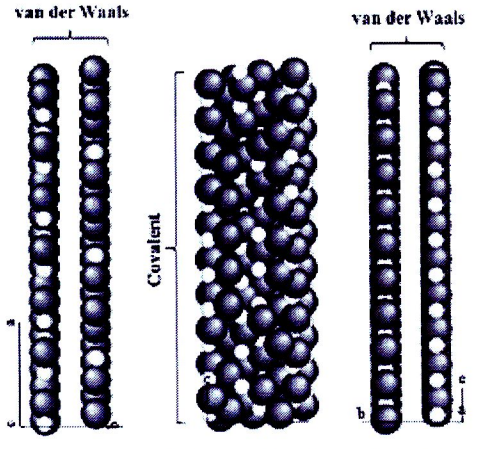

Fig. 5. Consistent modeling of Bi_2S_3 structure. (White balls = Bi^{3+}, Black balls = S^{2-}).

the solution. HEC chain molecules were long enough to entangle the nuclei in the solution to form very tiny spheres with active sites on the surfaces. Nanocrystals grew out of the active sites. Simultaneously, HEC molecules adsorbed on the side walls of the nanocrystals, of which their lateral growth was inhibited to some extent. The tips were the most active, and these nanocrystals became lengthened [23]. Their Bi–S inherent chain type structure [2,13,23,24,28] also promoted the formation of nanocrystals, growing from cores. Thus Bi_2S_3 nanorods with homogeneous diameter grew out of the active sites on the spheres, and urchin-like colonies of regular nanorods were fully synthesized. In 0.50 g HEC-added solution, HEC in the solution became excessive. The tiny spheres with active sites on surfaces and the growing nanorods out of cores were inhibited – causing the product to be incomplete urchin-like colonies. When more HEC was added until the solution contained 1.00 g HEC, the extent of inhibiting became more powerful, and the urchin-like colonies were not able to be synthesized. In the present research, regular nanorods of complete urchin-like colonies were synthesized by the 200 °C and 20 h hydrothermal reaction of bismuth nitrate ($Bi(NO_3)_3$) and thiourea (NH_2CSNH_2) in an acid-catalyst solution containing 0.25 g HEC. Schematic diagram for the formation of the as-synthesized Bi_2S_3 with different morphologies using different amounts of HEC is shown in Fig. 6. The stability and reliability of using polymers as templates were proved by other experiments, as follows. The uniformity in length and diameter of nanowires was able to be improved by the addition of some polymers (polyacrylonitrile (PAN) by template synthesis of CdS/PAN composited nanowires under de-aerated solutions [29], polyacrylamide (PAA) by polymer-controlled growth of CdS nanowires [30], and poly (vinyl alcohol) (PVA) by solvothermal synthesis of CdSe and CdTe nanowires [31]) as coordination agents to stabilize ionic concentrations of the solutions. Different polymeric templates (PVA, polyethylene glycol (PEG), and polyvinylpyrrolidone (PVP)) were used to control shapes and sizes of CdS by hydrothermal method. These products were composed of a number of nanorods in clusters, flower-like clusters of nanospears, nanorods and nanoplates in polymer-free, PVA-, PEG- and PVP-added solutions [23].

3.5. Ultraviolet–visible absorption

The UV–vis absorption spectra of the orthorhombic Bi_2S_3 synthesized in the solutions containing different amounts of HEC at 200 °C for 20 h are shown in Fig. 7. The absorption spectra of the products synthesized under different conditions were used to determine their energy band gaps, corresponding to the electronic transition between conduction and valence bands. In the high energy region of the absorption edge, the absorption is monotonously increased with the increasing of photon energy, represented by a straight line

$$\alpha h\nu = (h\nu - Eg)^n \quad (4)$$

where α, h, ν, E_g and n are the absorbance, Planck constant, photon frequency, Tauc optical band gap, and pure number associated with the different types of electronic transitions. For $n = 1/2, 2, 3/2$ and 3,

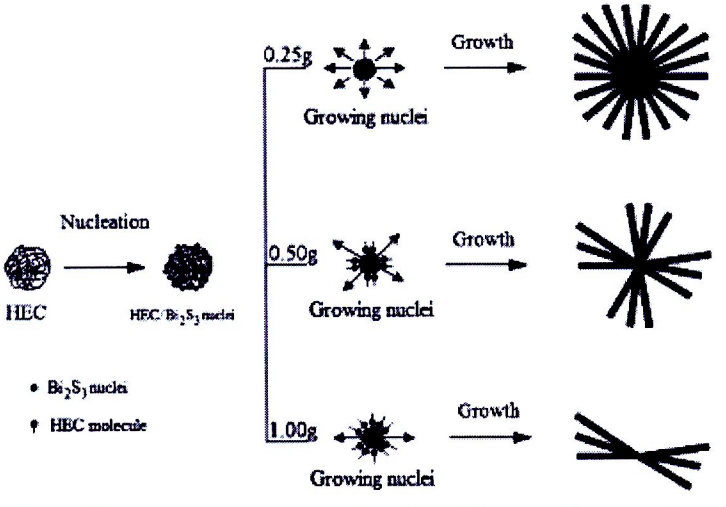

Fig. 6. Schematic diagram for the formation of Bi_2S_3 in the solutions containing 0.25 g, 0.50 g and 1.00 g HEC. The arrows on the growing nuclei were the allowed growth directions.

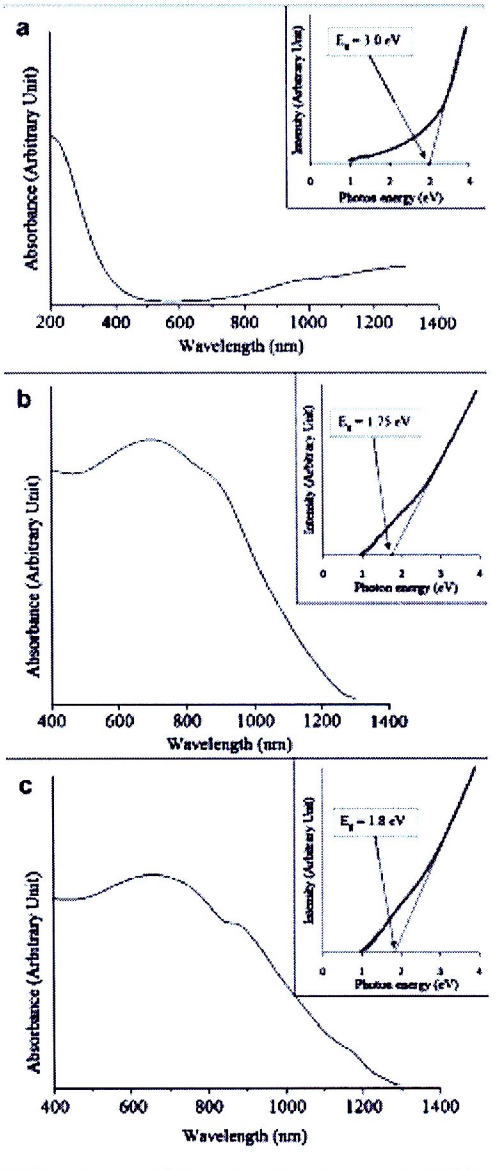

Fig. 7. UV–vis absorption of Bi_2S_3 hydrothermally synthesized in the (a) HEC-free, (b) 0.25 g HEC-added, and (c) 1.00 g HEC-added solutions at 200 °C for 20 h.

the transitions are the direct allowed, indirect allowed, direct forbidden, and indirect forbidden, respectively [19–21,24]. For orthorhombic Bi_2S_3, the pure number equals to 1/2 [21,24,32]. The direct band gaps of Bi_2S_3 with the shapes of nanorods, complete urchin-like colonies, and highly crystalline nanorods were estimated to be 3.0, 1.75, and 1.8 eV, respectively. These differences were influenced by not only the morphology but also the crystalline degree. The difference in energy band gap was possibly influenced by the synthesis process, morphologies, average crystallite size, and

Table 1
Bi_2S_3 nanostructures synthesized by different conditions and methods.

	Starting materials	Procedures	Products
1	$Bi(NO_3)_3 \cdot 5H_2O$ + diaspylic acid + H_2O	80–160 °C and 5–18 h hydrothermal reaction (HR)	Nanoparticles (NPs), nanorods (NRs) nanobelts (NBs) and nanoflowers ($NFIs$) [19]
2	$Bi(NO_3)_3 \cdot 5H_2O$ + thiourea (TU) + citric acid + H_2O	140 °C and 10 h HR	Network nanostructure of cross-linked single-crystalline nanowires (NWs) [10]
3	$Bi(NO_3)_3 \cdot 5H_2O$ + TU + H_2O	140 °C HR for different lengths of time	Urchin-like nanostructures of needle
4	$Bi(NO_3)_3 \cdot 5H_2O$ + $C_{10}H_{14}N_2O_8Na_2 \cdot 2H_2O$ ($EDTA\ Na_2$) + L-cysteine + H_2O	180 °C and 12 h HR	NRs, solid NRs, and NWs [11]
5	$Bi(NO_3)_3 \cdot 5H_2O$ + TU + H_2O + HNO_3	180 °C and 12 h HR	Chrysanthemum-like microcrystals [12]
6	$Bi(NO_3)_3 \cdot 5H_2O$ + TU + H_2O	140 °C and 10 h seed-assisted HR	NRs and nanostructured flowers [33]
7	$Bi(NO_3)_3 \cdot 5H_2O$ + different solvents (acetone, MeOH, $EtOH$, H_2O, ethylene glycol (EG) and glycerol) + $Na_2S \cdot 9H_2O$ + urea + H_2O	120 °C and 12 h solvothermal reaction (SR)	3D nanoflake architecture [15]
8	NaOH + EtOH + thioglycolic acid + $Bi(NO_3)_3 \cdot 5H_2O$ in N_2 stream to form $Bi(SCOPh)_3$ precursor (PC) in ice-bath for 15 min. Products with different morphologies were synthesized.		Nanotubes (NTs) and NRs [34]
	(8.1) PC + $C_{12}H_{25}SH$ + $[CH_3(CH_2)_3]_2PO$	150 °C and 1 h heat in N_2 at 70 °C + BOH (process)	NRs
	(8.2) PC + PVP + EG	150 °C and 1 h heat	Dandelion-like nanostructure
	(8.3) PC + pyridine + H_2O	1 h reflux at room temperature (T_r)	Nanoleaves (NLs)
	(8.4) $Bi(NO_3)_3 \cdot 5H_2O$ + pyridine + NaOH + H_2O	150 °C and 3.5 h HR	$NFIs$
	(8.5) $Bi(NO_3)_3 \cdot 5H_2O$ + pyridine + NaOH + diphenylalanine (ref) + H_2O	150 °C and 3.5 h HR	Nanoflakes [16]
9	$Bi(NO_3)_3 \cdot 5H_2O$ + TU + H_2O + HNO_3 + PVP	200 °C and 1 h by 300 W microwave (MCW) – HR	Flower-like structure [21]
10	$Bi(NO_3)_3 \cdot 5H_2O$ + $Na_2S \cdot 5H_2O$ + NaOH + eq EtOH (dissolute) mixed solvent	150 °C and 4 h MCW-SR	1D NWs [24]
11	$Bi(NO_3)_3 \cdot 5H_2O$ + TU + EG	800 W and 5 min microwave-radiation ($MCWR$)	3D flower-like superstructures [2]
12	$Bi(NO_3)_3 \cdot 5H_2O$ + thioacetamide (TAA) or TU + different solvents (H_2O, EG, and propylene glycol) + HNO_3	180 W and 20 min MCWR	NPs, NRs, and $NFIs$ [35]

15	$Bi(NO_3)_3$·5H$_2$O + TU + EG	197 °C and 30 min rapid pulsed process (refluxing process)	Urchin-like patterns of NRs [36]
16	Bismuth citrate + TU + CTAB + EG	160 °C and 2 h refluxing	3D monoflakes [37]
17	$Bi(NO_3)_3$·5H$_2$O + TAA + HCl + H$_2$O	15 °C and 5 d high yield precipitation	NR bundles, 3D cluster-like nanostructures [38]
18	$Bi(NO_3)_3$·5H$_2$O + $Na_2S_2O_3$ + EDTA or methanediamine-(TEA) or sodium tartrate) + H_2O, $Bi(NO_3)_3$·5H$_2$O + DMA + TEA + H_2O, $Bi(NO_3)_3$·5H$_2$O + $Na_2S_2O_3$ + TEA + N, N dimethylformamide + H_2O	343 K and 120 min solvothermal method	NRs [39]
19	$Bi(NO_3)_3$·5H$_2$O + TAA + nitrilotriacetic acid + H_2O	25 °C and 5 h photochemical synthesis (UV radiation)	Nanofibers [40]
20	Bismuth nitrate + $Na_2S_2O_3$ + EDTA in acidic medium	Chemical bath deposition at T_r	Nanostructured thin film on glass substrate [41]
21	$Bi(NO_3)_3$·5H$_2$O + $Na_2S_2O_3$·5H$_2$O + Na$_2$EDTA·2H$_2$O + H_2O (pH 4.5, adjusted using NH_4OH)	3 V cathodic electrodeposition	Thin films of NRs on indium tin oxide (ITO) glass [42]

degree of structural order-disorder. In the present research, Bi_2S_3 with 1.75 eV and 1.8 eV band gaps are promising candidates for using as solar energy converting devices [5,32].

3.6. Bi_2S_3 synthesized by other researchers

Bi_2S_3 nanostructures with different morphologies were also synthesized by hydrothermal method using different starting materials and conditions, as well as by other methods, shown in Table 1. It should be noted that the morphologies of the present and previous reports were controlled by several parameters, such as Bi and S sources, additives, pH values, solvents, temperatures, pressures, lengths of time, and synthesis methods.

4. Conclusions

Orthorhombic Bi_2S_3 regular and irregular nanorods were successfully synthesized from bismuth nitrate ($Bi(NO_3)_3$) and thiourea (NH_2CSNH_2) in the acid-catalyst solutions containing different amounts of HEC by the 200 °C and 20 h hydrothermal reactions. Both the interpreted and simulated patterns show that all products were orthorhombic Bi_2S_3 with no detection of any impurities. Those of a cluster of irregular nanorods, complete urchin-like colonies of regular nanorods, and highly crystalline regular nanorods were hydrothermally synthesized in the HEC-free, 0.25 g HEC-added, and 1.00 g HEC-added solutions, with their direct allowed band gaps of 3.00, 1.75 and 1.8 eV, respectively.

Acknowledgements

We wish to give thank the Thailand's Office of the Higher Education Commission for providing financial support through the National Research University Project, and the National Research Council of Thailand for financial Support.

References

[1] J. Ota, S.K. Srivastava, J. Phys. Chem. C 111 (2007) 12280–12284.
[2] J. Liu, Q. Han, X. Yang, L. Li, X. Wang, Mater. Lett. 61 (2007) 2883–2886.
[3] C.J. Tang, G.Z. Wang, H.Q. Wang, Y.X. Zhang, G.H. Li, Mater. Lett. 62 (2008) 3663–3665.
[4] M.W. Shao, M.S. Mo, Y. Cui, C. Chen, Y.T. Qian, J. Cryst. Growth 233 (2001) 799–802.
[5] F. Wei, J. Zhang, L. Wang, Z.K. Zhang, Cryst. Growth Des. 6 (2006) 1942–1944.
[6] W. Lou, M. Chen, X. Wang, W. Liu, Chem. Mater. 19 (2007) 872–878.
[7] Y. Yu, C.H. Jin, R.H. Wang, Q. Chen, L.M. Peng, J. Phys. Chem. B 109 (2005) 18772–18776.
[8] Z. Quan, C. Li, X. Zhang, J. Yang, P. Yang, C. Zhang, J. Lin, Cryst. Growth Des. 8 (2008) 2384–2392.
[9] M. Salavati-Niasari, D. Ghanbari, F. Davar, J. Alloys Compd. 488 (2009) 442–447.
[10] C.J. Tang, J.F. Su, Q.B. Hu, Y.X. Yang, C.Q. Wang, C.H. Zhao, C.H. Zang, Y.S. Zhang, Solid State Sci. 13 (2011) 1152–1156.
[11] C. Yang, C. Wang, F. Su, C. Zang, Y. Yang, Z. Zong, Y. Zhang, Solid State Sci. 12 (2010) 1352–1356.
[12] J. Jiang, G. Gao, R. Yu, C. Qiu, X. Liu, Solid State Sci. 13 (2011) 356–360.
[13] J. Liu, Q. Han, X. Yang, L. Li, X. Wang, Mater. Lett. 61 (2007) 3425–3428.
[14] C. Xie, Z.P. Qiao, M.H. Zeng, X.M. Chen, S.L. Gao, Cryst. Growth Des. 4 (2004) 513–515.
[15] C.J. Tang, Y.X. Zhang, X.C. Dou, G.H. Li, J. Cryst. Growth 312 (2010) 992–997.
[16] L. Tian, H.Y. Tan, J.J. Vittal, Cryst. Growth Des. 8 (2008) 734–738.
[17] B. Zhang, X. Ye, W. Hou, Y. Zhao, Y. Xie, J. Phys. Chem. B 110 (2006) 8978–8985.
[18] T. Thongtem, C. Pilapong, S. Thongtem, Curr. Appl. Phys. 9 (2009) 1272–1277.
[19] J.C. Sczancoski, M.O.R. Somtu, L.S. Cavalcante, M.R. Joya, P.S. Pizani, J.A. Varela, E. Longo, M.S. Li, J.A. Andrés, J. Phys. Chem. C 113 (2009) 5812–5822.
[20] J.C. Sczancoski, L.S. Cavalcante, M.R. Joya, J.W.M. Espinosa, P.S. Pizani, J.A. Varela, E. Longo, J. Col. Interf. Sci. 330 (2009) 227–236.
[21] T. Thongtem, C. Pilapong, J. Kaowichan, A. Phuruangrat, S. Thongtem, J. Alloys Compd. 500 (2010) 195–199.
[22] Powder Diffract. File, JCPDS-ICDD, 12 Campus Boulevard, Newtown Square, PA 19073–3273, U.S.A. 2001.
[23] C. Pilapong, T. Thongtem, S. Thongtem, J. Phys. Chem. Solids 71 (2010) 712–715.

[24] W. Li, Mater. Lett. 62 (2008) 243–245.
[25] K.W. Andrews, D.J. Dyson, S.R. Keown, Interpret. Electr. Diffract. Plenum Press, New York, 1971.
[26] D.B. Williams, C.B. Carter, Transmis. Electr. Microscopy, Plenum Press, New York, 1996.
[27] C. Boudias, D. Monceau, CaRIne Crystallography 3.1, DIVERGENT S.A., Centre de Transfert, 60200 Compiègne, France, 1989–1998.
[28] Z. Liu, D. Xu, J. Liang, W. Lin, W. Yu, Y. Qian, J. Solid State Chem. 178 (2005) 950–955.
[29] M. Chen, Y. Xie, H. Chen, X. Qian, Y. Zhu, Y. Qian, J. Coll. Interf. Sci. 239 (2000) 217–221.
[30] J.H. Zhan, X.C. Yang, D.W. Wang, S.D. Li, Y. Xie, Y. Xia, Y. Qian, Adv. Mater. 12 (2000) 1348–1351.
[31] Q. Yang, K. Tang, C. Wang, Y. Qian, S. Zhang, J. Phys. Chem. B 106 (2002) 9227–9230.
[32] V.V. Kuratieva, S.N. Katorka, C.H. Brosseau, Mater. Chem. Phys. 64 (2000) 166–169.
[33] A. Phuruangrat, T. Thongtem, S. Thongtem, Mater. Lett. 63 (2009) 1486–1488.
[34] C. Zhu, P. Liu, J. Zhou, X. Bian, X. Wang, J. Li, B. Chen, Mater. Lett. 62 (2008) 2335–2338.
[35] T. Thongtem, A. Phuruangrat, S. Wannapop, S. Thongtem, Mater. Lett. 64 (2010) 122–124.
[36] C. Shen, D. Chen, K. Tang, F. Li, Y. Qian, Chem. Phys. Lett. 370 (2003) 334–337.
[37] J. Wu, F. Qin, F.Y.F. Chan, C. Cheng, H. Li, Z. Lu, R. Chen, Mater. Lett. 64 (2010) 287–290.
[38] L. Dong, Y. Chu, W. Zhang, Mater. Lett. 62 (2008) 4286–4272.
[39] H. Wang, J.J. Zhu, J.M. Zhu, H.Y. Chen, J. Phys. Chem. B 106 (2002) 3848–3854.
[40] W.B. Zhao, J.J. Zhu, Y. Zhao, H.Y. Chen, Mater. Sci. Eng. B 110 (2004) 307–313.
[41] A.U. Ubale, Mater. Chem. Phys. 121 (2010) 555–560.
[42] W. Yan, H. Jian-feng, C. Li-yuh, Z. Hui, H. Hai-yan, W. Jian-peng, Appl. Surf. Sci. 255 (2009) 7749–7753.

Journal of Alloys and Compounds 496 (2010) 129–132

Contents lists available at ScienceDirect

Journal of Alloys and Compounds

journal homepage: www.elsevier.com/locate/jallcom

Letter

Synthesis of novel ZnS/$ZnAl_2S_4$ core/shell nanocomposites using a facile solvothermal route

Titipun Thongtem[a,*], Chalermchai Pilapong[a], Somchai Thongtem[b]

[a] Department of Chemistry, Faculty of Science, Chiang Mai University, Chiang Mai 50200, Thailand
[b] Department of Physics and Materials Science, Faculty of Science, Chiang Mai University, Chiang Mai 50200, Thailand

ARTICLE INFO

Article history:
Received 13 January 2010
Received in revised form 14 February 2010
Accepted 16 February 2010
Available online 24 February 2010

Keywords:
Electron microscopy
Luminescence
Nanocomposites
Semiconductors
X-ray techniques

ABSTRACT

Novel ZnS/$ZnAl_2S_4$ core/shell nanocomposites were successfully synthesized by a surfactant-free solvothermal reaction at 200 °C for 10 h. XRD, FESEM, TEM, and photoluminescence (PL) were used to characterize these novel nanocomposites—build-up of zinc blende ZnS nanorod cores and wurtzite $ZnAl_2S_4$ shells. PL emission of ZnS nanorod cores were influenced by $ZnAl_2S_4$ shells covered around them. A formation mechanism of ZnS/$ZnAl_2S_4$ core/shell nanocomposites was also explained to relate with these results.

1. Introduction

Presently, nanocomposites have attracted much attention to a number of material scientists and engineers, due to their novel properties. These were caused by small size, large surface area and quantum-dimension, which are able to improve their physical and chemical properties. Different nanocomposites, including core/shell Ag/Au nanoparticles [1], metal-semiconductor Zn–ZnO core–shell nanobelts and nanotubes [2], CdS/ZnS core/shell nanocrystals [3], iron oxide/polystyrene core/shell nanoparticles [4], and TiO_2/SiO_2 core/shell nanocable arrays [5] were successfully synthesized. To the best of our knowledge, there are no reports on the synthesis of binary semiconductor–ternary semiconductor core–shell nanocomposites, which have promising properties for optoelectronic and photocatalytic applications.

As an important II–VI semiconductor with unique optical and electrical properties, ZnS with 3.7 eV band gap at 300 K, has shown a wide range of technological applications in electroluminescent and non-linear optical devices [6], and base material for cathode-ray tubes [7]. For semiconducting ternary chalcogenides, AB_2C_4 (A = Cu, Ag, Zn, Cd, etc.; B = Al, Ga, In; C = S, Se, Te) are also very attractive, due to their unique thermoelectric and photocatalytic properties [8–10]. One of them is $ZnAl_2S_4$, which has different structures [11]. Thus novel ZnS/$ZnAl_2S_4$

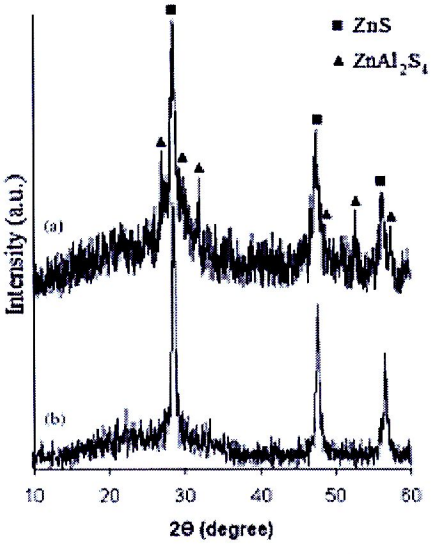

Fig. 1. XRD spectra of (a) ZnS/$ZnAl_2S_4$ nanocomposites and (b) ZnS nanorods.

* Corresponding author. Tel.: +66 53 943344; fax: +66 53 892277.
E-mail address: ttpthongtem@hotmail.com (T. Thongtem).

0925-8388/$ – see front matter © 2010 Elsevier B.V. All rights reserved.
doi:10.1016/j.jallcom.2010.02.134

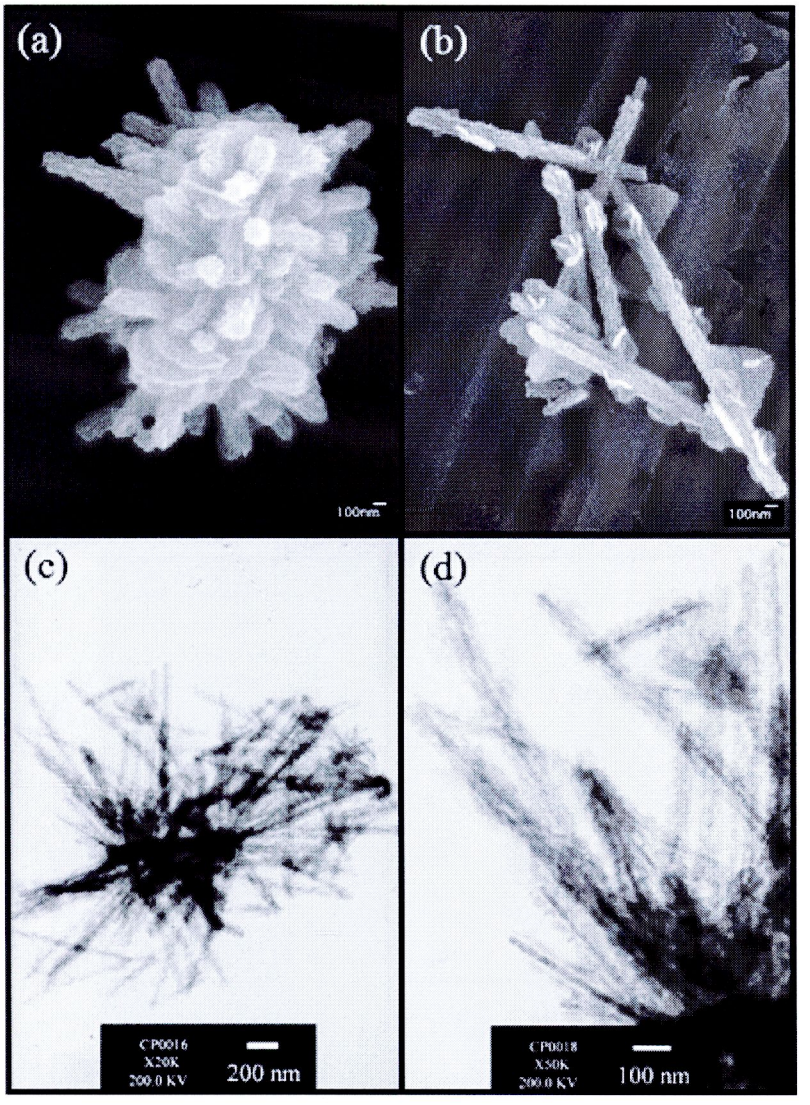

Fig. 2. (a and b) FESEM and (c and d) TEM images of ZnS/$ZnAl_2S_4$ core/shell nanocomposites.

core/shell nanocomposites synthesized via a facile solvothermal route without the use of any surfactants or additives, are reported.

2. Experiment

For this typical procedure, 0.1 mmol $Zn(NO_3)_2 \cdot 6H_2O$, 0.2 mmol $AlCl_3$ and 0.6 mmol thiourea (excess) were dissolved in 30 ml propylene glycol. Similar solution without $AlCl_3$ adding was also prepared. The reactions solvothermally proceeded at 200 °C for 10 h to form precipitates. After washing with DI water and 95% ethanol, and drying at 70 °C for 24 h, these products were characterized to determine their phases, morphologies and photoluminescence.

3. Results and discussion

XRD spectra (Fig. 1) were specified as ZnS/$ZnAl_2S_4$ nanocomposites (top) and ZnS (bottom), corresponding to the JCPDS database nos. 05-0566 for cubic zinc blende ZnS (a = 5.4060 Å) and 32-1458 for hcp wurtzite $ZnAl_2S_4$ (a = 3.7550 Å, c = 6.1320 Å) [11]. The top has composited diffraction peaks arising from both zinc blende ZnS (cubic) and wurtzite $ZnAl_2S_4$ (hcp). Calculated lattice constant [12] of cubic ZnS is a = 5.40 Å—very close to the JCPDS database [11]. For hexagonal $ZnAl_2S_4$, it is composed of layer-structured atoms of S–Zn–S–Al–S–Al–S, repeated in sequence along the c-axis [13]. Cal-

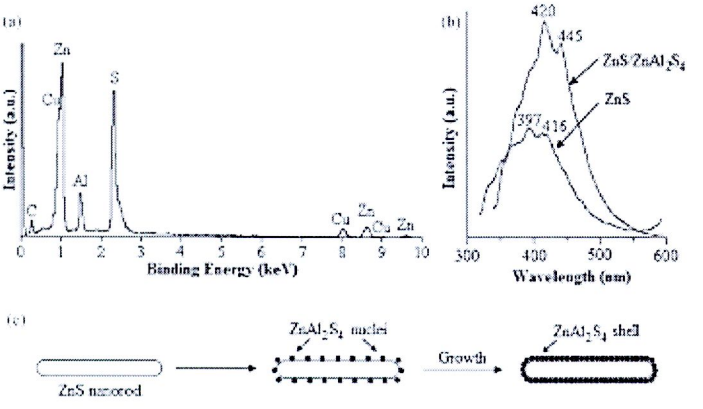

Fig. 3. (a) EDX and (b) PL spectra of ZnS/ZnAl$_2$S$_4$ core/shell nanocomposites and ZnS nanorods. (c) Schematic diagram used to explain the formation of ZnS/ZnAl$_2$S$_4$ core/shell nanocomposites.

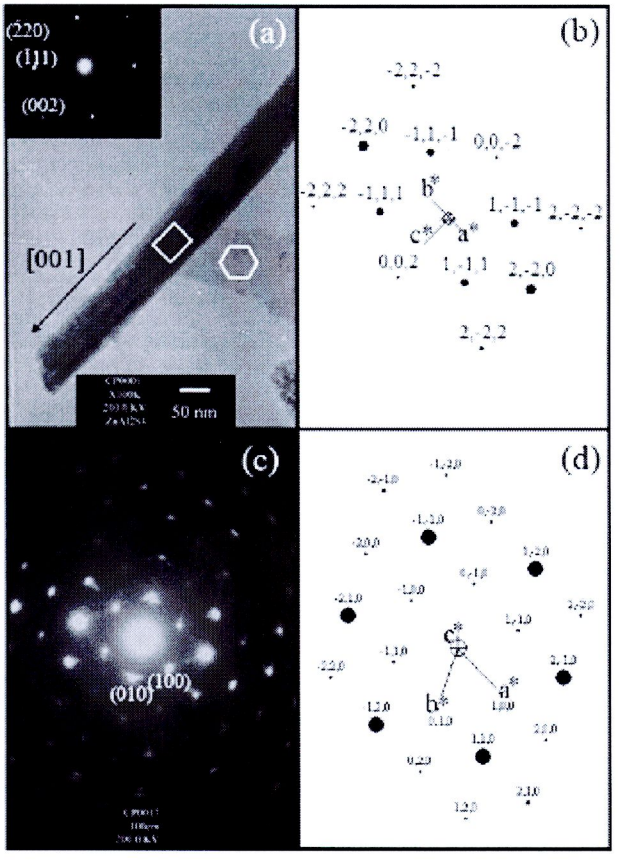

Fig. 4. TEM image (a) and SAED patterns of ZnS core (inset of a) and ZnAl$_2$S$_4$ shell (c) with their corresponding simulated patterns (b and d).

culated lattice constants [12] are a = 3.75 Å and c = 6.05 Å. The last is less than its JCPDS database [11], due to the more compact layered structure of $ZnAl_2S_4$ along the c-axis.

FESEM and TEM images (Fig. 2) show morphologies of ZnS/$ZnAl_2S_4$ core/shell nanocomposites, composed of a number of nanorods with rough surfaces, aligning in different orientations. Nanorod cores were covered with shells of assemblies of nanoparticles. The difference of crystal structures of cubic ZnS cores and hcp wurtzite $ZnAl_2S_4$ shells—the mismatched interface, was able to generate defects in the composites. The defect generation in other products was also explained: ZnS–ZnO heterogeneous microstructured flowers by Nie et al. [14], ZnO–ZnS nanocomposites by Li et al. [15], and ZnO–ZnS core–shell microspindles by Li et al. [16]. EDX spectrum (Fig. 3a) revealed the presence of Zn, Al and S containing in these nanocomposites [17]. Cu and C belonging to a copper stub and carbon tape, were also detected. When no $AlCl_3$ was added in the solution, the product is in the shape of nanorods (unshown result).

To identify the ZnS cores and $ZnAl_2S_4$ shells, the nanocomposites were put in a beaker containing 95% ethanol. Ultrasonic oscillating proceeded for 1 h to separate shells from nanorod cores. The solution of dispersed nanorods and shells was dropped on a copper grid and dried in ambient atmosphere. By using TEM, a nanorod with its growth in the [0 0 1] direction, and its nearby shell (Fig. 4a) were clearly detected. This growth direction is in accordance with that of ZnS nanorods synthesized by Zhu et al. [18]. Two SAED patterns at a rectangle and hexagon of Fig. 4a were indexed [19] and interpreted as zinc blende ZnS core (Fig. 4a (inset)) and wurtzite $ZnAl_2S_4$ shell (Fig. 4c) [11]. It is worth noting that these interpreted diffraction patterns are in good accordance with their corresponding simulations [20] (Fig. 4b and d).

By using a 300 nm excitation wavelength at room temperature, PL emissions (Fig. 3b) of ZnS/$ZnAl_2S_4$ core/shell nanocomposites and pure ZnS nanorods were determined. There were two distinct peaks at 397 and 416 nm for pure ZnS nanorods, originating from self-activated centers and defects, respectively [21]. PL emission of ZnS/$ZnAl_2S_4$ core/shell nanocomposites is at 420 and 445 nm, which are red-shift relative to those of pure ZnS nanorods. The intensity is obviously enhanced. These facts were caused by defects in the nanocomposites [14].

To synthesize ZnS/$ZnAl_2S_4$ core/shell nanocomposites by the solvothermal reaction of $Zn(NO_3)_2{\cdot}6H_2O$, $AlCl_3$ and thiourea in propylene glycol at 200 °C for 10 h, ZnS began to exist and grew to form nanorods with different orientations. Zn^{2+} ions in the solution became lesser with the prolonged time. Subsequently, $ZnAl_2S_4$ began to nucleate on ZnS nanorods (rough surfaces). As time passed, more $ZnAl_2S_4$ nanoparticles were synthesized to form shells of assemblies of nanoparticles around ZnS nanorod cores (Fig. 3c). Only ZnS nanorods were synthesized in the solution with no $AlCl_3$ adding.

4. Conclusions

ZnS/$ZnAl_2S_4$ core/shell nanocomposites and ZnS nanorods were successfully synthesized by the solvothermal reactions at 200 °C for 10 h. The nanocomposites of zinc blende ZnS nanorod cores covered with wurtzite $ZnAl_2S_4$ shells, and bare ZnS nanorods were detected. Their PL emissions were at approximately 397 nm for pure ZnS nanorods, originating from self-activated centers, and 420 nm for ZnS/$ZnAl_2S_4$ core/shell nanocomposites. The presence of $ZnAl_2S_4$ shells covered on ZnS nanorods is able to generate more defects in the composites, which can play the role in their optical properties. A formation mechanism of ZnS/$ZnAl_2S_4$ core/shell nanocomposites was also proposed for the present research.

Acknowledgement

This research was supported by the National Research University Project for Chiang Mai University, Commission on Higher Education, Ministry of Education, Thailand.

References

[1] Y.W. Cao, R. Jin, C.A. Mirkin, J. Am. Chem. Soc. 123 (2001) 7961–7962.
[2] X.Y. Kong, Y. Ding, Z.L. Wang, J. Phys. Chem. B 108 (2004) 570–574.
[3] Y. Yang, O. Chen, A. Angerhofer, Y.C. Cao, J. Am. Chem. Soc. 128 (2006) 12428–12429.
[4] C. Li, J. Fan, R. Jiang, Y. Cao, Chem. Mater. 16 (2004) 1835–1837.
[5] H. Zhang, X. Luo, J. Xu, B. Xiang, D. Yu, J. Phys. Chem. B 108 (2004) 14866–14868.
[6] H.P. Soni, D. Parmar, N. Patel, M. Chawda, D. Bodas, Mater. Lett. 62 (2008) 2700–2703.
[7] M. Bredol, J. Merikhi, J. Mater. Sci. 33 (1998) 471–476.
[8] X. Gou, F. Cheng, Y. Shi, L. Zhang, S. Peng, J. Chen, P. Shen, J. Am. Chem. Soc. 128 (2006) 7222–7229.
[9] Y. Li, R. Dillert, D. Bahnemann, Thin Solid Films 516 (2008) 4988–4992.
[10] S. Shen, L. Zhao, L. Guo, Mater. Res. Bull. 44 (2009) 100–105.
[11] Powder Diffraction File, JCPDS-ICDD, 12 Campus Boulevard, Newtown Square, PA 19073-3273, U.S.A. (2001).
[12] C. Suryanarayana, M.G. Norton, X-ray Diffraction—A Practical Approach, Plenum Press, New York, 1998.
[13] S. Shen, L. Zhao, L. Guo, Int. J. Hydrogen Energ. 33 (2008) 4501–4510.
[14] Y. Ni, S. Yang, J. Hong, L. Zhang, W. Wu, Z. Yang, J. Phys. Chem. C 112 (2008) 8200–8205.
[15] F. Li, Y. Jiang, L. Hu, L. Liu, Z. Li, X. Huang, J. Alloys Compd. 474 (2009) 531–535.
[16] F. Li, W. Bi, L. Liu, Z. Li, X. Huang, Colloids Surf. A 334 (2009) 160–164.
[17] X-ray Absorption and Emission Energies, Oxford Instrum. Analyt., Halifax Rd., High Wycombe Bucks HP12 3SE, U.K.
[18] H. Tong, Y.J. Zhu, L.X. Yang, L. Li, L. Zhang, J. Chang, L.Q. An, S.W. Wang, J. Phys. Chem. C 111 (2007) 3893–3900.
[19] D.B. Williams, C.B. Carter, Transmission Electron Microscopy—A Textbook for Materials Science, Plenum Press, New York, 1996.
[20] C. Boudias, D. Monceau, CaRIne Crystallography 3.1, DIVERGENT S.A., Centre de Transfert, 60200 Compiègne, France, 1989–1998.
[21] J. Hu, G. Wang, C. Guo, D. Li, L. Zhang, J. Zhao, J. Lumin. 122–123 (2007) 172–175.

ELSEVIER Science Press

Trans. Nonferrous Met. Soc. China 19(2009) s105-s109

Transactions of Nonferrous Metals Society of China

www.tnmsc.cn

Silica gel-assisted solvothermal production of CdS, Cu_xS (x=1, 2) and ZnS with different morphologies

Titipun THONGTEM[1], Chalermchai PILAPONG[1], Somchai THONGTEM[2]

1. Department of Chemistry and Center for Innovation in Chemistry, Faculty of Science, Chiang Mai University, Chiang Mai, 50200, Thailand;
2. Department of Physics and Materials Science, Faculty of Science, Chiang Mai University, Chiang Mai, 50200, Thailand

Received 2 March 2009; accepted 30 May 2009

Abstract: CdS, Cu_xS (x=1, 2) and ZnS with different morphologies were produced by the solvothermal reactions of $M(CH_3COO)_2{\cdot}2H_2O$ (M=Cd, Cu and Zn) and NH_2CSNH_2 in hexane with and without silica gel as a hard template at 200 ℃ for 24 h. The product phases were detected using X-ray diffraction (XRD). Different morphologies were characterized using a scanning electron microscope (SEM). The existence of silica gel in modeling morphologies of the sulfides was characterized using Fourier transform infrared (FTIR) spectrometer. Raman spectra of different products show the vibrations at the same wavenumbers, although they are composed of different morphologies. Photoluminescence (PL) emissions of the corresponding phases with different morphologies are at the same values, but their intensities are increased by template adding.

Key words: solvothermal reaction; silica gel; CdS; Cu_xS; ZnS

1 Introduction

Presently, inorganic sulfides such as CdS, CuS, Cu_2S and ZnS have high scientific and technological interest as photonic crystals. CdS is a semiconducting material having a direct-band gap of 2.42 eV, and is able to apply for light-emitting diodes and nonlinear optics[1]. Cu_xS (x=1, 2) are able to apply for solar cells, solar absorbers, selective radiation filters for architectural windows and electroconductive films on polymers[2]. Their mixed phases are supposed to be the stoichiometric compounds. In the case of ZnS, it has a wide band gap of 3.66 eV at 300 K and shows different luminescent properties, such as photoluminescence, electroluminescence, mechanoluminescence and thermal luminescence[3]. There are different processes used to produce the sulfides, such as CdS nanoparticles by chemical process[4], CdS by free surfactant solvothermal synthesis[5], Cu_xS (x=1, 2) by asynchronous-pulse ultrasonic spray pyrolysis[2], nano- and micro-sized CuS crystals by cyclic microwave radiation[6], CuS with different morphologies by solvothermal-microwave process[7], CuS nanoparticles by sonochemistry[8], ZnS nanoballs, nanoparticles and based materials by microwave-assisted synthesis[9-11], ZnS microspheres and hollow nanospheres by hydrothermal synthesis[12], and ZnS nanoparticles by mechanochemical synthesis[13].

Recently, there are a wide variety of porous materials that have been used as the templates to model the product morphologies[14]. Among them are soft templates (surfactants) and hard templates (active carbon and mesostructured silica gel)[14-15]. There is the limitation of using active carbon, which may be oxidized by the infiltrated or metallic salts[14]. Therefore, a more inert hard template such as porous silica gel is appropriate for assisting the formation of high-surface area (nanostructured) inorganic materials[14-15]. Silica gel is also readily available, inexpensive and easy to be washed out by water. In the present research, CdS, CuS-Cu_2S mixture and ZnS with different morphologies were solvothermally produced with and without adding silica gel. The effects of the template on the products were also studied using different techniques.

Corresponding author: Titipun THONGTEM; Tel: +66-53-943344; Fax: +66-53-892277; E-mail: ttpthongtem@yahoo.com, ttpthongtem@hotmail.com

2 Experimental

Each 0.005 mol of metal acetates [$Cd(CH_3COOH)_2 \cdot 2H_2O$, $Cu(CH_3COOH)_2 \cdot 2H_2O$, $Zn(CH_3COOH)_2 \cdot 2H_2O$] and NH_2CSNH_2 was separately dissolved in 35 mL hexane and mixed in Teflon containers with and without 0.25 g silica gel as a hard template. The reactions solvothermally proceeded at 200 ℃ for 24 h. The precipitates were washed with distilled water and 95% ethanol, and dried at 70 ℃ for 24 h. The products (Table 1) were intensively characterized using a X-ray diffractometer (XRD) operated at 20 kV, 15 mA and using K_α line from a Cu target, a scanning electron microscope (SEM) operated at 15 kV, a Fourier transform infrared (FTIR) spectrometer with KBr as diluting agent and operated in the range 738−4 000 cm^{-1}, a Raman spectrometer using 50 mW Ar laser with λ=514.5 nm, and a photoluminescence (PL) spectrometer using 250, 220 and 230 nm excitation wavelengths at room temperature for CdS, CuS-Cu_2S mixture and ZnS, respectively.

Table 1 Different codes of products

Product code	Reactants	Template
N1	$Cd(CH_3COOH)_2 \cdot 2H_2O$, NH_2CSNH_2	-
N2	$Cu(CH_3COOH)_2 \cdot 2H_2O$, NH_2CSNH_2	-
N3	$Zn(CH_3COOH)_2 \cdot 2H_2O$, NH_2CSNH_2	-
S1	$Cd(CH_3COOH)_2 \cdot 2H_2O$, NH_2CSNH_2	Silica gel
S2	$Cu(CH_3COOH)_2 \cdot 2H_2O$, NH_2CSNH_2	Silica gel
S3	$Zn(CH_3COOH)_2 \cdot 2H_2O$, NH_2CSNH_2	Silica gel

3 Results and discussion

3.1 XRD analysis

The crystallographic planes of XRD spectra (Fig.1) were indexed using Bragg's law for X-ray diffraction and compared with those of the JCPDS software with reference codes 01-0647, 03-0724, 12-0175 and 01-0792 for CdS (cubic), covellite CuS (hcp), Cu_2S (cubic) and sphalerite ZnS (cubic), respectively[16]. The products are composed of CdS (cubic) for N1 and S1, a mixture of covellite CuS (hcp) and Cu_2S (cubic) labeled with the asterisks (*) for N2 and S2, and sphalerite ZnS (cubic) for N3 and S3. XRD spectrum of silica gel (Fig.1) is also shown for comparison. When silica gel was used, the product spectra still correspond to the same phases as in the template-free solutions did. XRD intensities become higher, showing that silica gel functions as a template to model atoms in more perfect orders. These reflect the degree or extent of the crystals. A small amount of silica

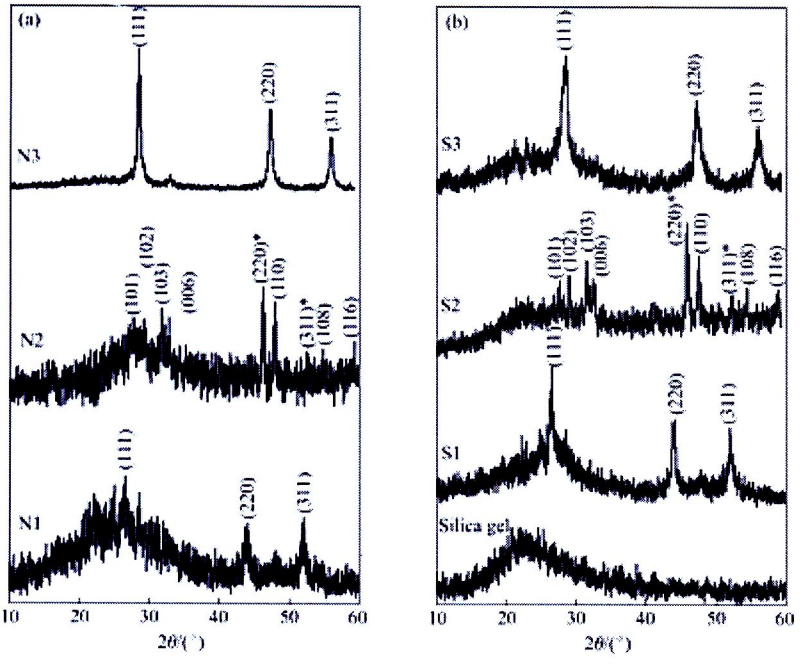

Fig.1 XRD spectra of different products and silica gel

gel remains in the products although they have been washed out by water. The calculated lattice parameter [17](Table 2) are very close to those of the corresponding JCPDS software[16].

Table 2 Calculated lattice parameters of products

Product	Silica gel-free		Containing silica gel	
	a/nm	c/nm	a/nm	c/nm
CdS (cubic)	0.582	-	0.581	-
CuS (hcp)	0.378	1.636	0.379	1.640
Cu_2S (cubic)	0.557	-	0.558	-
ZnS (cubic)	0.540	-	0.539	-

3.2 SEM analysis

The SEM images show the change of product morphologies, caused by silica gel. In template-free solutions, N1 (Fig.2(a)) is composed of nanosized spherical particles. Each appears as rough surface. But for N2 and N3 (Figs.2(b) and 2(c)), they are nanoplates in cluster and a bulk of nanoparticles, respectively. When silica gel is added to the solutions, the process is divided into three steps: (1) the template randomly diffuses through the solutions, (2) the 200 ℃ solvothermal reaction proceeds, and (3) after cooling to room temperature, the template is removed by water. Silica gel functions as a hard template and models the products into some specified morphologies [14-15]. S1, S2 and S3 (Figs.2(d), 2(e) and 2(f)) are composed of elongated particles with clusters of nanoparticles at their tips, hexagonal particles and spherical particles, respectively. At higher magnification, each of the spherical particles (Fig.2(f)) is composed of nanoparticles with different sizes. The results show that silica gel played the role in the product morphologies.

3.3 FTIR analysis

The FTIR spectra of silica gel, S1, S2 and S3 (Fig.3) were analyzed using a transmittance mode. For silica gel, its spectrum shows the broad band of stretching vibration of hydroxyl groups on its surface at 3 438 cm^{-1}. The bands at 1 098 and 797 cm^{-1} are assigned to the Si—O stretching vibration and Si—O—Si bending vibration,

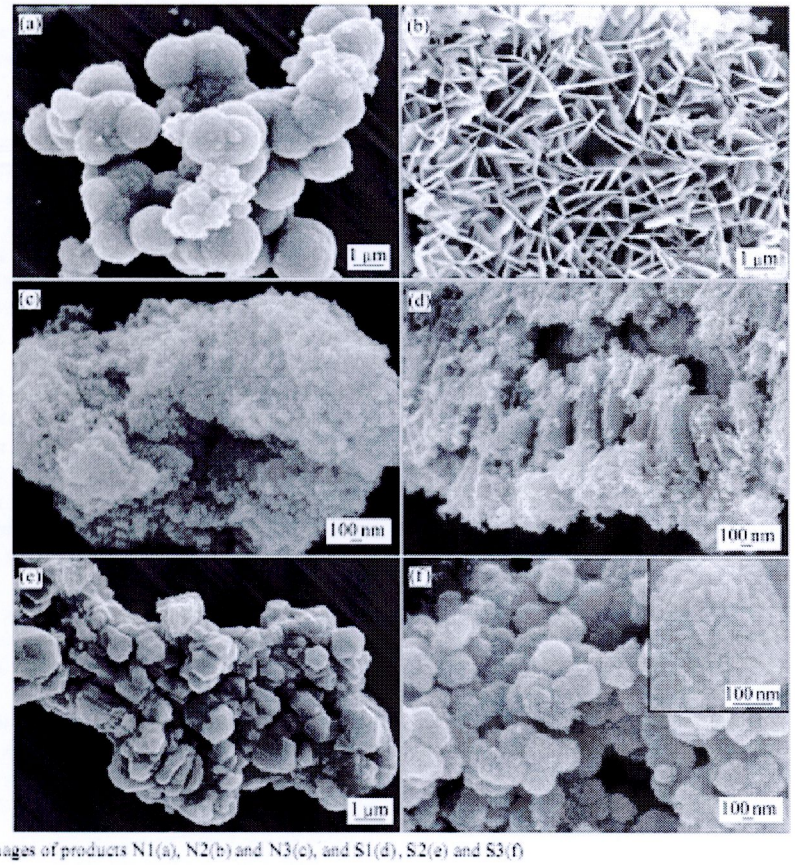

Fig.2 SEM images of products N1(a), N2(b) and N3(c), and S1(d), S2(e) and S3(f)

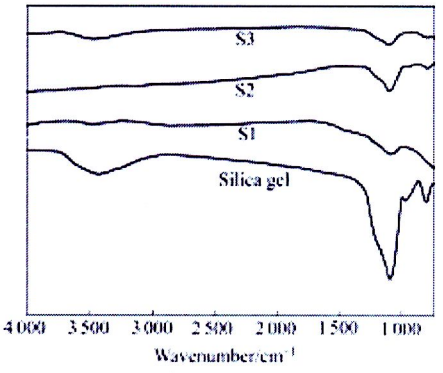

Fig.3 FTIR spectra of silica gel, S1, S2 and S3

respectively. The band at 974 cm^{-1} corresponds to the Si—OH stretching vibration[18]. But for S1, S2 and S3, some of the vibration peaks belonging to silica gel no longer exist. The stretching vibration of Si—O still exists but its intensity becomes lower. The analysis shows that silica gel functions as a template which was subsequently washed out by water. Only the residues remain in the products. The results are in accordance with those of the XRD analysis.

3.4 Raman spectral analysis

The Raman spectra of N1 and S1 (Fig.4(a)) show two main peaks corresponding to the first and second longitudinal optical (LO) phonon modes, which are polarized in the x-z face with strong coupling to the exciton along c axis[1]. The 1LO and 2LO corresponding to the fundamental and overtone modes[1, 19] are detected at 300 and 599 cm^{-1}, respectively. Each of the vibrations is at the same wavenumbers although the products are synthesized with and without using silica gel. They are in accordance with other results[20]. In the solution containing silica gel, atoms are modeled in perfect lattice and the intensity becomes higher. But for those of N2 and S2 (Fig.4(b)), the spectra are very narrow. Their vibrations are in the same wavenumbers at 474 cm^{-1}, corresponding to lattice vibrations. The present results are in accordance with those of CuS thin films[2]. The intensity of the product synthesized in the solution containing silica gel becomes higher as well. The Raman analysis of ZnS does not show any prominent peaks in the spectra of both N2 and S2.

3.5 Photoluminescence (PL) analysis

The PL spectra of CdS, CuS-Cu_2S mixture and ZnS (Fig.5) were determined at ambient temperature using 250 nm, 220 nm and 230 nm excitation wavelengths, respectively. The distinct PL emissions are detected at 616 nm, 340 nm and 362 nm, which are very close to the

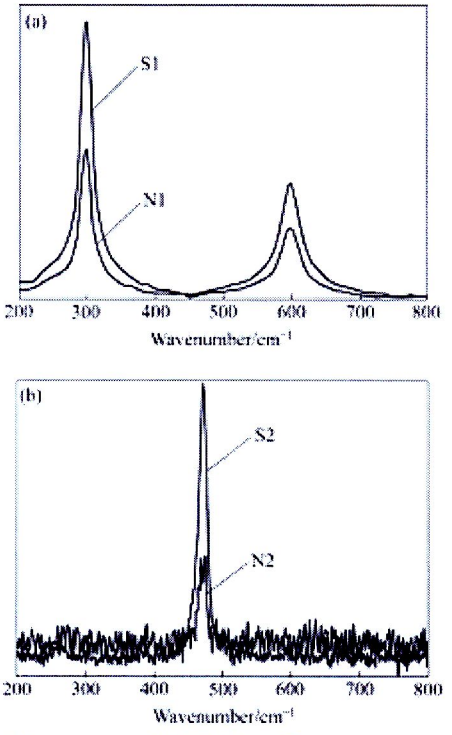

Fig.4 Raman spectra of N1, S1, N2 and S2

previous reports for CdS[4, 21], CuS[22] and ZnS[9, 23]. Emission caused by defects of ZnS[23] is also detected at 423 nm. For the present analysis, photon energies are lost during the characterization and the emissions of longer wavelengths are detected. Their intensities are influenced by several parameters such as shapes, sizes, and crystallinities, which are controlled by the template. In the solution containing silica gel, atoms are modeled in perfect lattices and higher intensities are clearly detected. These results thus show that silica gel has the influence on PL emissions of the products.

4 Conclusions

CdS (cubic), mixed phases of covellite CuS (hcp) and Cu_2S (cubic), and sphalerite ZnS (cubic) with different morphologies were successfully produced by the solvothermal process with and without using silica gel as a hard template. Their morphologies changed from the spherical particles to elongated particles with clusters of nanoparticles at their tips for CdS, nanoplates in cluster to hexagonal particles for CuS-Cu_2S mixture, and a bulk of nanoparticles to spherical particles for ZnS by silica gel adding. A small amount of silica gel was also

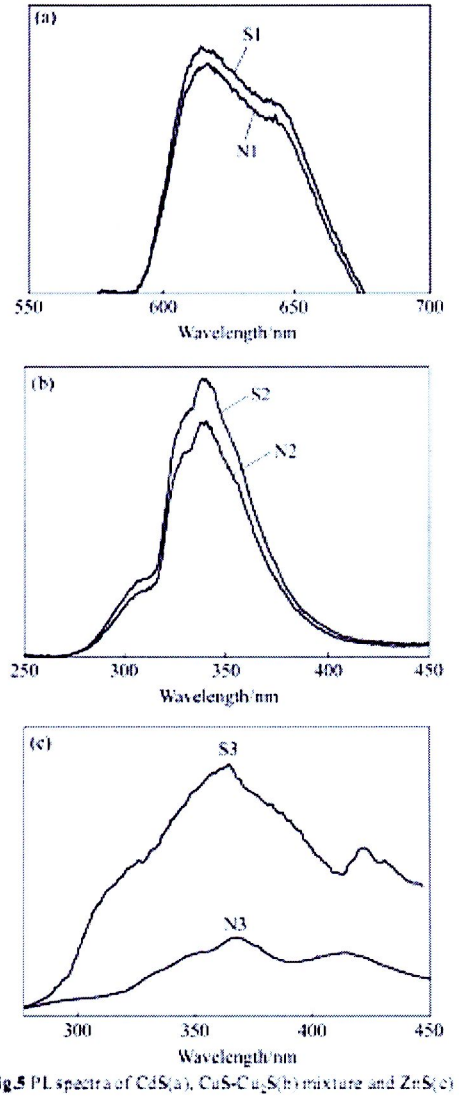

Fig.5 PL spectra of CdS(a), CuS-Cu_2S(b) mixture and ZnS(c)

detected after the products were washed out. Intensities of Raman and photoluminescence spectra were increased by using silica gel as a hard template. But for their wavenumbers and wavelengths, they remained at the same values.

Acknowledgements

We are extremely grateful to the Thailand Research Fund (TRF), and Center for Innovation in Chemistry (PERCH-CIC), Commission on Higher Education (CHE), Ministry of Education (CCHE), Thailand, for financial support.

References

[1] PAN A, LIU R, YANG Q, ZHU Y, YANG G, ZOU B, CHEN K. Simulated emissions in aligned CdS nanowires at room temperature[J]. J Phys Chem B, 2005, 109: 24268−24272.

[2] WANG S Y, WANG W, LU Z H. Asynchronous-pulse ultrasonic spray pyrolysis deposition of Cu_xS (x=1, 2) thin films[J]. Mater Sci Eng B, 2003, 103: 164−168.

[3] PANDA S K, CHAUDHURI S. Chelating ligand-mediated synthesis of hollow ZnS microspheres and its optical properties[J]. J Coll Interf Sci, 2007, 313: 338−344.

[4] HERNANDEZ J R L, DE SOUZA-PARISE M, MORAIS P C. Optical investigation of the red band emission of CdS nanoparticles[J]. Surf Sci, 2007, 601: 3905−3908.

[5] THONGTEM T, PHURUANGRAT A, THONGTEM S. Free surfactant synthesis of microcrystalline CdS by solvothermal reaction[J]. Mater Lett, 2007, 61: 3235−3238.

[6] THONGTEM T, PHURUANGRAT A, THONGTEM S. Synthesis and analysis of CuS with different morphologies using cyclic microwave irradiation[J]. J Mater Sci, 2007, 42: 9316−9323.

[7] THONGTEM T, PHURUANGRAT A, THONGTEM S. Formation of CuS with flower-like, hollow spherical, and tubular structures using the solvothermal-microwave process[J]. Curr Appl Phys, 2009, 9: 195−200.

[8] XU J Z, XU S, GENG J, LIG X, ZHU J J. The fabrication of hollow spherical copper sulfide nanoparticle assemblies with 2-hydroxypropyl-β-cyclodextrin as a template under sonication[J]. Ultrason Sonochem, 2008, 15: 45−454.

[9] ZHAO Y, HONG J M, ZHU J J. Microwave-assisted self-assembled ZnS nanoballs[J]. J Cryst Growth, 2004, 270: 438−445.

[10] YANG H, HUANG C, SU X, TANG A. Microwave-assisted synthesis and luminescent properties of pure and doped ZnS nanoparticles[J]. J Alloys Comp, 2005, 402: 274−277.

[11] MANOHARAN S S, GOYAL S, RAO M L, NAIR M S, PRADHAN A. Microwave synthesis and characterization of doped ZnS based phosphor materials[J]. Mater Res Bull, 2003, 38: 1039−1047.

[12] JIANG C, ZHANG W, ZOU G, YU W, QIAN Y. Hydrothermal synthesis and characterization of ZnS microspheres and hollow nanospheres[J]. Mater Chem Phys, 2007, 103: 24−27.

[13] TSUZUKI T, MCCORMICK P G. Mechanochemical synthesis of metal sulphide nanoparticles[J]. NanoStruct Mater, 1999, 12: 75−78.

[14] FUERTES A B. A general and low-cost synthetic route to high-surface area metal oxides through a silica xerogel template[J]. J Phys Chem Solids, 2005, 66: 741−744.

[15] CABANA J, VALDÉS-SOLÍS T, PALACÍN M R, ORO-SOLÉ J, FUERTES A, MARBAN G, FUERTES A B. Enhanced high rate performance of $LiMn_2O_4$ spinel nanoparticles synthesized by a nanotemplate route[J]. J Power Sours, 2007, 166: 492−498.

[16] Powder Diffraction Files[S]. JCPDS-ICDD. USA, PA 19073-3273, 2001.

[17] SURYANARAYANA C, NORTON M G. X-ray diffraction, a practical approach[M]. New York: Plenum Press, 1998: 23−253.

[18] VIJAYALAKSHMI U, BALAMURUGAN A, RAJESWARI S. Synthesis and characterization of porous silica gels for biomedical applications[J]. Trends Biomater Artif Organs, 2005, 18: 101−105.

[19] LI C, YANG X, YANG B, YAN Y, QIAN Y. Growth of macrotubular complexes as precursors to synthesize nanocrystalline ZnS and CdS[J]. J Cryst Growth, 2006, 291: 45−51.

[20] SHEN X P, YUAN A H, WANG F, HONG J M, XU Z. Fabrication of well-aligned CdS nanotubes by CVD-template method[J]. Solid State Comm, 2005, 133: 19−22.

[21] XIA Q, CHEN X, ZHAO K, LIU J. Synthesis and characterizations of polycrystalline walnut-like CdS nanoparticle by solvothermal method with PVP as stabilizer[J]. Mater Chem Phys, 2008, 111: 98−105.

[22] ZHANG J, ZHANG Z. Hydrothermal synthesis and optical properties of CuS nanoplates[J]. Mater Lett, 2008, 62: 2279−2281.

[23] JING H, ZHU Y J, YANG L X, LI L, ZHANG L, CHANG J, AN L Q, WANG S W. Self-assembled ZnS nanostructured spheres: Controllable crystal phase and morphology[J]. J Phys Chem C, 2007, 111: 3893−3900.

(Edited by YUAN Sai-qian)